BAKU STATE UNIVERSITY

8th INTERNATIONAL CONFERENCE

MODERN TRENDS IN PHYSICS

DEDICATED TO THE 100th ANNIVERSARY OF NATIONAL LEADER HEYDAR ALIYEV

NOVEMBER 30 - DECEMBER 1, 2023

BAKU STATE UNIVERSITY

BAKU, AZERBAIJAN

BOOK OF ABSTRACTS

BAKU-2023

Book of abstracts. 8th International Conference MTP-2023: Modern Trends in Physics, dedicated to the 100th anniversary of National Leader Heydar Aliyev, November 30 – December 01, 2023. Baku State University, Baku, Azerbaijan. 184 p.

ISBN: 978-9952-546-49-1

ORGANIZING COMMITTEE:

Chairman:

Huseyn Mammadov – Vice Rector for Science and Innovations, Baku State University (BSU), Azerbaijan

Deputy chairman:

Bakhtiyar Pashaev – Dean of Physics Faculty, BSU, Azerbaijan

Members:

Sadiyar Rahimov – Director of Institute for Physical Problems, BSU, Azerbaijan

Vusal Mammadov – Deputy Dean for Academic Affairs of the Physics Faculty, BSU, Azerbaijan

Shahla Hajiyeva – Deputy Dean for Scientific Affairs of the Physics Faculty, BSU, Azerbaijan

Yegana Aliyeva – Scientific secretary, BSU, Azerbaijan

Mahir Pirguliyev – Head of the Rector's Secretariat, BSU, Azerbaijan

Mustafa Muradov – Deputy Director for Education, Programs and Cooperation of Excellence Center for Research, Development and Innovations, BSU, Azerbaijan

Zohrab Aghamaliyev – Deputy Director for R&D and Innovations of Excellence Center for Research, Development and Innovations, BSU, Azerbaijan

Ilyas Nasibov – Director of Student Scientific-Technical Creativity Center, BSU, Azerbaijan

Mirnamik Bashirov – Head of the Department of Doctorate, BSU, Azerbaijan

Majid Gojayev – Associate Professor, Theoretical Physics Department, BSU, Azerbaijan

Goncha Eyvazova – Leading researcher, EC Nano Research Lab, BSU, Azerbaijan

Lala Gahramanli – Leading researcher, EC Nano Research Lab, BSU, Azerbaijan

Sara Rahimzade – Specialist of Physics faculty, BSU, Azerbaijan

PROGRAM COMMITTEE:

Chairman:

Aydin Kazimzade – Rector's advisor for Science and Education, BSU, Azerbaijan

Members:

Oktay Gasimov – Director of Institute of Biophysics, Ministry of Science and Education, Azerbaijan

Sajid Qamar – Rector of COMSATS University, Pakistan

Mais Suleymanov – Director of the Centre for Organization of Scientific Activity and Innovations, BSU, Azerbaijan

Eldar Masimov – Head of the Department of Matter Structure, BSU, Azerbaijan

Ahmad Abdinov – Head of the Department of Physical Electronics, BSU, Azerbaijan

Vagif Salmanov – Head of the Department of Semiconductor Physics, BSU, Azerbaijan

Rena Gasimova – Head of the Department of Optics and Molecular Physics, BSU, Azerbaijan

Maarif Jafarov – Head of the Department of Chemical Physics of Nanomaterials, BSU, Azerbaijan

Kamala Alisheva – Head of the Department of Astrophysics, BSU, Azerbaijan

Mammad Rajabov – Head of the Department of Theoretical Physics, BSU, Azerbaijan

Mehdi Mahmudov – Head of the Department of Solid State Physics, BSU, Azerbaijan

CONTENT

INNOVATIVE APPLICATIONS OF ADVANCED 2D MATERIALS
Bellucci S. 19

PHYSICS OF DOUBLY HEAVY BARYONS
Aliyev T. 20

FUNDAMENTAL AND APPLIED PHYSICS WITH REACTOR NEUTRINOS
Yakushev E. 21

COMPARATIVE ANALYSIS OF MEMBRANE PROPERTIES OF HUMAN LUNG CARCINOMA AND NORMAL CELLS: RELEVANCE FOR DRUG DELIVERY
[1*]Gasymov O.K., [2]Aliyev J.A. 22

MAGNETOHYDRODYNAMIC KELVIN-HELMHOLTZ INSTABILITIES OF SUPERSONIC SHEAR LAYERS WITH FINITE INTERFACE THICKNESS AND HEAT FLUX IN ANISOTROPIC SPACE PLASMAS
[1*]Dzhalilov N.S., [2]Ismayilli R. 23

THERMODYNAMIC SIGNATURES AND PHASE TRANSITIONS IN HIGH-ENERGY HADRONIC AND NUCLEAR COLLISIONS
[1*]Ajaz M., [2]Waqas M., [3]Alrebdi H.I., [1]Badshah M. 24

TRAVELLING OF SINE-GORDON SOLITONS IN NETWORK OF JOSEPHSON JUNCTION ARRAYS
[1,3*]Askerzade I.N., [2]Matrasulov D., [1]Salati M. 25

EXTENDED LINEAR-SIGMA MODEL: MASS SPECTRUM OF CHARMED MESONS
[1*]Tawfik A., [2]Ahmadov A. 25

THE SEARCH FOR A RARE PROCESS FOR HIGGS BOSON PRODUCTION BY APPLYING A NEW EVOLUTIONARY ALGORITHM WHICH CONSTRUCT A OPTIMIZED NEURAL NETWORK IN AN IRREGULAR HYPERPARAMETER SPACE
[1,2*]Huseynov N.A., [2]Boyko I.R., [2]Yeletskikh I.V., [2]Didenko A.R., [2]Koval O.A. 26

GEOGRAPHY OF OBSERVATION OF THE OWN REFLECTED RADIATION
Rustamov R.B. 26

EXPLORING THE CROSS SECTIONS OF DIRECT REACTIONS IN THE SU(5) REPRESENTATION
[1*]Abdulvahabova S.G., [2]Afandiyeva I.G., [2]Ahmedov R.A. 27

SEARCH FOR THE EXPERIMENTAL SIGNATURE OF THE STRINGS AT THE LHC
Suleymanov M.K. 28

FREQUENCY OF TRANSVERSE AND LONGITUDINAL THERMOMAGNETIC WAVES IN CERTAIN ANISOTROPIC CONDUCTING MEDIA

*Maharramova A.A., Hasanov E.R. 30

SPECTRAL INVESTIGATIONS OF THE ALGOL-TYPE BINARY STAR U SAGITTAE
[1,2]Rustamov B.N., [1]Mikailov Kh.M., [1]Alisheva K.I., [2]Mammadova S.O., [2*]Aliyeva V.I. 31

AXIAL-VECTOR CHARGE RADIUS OF NUCLEONS IN THE SOFT-WALL MODEL OF HOLOGRAPHIC QCD AT FINITE TEMPERATURE
[1*]Nasibova N., [2]Mamedov Sh. 32

METALLICITY OF THE STAR HR 4294(A5III)
[1,2]Samedov Z.A., [1]Rajabova S.Sh., [2]Rustem U.R., [2*]Hajiyeva G.M. 34

INVESTIGATING THE STRUCTURAL AND OPTICAL PROPERTIES OF $Cu_xCo_{3-x}O_4$ NANOPARTICLES SYNTHESIZED BY SONOCHEMICAL METHOD
*Mammadyarova S.J., Muradov M.B., Eyvazova G.M., Balayeva O.O. 35

DOUBLE QUADRATIC PHOTODETECTION BASED GAAS/ALGAAS STEPPED QUANTUM WELL IN A TERAHERTZ AND FAR INFRARED RANGE
[1*]Salhi W., [1]Rajira A., [1]Samyh A., [2]Akabli H., [1]Abounadi A., [1]Almaggoussi A. .. 36

DLTS SPECTROSCOPY OF RADIATION DEFECTS
IN SILICON WITH PLATINUM IMPURITY
Utamuradova Sh., *Rakhmanov D. 37

TWO-DIMENSIONAL ENERGY STRUCTURE OF SCHOTTKY DIODES
*Mamedov R.K., Aslanova A.R. 38

SELF-POWERED TRANSMISSION LINE MONITORING SENSORS BASED ON TRIBOELECTRIC NANOGENERATORS WITH MAGNETIC NANOPARTICLES /NYLON NANOCOMPOSITE FILMS
*Gulahmadov O.G., Muradov M.B., Mamedov H.M., Qahramanli L.R., Jiseok K. 40

ACOUSTIC WEYL METAMATERIALS BASED SPACE-TIME CRYSTALS
WITH TOPOLOGICAL STATES
[1]Ozer Z., [2,3*]Mamedov A.M., [2]Ozbay E. 41

CONTROLLING THE UNCONTROLLABLE: QUANTUM CONTROL OF OPEN SYSTEM DYNAMICS
[1,2*]Kallush Sh., [1]Dann R., [1]Kosloff R. 43

SYNTHESIS OF AgNWs/PVA NANOCOMPOSITE AND EXAMINATION
OF THE IMPACT OF SULFIDATION ON ITS STRUCTURAL CHARACTERISTICS
*Addayeva Z.R., Muradov M.B., Eyvazova G.M., Mammadyarova S.J., Baghirov M.A. 43

THE USE OF MULTI-QUANTUM ABSORPTION FOR THE STUDY OF
SEMICONDUCTOR MULTILAYER STRUCTURES

*Salmanov V.M., Huseynov A.G., Mamedov R.M., Hasanova L.G., Mahammadov A.Z., Ahmadova F.Sh., Mammadova T.A. 45

ELECTRONIC BAND STRUCTURE OF $Cd_{1-x}Fe_xSe$
[1,2*]Mehrabova M.A., [3,4]Allahyarov E.A., [5]Hasanov N.H., [6]Gasimova N.R. 46

CdS NANOPARTICLES SYNTHESIZED BY LASER ABLATION
Jafarov M.A., *Salmanov V.M., Huseynov A.G., Mamedov R.M., Abasova A.Z., Jahangirova S.A., Ahmadova F.Sh., Mammadova T.A. 47

STATE OF THE ART IN CANCER THERAPY: COMBINED THERAPY AND THE MAIN FACTORS LIMITING OR ENHANCING THE EFFICACY OF PROTON THERAPY
[1]*Chirakadze A., [1]Mitagvaria N., [1]Chubinidze G., [1]Dvali N., [1]Khuskivadze N., [2]Shanidze R., [2]Abuladze M., [3]Palavandishvili G. 48

ALKALI METAL SALT SOLUTION BASED SYNERGISTIC CANCER THERAPY COMBINED
WITH ANTICANCER METAL OXIDE NANOPARTICLES: ACUTE TOXICITY STUDY
[1*]Chubinidze G., [1]Mitagvaria N., [1]Chirakadze A., [1]Dvali N., [1]Khuskivadze N., [1]Chichua T., [2]Chikadze N., [3]Khomeriki I., [3]Buachidze Z., [4]Abuladze M..... 50

BAND STRUCTURE, DIELECTRIC FUNCTION AND REFLECTION COEFFICIENT OF CHAIN $TlGaTe_2$
[1]Abdullayev A.P., [1*]Gafarova D.M., [1]Musazade I.V., [2]Ismayılov T.I. 51

ELECTRONIC AND MAGNETIC PROPERTIES OF AG-DOPED (6,0) SINGLE-WALLED ZnO NANOTUBES
[1*]Jafarova V.N., [2]Mamedov N.T. 52

DEVELOPMENT OF SELECTIVE INHIBITORS FOR THE TUMOR-ASSOCIATED CARBONIC ANHYDRASES
[1*]Akdemir A., [2]Demir-Yazıcı K., [2]Trawally M., [2]Guzel-Akdemir O. 53

ACOUSTIC METAMATERIALS FOR AERONAUTIC APPLICATIONS: A REVIEW
[1,2*]Mamedov A.M., [1]Ekmel Ozbay 54

JANUS MATERIALS: INDIRECT (Λ-Γ)-TO-INDIRECT (K-Γ) CROSSOVER IN FEW MONOLAYER MoS_2
[1,2]Mamedov N.T. 56

REPULSION DRIVEN METALLIC PHASE IN THE GROUND STATE OF THE HALF-FILLED T-T' IONIC HUBBARD CHAIN
[1]Rossini G.L., [2]Japaridze G.I. 56

MONTE CARLO PREDICTIONS FOR AND ϕ(1020)° and K* (892)° MESONS PRODUCTION AT LHC ENERGIES IN HADRON-HADRON AND HEAVY ION COLLISIONS
Yasir A.S. 57

IR LASER-INDUCED ABLATIVE DEPOSITION OF POLYMER BASED COMPOSITES
Gilev J.B. 58

EARTH-ABUNDANT COMPOUND SEMICONDUCTORS FOR SOLAR ENERGY CONVERSION
[1,2*]Schorr S. 59

KNOCKING OUT OF NEUTRON BY THE PROTON FROM NUCLEUS
[*]Abdulvahabova S.G., Bayramova T.O. 60

SPECTRAL OBSERVATIONS OF THE SYMBIOTIC STAR AG PEGASI
[1]Mikailov Kh.M., [2*]Rustamova A.B., [1,2]Rustamov B.N., [2]Alekberov I.A. 61

STUDY OF THE ASSOCIATIVE PRODUCTION OF THE HIGGS BOSON WITH THE Z-BOSON USING MVA METHODS
Ahmadov F.N. 63

TEMPERATURES OF THE CENTRAL STARS OF PLANETARY NEBULAE NGC 2392, NGC 1535, NGC 3242, IC 418
*Alili A.H., Alisheva K.I., Mikailov Kh.M. 64

PROMPT PHOTON PRODUCTION IN BREMSSTRAHLUNG AT NICA ENERGIES
[1*]Alizada M.R., [1]Ahmadov A.I., [2]Arbuzov A.B. 65

$f_2(1270)$ TENSOR MESON COUPLING CONSTANT FROM THE HARD-WALL AdS/QCD
[1*]Hashimli Z.I., [1,2,3]Mamedov S.A. 66

ON THE DIRECT CORRESPONDENCE BETWEEN THE TRIGONOMETRIC PÖSCHL-TELLER POTENTIAL WALL AND THE QUANTUM SINGULAR OSCILLATOR WITH THE POSITION-DEPENDENT MASS
Nagiyev Sh.M., [*]Jafarov E.I. 67

COULD QUARK STARS BE A SOURCE OF ULTRA-HIGH ENERGY COSMIC RAYS?
Suleymanov M.K. 68

π MESON-Σ BARYON COUPLING CONSTANT IN THE HARD-WALL AdS/QCD MODEL
[1,2*]Taghiyeva Sh.I., [1,3]Mamedov Sh.A. 69

SINGULARITY ATTENUATION IN GENERAL RELATIVITY WITH QUANTIZED FUNDAMENTAL METRIC
[1*]Tawfik A., [2]Dabash T., [3]Alshehri A. 70

APPLICATION OF THE DISTORED-WAVE APPROXIMATION TO THE ELECTRON'S SCATTERING ON THE ATOMS
Mirabutalibov M.M., [*]Aliyeva M.B. 71

SYNTHESIS OF NICKEL NANOPARTICLES WITH MAGNETIC PROPERTIES USING THE CARBOTHERMY METHOD

[1*]Bohatyrenko V.A., [2]Kamenskyh D.S., [2]Tkachenko T.V., [2]Khimach N.Y..... 72

SYNTHESIS AND CHARACTERIZATION OF VSi_2-SiC NANOCOMPOSITE POWDERS
Dondash D.O. 73

PREPARATION OF GO/AGNWS NANOCOMPOSITE AND INVESTIGATION OF THE EFFECT OF SULFIDATION AND ITS STRUCTURE AND OPTICAL CHARACTERISTICS
*Baghirov M.A., Muradov M.B., Eyvazova G.M., Mammadyarova S.J., Ahmadov X.I. 74

NANOPARTICLE FABRICATION OF $G_EB_{i2}T_{E4}$ VAN DER WAALS COMPOUND VIA THE BALL-MILLING METHOD
[1*]Mehtiyeva Kh. Z., [1,2] Amiraslanov I. R., [1,2]Aliev Z. S. 75

GRAPHENE OXIDE-POLYVINYL ALCOHOL NANOFIBROUS COMPOSITES: ELECTRICAL PROPERTIES
[1]Khanmamadova E.A., [1]Abaszade R.G., [2]Jafarov M.A., [3*]Safarov R.Y..... 77

EFFECTS OF Se/(Sn+Zn+Sn) RATIO ON THE PROPERTIES OF SINGLE-STEP ELECTRODEPOSITED $Cu_2ZnSnSe_4$ THIN FILMS
[1,2*]El Otmani R., [4]El Khouja O., [1]El Manouni A., [4]Galca A.C., [2,3]Almaggoussi A. 77

INTERACTION OF α-In_2Se_3 CRYSTALS WITH 4-AMINOPYRIDINE
[1]Rahimli A.B., [1.2]Aliev Z.S., [1.2*]Amiraslanov I.R. 78

MICRO-PIXEL HIGH Z SEMICONDUCTOR MATERIALS AS IMAGING DETECTORS
[*]Guliyev E., Hamzayeva R. 80

COMPARATIVE ACOUSTIC ANALYSIS OF FIVE RENOWNED OPERATIC TENORS
Bruseldorff A.S. 80

INFLUENCE OF GAMMA RADIATION ON THE CRYSTALLISATION OF PVS/CdS NANOCOMPOSITES
Gasimova A.I., Nuriyev M.A. 82

BAND GAP AND WAVE PROPAGATION ON PVDF BASED TOPOLOGICAL HAUSDORFF AND SERPINSKI DIMENSION OF QUASI-FRACTAL PHONONIC CRYSTALS: FINITE ELEMENTS ANALYSIS
[1]Palaz S., [2]Ozer Z., [3,4]Mamedov A.M., [3]Ozbay E. 83

COMPARISON OF THE PHYSICAL PROPERTIES OF CDXZN1-XS-BASED NANOCOMPOSITE MATERIALS PRODUCED VIA SONOCHEMICAL AND SILAR APPROACHES
[1*]Gahramanli L.R., [1]Muradov M.B., [1]Eyvazova G.M., [2]Ákos Kukovecz 84

PROMISING CARBONS FROM LIGNOCELLULOSIC RAW MATERIALS AND THEIR PROCESSING WASTE
[1]Doroshenko S.O., [1*]Tkachenko T.V., [2]Tamarkina Y.V., [2]Kucherenko V.O., [3]Jafarov M.A., [1,4]Kamenskyh D.S., [1]Povazhny V.A., [1]Yevdokymenko V.O. 85

LASER ABLATION ZnCdO THIN FILMS
Jafarov M.A., Mammadov H.M., *Mammadov V.U., Nasirov E.F..... 86

THE EFFECT OF CHARACTERISTIC LENGTHS ON THE NONSTATIONARY CONVERSION OF FREQUENCIES OF ULTRA SHORT LIGHT PULSES
Amirov Sh.Sh. 87

SOLUTION OF REDUCED EQUATIONS FOR THE PROPAGATION OF AN ULTRASHORT LASER PULSE IN A METAMATERIAL
*Ahmadova A.R., Kasumova R.J., Safarova G.A. 88

INFLUENCE OF RARE EARTH METALS ON ELECTROPHYSICAL PROPERTIES OF GES LAYERED MONOCRYSTALLINE
Dashdemirov A.O., *Alekperov A.S. 90

MODIFICATION OF SLC-0111 AS NOVEL CARBONIC ANHYDRASE INHIBITORS
*Guliyeva L., Trawally M., Demir-Yazıcı K., Guzel-Akdemir O. 90

RADIOBIOLOGICAL RESEARCH AT JINR ACCELERATORS
Bugay A.N. 91

INTERACTION MECHANISM OF GLYCYRRHIZIN FOR THE COVID-19 TREATMENT
*Galandarli L.E., Akverdieva G.A. 92

DARK-INDUCED CHLOROFILL DEGRADATION IN COTTON PLANTS SEEDLINGS
*Ahmadov I.S., Eyvazova G.M., Hasanova F.V., Babanlı S.T. 93

STRUCTURAL ORGANIZATION OF LACTOFERROXINE C
*Agayeva L.N., Abdinova A.A., Akhmedova S.R., Akhmedov N.F. 94

ULTRASTRUCTURAL CHARACTERISTICS OF THE ACCUMULATION OF IRON NANOPARTICLES IN INTESTINE AND LIVER OF COMMON CARP (*CYPRINUS CARPIO* LINNAEUS, 1758)
*Mammadov Ch.A., Hajiyeva A.D., Khalilov R.I. 95

TEMPERATURE-INDUCED PHASE TRANSITIONS OF LIPIDS EXTRACTED FROM HUMAN LUNG CARCINOMA AND NORMAL CELLS
[1*]Aydemirova A.H., [1]Bakhishova M.J., [1]Aslanov R.B., [1,2]Melikova L.A., [1]Gasymov O.K. 96

MOLECULAR MODELING APPLIED TO THE NEW CHEMICAL COMPOUNDS
*Akverdieva G.A, Demukhamedova S.D. 97

REFRACTOMETRIC INVESTIGATION OF THE HYDRATION PROCESS IN ELECTROLYTES
Masimov E.A., Pashayev B.G., Shahbazova G.M., *Teymurova J.Z. 99

NON-LETHAL TESTING OF THE ACUTE TOXICITY OF NEWLY DEVELOPED COMBINED CANCER TREATMENT MODALITIES AGAINST CHICK EMBRYOS AND WARM BLOODED MAMMALS

[1]*Mitagvaria N., [1]Chirakadze A., [1]Chubinidze G., [1]Dvali N., [1]Khuskivadze N., [2]Shanidze R., [2]Abuladze M., [3]Khomeriki I., [3]Tserodze K. 100

ALKALI METAL SALT SOLUTION BASED COMBINED CANCER THERAPY AND THE "HIGH PH THERAPY" CONCEPT
[1*]Khuskivadze N., [1]Chubinidze G., [1]Mitagvaria N., [1]Chirakadze A., [1]Dvali N., [1]Chichua T., [2]Abuladze M., [3]Khomeriki I., [3]Buachidze Z. 102

ISOTOPIC ENRICHED BORON AND BORON NITRIDE NANOMATERIALS FOR PROTON-BORON CAPTURE AND BORON NEUTRON CAPTURE THERAPY OF CANCER
[1*]Dvali N., [1]Khuskivadze N., [1]Chubinidze G., [1]Mitagvaria N., [1]Chirakadze A., [1]Chichua T., [2]Chikadze N., [3]Khomeriki I., [3]Buachidze Z..... 103

VISIBLE LIGHT AND INFRARED OVOSCOPIC STUDY, PLETHYSMOGRAPHY AND SONOGRAPHY OF BIRD EMBRYOS AND LONG TERM MONITORING OF BEHAVIORAL AND PHYSIOLOGICAL PARAMETER OF WHITE RATS IN TESTING OF ACUTE TOXICITY OF DRUGS
[1*]Chichua,T., [1]Dvali N., [1]Khuskivadze N., [1]Chubinidze G., [1]Mitagvaria N., [1]Chirakadze A., [2]Chikadze N., [3]Khomeriki I., [3]Buachidze Z..... 104

THE PRODUCTION OF $\boldsymbol{AAA}$-BOSONS IN $\boldsymbol{e-e+}$-ANNIHILATION
Abdullayev S.K., *Gojayev M.Sh. 105

CURRENT OSCILLATIONS IN SEMICONDUCTORS
*Rzayeva U., Hasanov E. 107

ANALYTICAL SOLUTION OF THE DIRAC EQUATION FOR THE LINEAR COMBINATION OF THE MANNING-ROSEN AND YUKAWA POTENTIAL IN THE CASE OF EXACT SPIN SYMMETRY
*Ahmadov A.I., Aslanova S.M. 108

PAIRED SPIN CORRELATIONS OF ELECTRONS, POSITRONS AND γ - QUANTA IN THE PROCESS OF PHOTOLOGY OF $\boldsymbol{e+e-}$-PAIRS ON NUCLEI WITH ACCOUNT OF RECOIL EFFECTS AND NUCLEI STRUCTURE
Rajabov M.R. 110

OPTICAL PROPERTIES OF $PBMOO_4$ CRYSTALS DETERMINED BY SPECTROSCOPIC ELLIPSOMETRY
[1*]Darvishov N.H., [1]Rustamov F.A., [1]Mamedov M.Z., [1,2]Gasanly N.M. 110

THE TEMPERATURE DEPENDENT DIELECTRICAL PROPERTIES OF PtSi/nSi SCHOTTKY DIODES
[1*]Afandiyeva I.M., [1]Lebedeva N.N., [1]Akhundov Ch.G., [1]Bagirova S.E., [2]Babayeva R.F. 111

ACTIVATION ENERGY OF GAMMA-IRRADIATED HDPE+ %A-AL_2O_3 NANOCOMPOSITES

Nabieva A.N. 112

DIELECTRIC PROPERTIES OF POLYPROPYLENE/ZnO BASED NANOCOMPOSITES
*Nuriyeva S.G., Gasimova J.N., Shirinova H.A., Karimova A.H., Gahramanli L.R. 114

ELECTRICAL CONDUCTIVITY OF $FEGA_{0.4}IN_{1.6}SE_4$ CRYSTAL IN ALTERNATING ELECTRIC FIELD
[1*]Niftiyev N.N., [1,2]Mammadov F.M., [1]Aghayeva R.M., [3]Muradov M.B..... 114

NICKEL-CONTAINING THERMOPLASTIC ELASTOMER NANOCOMPOSITES BASED ON POLYPROPYLENE
*Guliyeva T.M., Kurbanova N.I..... 116

OBTAINING AND STUDYING THE PROPERTIES OF NANOCOMPOSITES BASED ON A MIXTURE OF POLYETHYLENES OF HIGH AND LOW PRESSURE WITH METAL-CONTAINING NANO FILLERS
[1*]Mamedova G.H., [2]Kurbanova N.I..... 117

PHOTOLUMINESCENCE SPECTRA OF POLYCRYSTALLINE CVD ZnSe WHEN CHANGING THE WAVELENGTH OF EXCITATION LIGHT
[1*]Musayev M.A., [2]Huseynov J.I., [1]Askerov D.J., [1]Abbasov I.I., [1]Hadiyeva A.A., [3]Mammadova A.J., [1]Hasimova N.N. 118

ELECTRONIC RAMAN SCATTERING IN $Hg_{1-x}Cd_xTe$
[1*]Ismayilov T., [1,2]Zeynalova S..... 119

THERMOELECTRIC EFFECTS IN SUPERLATTICES DUE TO ELECTRON SCATTERING BY SHORT-RANGE POTENTIAL
[1*]Figarova S.R., [2]Huseynov H.I. 120

TO THE TEMPERATURE DEPENDENCE OF PHOTOCONDUCTIVITY IN GeS LAYERED MONOCRYSTALLINE OF ER ADDITIVE ATOMS EFFECT
[1*]Alekperov A.S., [2]Ilyasova T.I., [3]Ismailov M.I. 121

TEMPERATURE DEPENDENCE of the KINETIC COEFFICIENTS of $Bi_{0.97}$ $Sb_{0.03}$ ALLOY
[1*]Musayev A.A., [2]Yuzbashov E.R..... 122

COMPARATIVE ADSORPTION STUDY OF Fe(III) IONS ONTO ODIFIED ADSORBENTS
*Eyyubova E.E.., Nagiyev Kh.J., Chyragov F.M. 123

SPATIAL STRUCTURE OF THE HUMEN β-CASOMORPHIN-7 MOLECULE
*Akhmedov N.A., Agayeva L.N., Ismailova L.I. 124

STRUCTURE OF THE IRON OXIDE Fe_xO_y COMPLEXES WITH GLUCOSE AND DI-GLUCOSE
Abbasova G.C., *Hajiyeva L.S. 125

EPR AND TEM STUDIES OF BIOLOGICAL SYSTEMS

*Nasibova A.N., Khalilov R.I. 126

UREA-ETHANOL-WATER SYSTEMS RESEARCH BY VISCOSIMETRY METHOD
[1*]Hajiyeva Sh.N., [1*]Ahmedova A.B., [2]Orucova N.F., [1]Babayeva F.Kh. 127

STRUCTURAL CHARACTERISTICS OF Kl IN AQUEOUS SOLUTION
Pashayev B.G..... 128

STRUCTURE AND CONFORMATION OF MACROMOLECULAR CHAIN IN WATER-PEG-KI SYSTEMS
Masimov E.A., Pashayev B.G., *Hajiyeva Sh.N. 130

SYNTHESIS AND STRUCTURAL PROPERTIES OF CHITOSAN AND CROSS-LINKED CHITOSAN COATED MAGNETITE NANOPARTICLES FOR ANTICANCER APPLICATIONS
[1*]Karimova A.H., [1]Mehdiyeva A.R., [2]Yagublu V., [1]Nuriyeva S.G., [2]Shirinova H.A., [1]Gahramanli L.R. 132

THE ROLE OF SPECTRAL TRAJECTORY CORRESPONDING TO VOICE ENERGY MAXIMA IN PERSON IDENTIFICATION
[1]Aliyev L.P., [2]Gaziyeva N.G., [1*]Guliyeva S.K..... 133

LASER ABLATION Si THIN FILMS
Mammadov V.U. 134

SYNTHESIS OF NEW COMPLEXES OF 1 PHENYL-2,3-DIMETHYLPYROZALON-5-AZO-4 PYROGALLOL REAGENT AND CETYLTRIMETHYLAMMONIUM BROMIDE WITH SILVER NANOPARTICLES
[1]*Imamaliyeva A., [2]Hajiyeva F., [3]Ciraqov F. 135

SPECTRAL TRAJECTORY REFLECTION OF THE INFLUENCE OF NEIGHBORING SOUNDS ON THE ENERGY MAXIMUM F2 OF A VOWEL SOUND
[1]Aliyev L.P., [2*]Gaziyeva N.G., [1]Guliyeva I. I., [1]Aghamaliyeva A.V. 137

MoS_2 THIN FILM: PREPARATION TECHNOLOGY AND CHARACTERIZATION
Bagiyev E.A..... 138

THE EFFECT OF NICKEL OXIDE NANOPARTICLES ON THE STRUCTURE AND PROPERTIES OF NANOCOMPOSITES BASED ON HIGH-PRESSURE POLYETHYLENE CONTAINING MULTIWALLED CARBON NANOTUBES
[1]*Kurbanova N.I., [1]Mirzoev N.A., [2]Zeynalov E.B., [3]Gadzhieva F.V., [3]Gahramanli L.R. 139

p-n JUNCTIONS BASED ON PbTe FILMS DOPED WITH OXYGEN
*Sarmasov S.N., Rahimov R.Sh. 140

COSMOLOGICAL MODELS
[1]*Jafarzade A.F., [2]Rajabov B.A..... 141

THE PRODUCTION OF ZAA-BOSONS IN $e-e+$-COLLISIONS

Abdullayev S.K., *Gojayev M.Sh. 142

BOUND STATE SOLUTIONS OF THE KLEIN-FOCK-GORDON EQUATION FOR THE DENQ-FAN POTENTIAL
[1]Aliyeva T.H., [2*]Dadashov E.A. 144

CURRENT FLUCTUATIONS IN IMPURITY SEMICONDUCTORS
[*]Aliyev S.R., Hasanov E.R. 145

IKEDA WITH LINEAR AND NON-LINEAR RELATIONSHIP COMBINED SYNCHRONIZATION BETWEEN SYSTEMS
[1*]Nuriyev R.A., [2]Pashayev B.G. 147

ELECTROMAGNETIC SHOWER IN CRYSTALS
Rajabov M.R. 148

LITERATURE REVIEW ON INCLUSION OF SOLAR PANEL SYSTEMS, BENEFITS AND CHALLENGES IN ALBANIA
Zeneli M. 149

DEFINITION OF ELECTRIC PARAMETERS OF Re/n-GaAs SCHOTTKY DIODE USING I–V MEASUREMENTS
[1*]Afandiyeva I.M., [1]Godjayev N.N., [3]Babayeva R.F. 150

EFFECT OF THERMAL TREATMENT METHODS ON MAGNETIC HYSTERESIS PROPERTIES OF Fe-Ni-Si-B BASED AMORPHOUS MAGNETS
Abdullayev A.P., [*]Rafiyev N.M., Isayeva A.A., Asgarova G.Z. 151

DIELECTRIC FUNCTION OF MoS_2 THIN FILMS
[*]Jalilli J.N., Alizade E.H., Hidiyev K.H., Mammadov D.A. 152

DEVELOPMENT OF METHODS FOR CONCENTRATING PALLADIUM WITH SYNTHETIC SORBENTS BASED ON A COPOLYMER OF MALEIC ANHYDRIDE WITH STYRENE
[*]Abilova U.M., Hajiyeva S.R., Chiraqov F.M. 154

THERMOELECTRIC CONVERTERS OF IR RADIATION BASED ON $Ag_3In_5Te_9$
[*]Rahimov R.Sh., Sarmasov S.N. 155

INFLUENCE OF ZINC-CONTAINING NANOPARTICLES ON THE PROPERTIES OF COMPOSITIONS BASED ON ISOTACTIC POLYPROPYLENE CONTAINING A MIXTURE OF $C_{60/70}$ FULLERENES
[1*]Dunyamalieva A.I., [1]Kurbanova N.I., [2]Zeynalov E.B. 156

INFLUENCE OF EXCHANGE INTERACTION AND BAND GAP ON THE THERMODYNAMIC PROPERTIES OF DILUTED MAGNETIC SEMICONDUCTOR FILMS
Figarova S.R., [*]Mahmudov M.M., Damirov R.Y. 157

THERMOPOWER IN A SEMICONDUCTOR QUANTUM WELL WITH MODIFIED PÖSCHL-TELLER CONFINING POTENTIAL
*Babayev M.M., Sultanova Kh.B. 158

INTERBAND LIGHT ABSORPTION IN QUANTUM FILM OF $Hg_{1-x}Cd_xTe$
*Ismayilov T.H., Aslanli A.F. 159

DETERMINATION OF BAND GAP OF $(AgSbTe_2)_{0.8}(PbTe)_{0.2}$ FROM ELECTROPHYSICAL AND OPTICAL PROPERTIES
[1,2*]Ragımov S.S., [3]Hashımova N.N. 160

STUDY OF PARTICLE ACCELERATION MECHANISMS IN THE ANISOTROPIC SOLAR WIND
Bashirov M.M. 161

SPATIAL STRUCTURE OF HEPTAPEPTIDE MOLECULE
*Ismailova L., Akhmedov N.A. 162

CONFORMATIONAL PARTICULARITIES OF ANTIBACTERIAL, ANTICANCER AND ANTIOXIDANT CYCLIC DIPEPTIDE CYCLO(D-TYR-D-PHE)
*Agaeva G.A., Agaeva U.T., Godjaev N.M. 163

KINETIC AND THERMODYNAMIC PARAMETERS OF Cl^- TRANSPORT IN PLANT ROOTS DUE TO CHANGES IN TEMPERATURES
*Abdiyev V., Aliyeva N. 165

MOLECULAR MODELING OF ILE-TRP DIPEPTIDE
*Rahimzade S.G., Akverdieva G.A. 166

THE BINDING OF IRON IONS WITH MELANINS OF PLANT ORIGIN
Bagirov R.M. 167

MODIFICATION OF ZINC-ALUMINIUM LAYERED DOUBLE HYDROXIDES WITH FULLERENE AND INVESTIGATION OF PHOTOCATALYTIC ACTIVITY OF OBTAINED NANOCOMPOSITES
*Israfilli T., Balayeva O. 168

INCORPORATED TiO_2 NANOPARTICLES INTO PVC POLYMER FOR ENHANCING THE DIELECTRIC PROPERTIES
Rahimli A.M. 170

MWCNT/CuS NWS BASED MATERIALS FOR PHOTOVOLTAICS
[1]Nuriyeva S.G., [1*]Jafarova S.R., [2]Aguas H. 171

SCHOTTKY DIODES BASED ON CdS SINGLE NANOBELTS
*Mamedov R.K., Aslanova A.R. 172

OPTICAL ABSORPTION AND PHOTOCONDUCTIVITY IN $Cu3In5S9$ SINGLE CRYSTAL
*Jahangirova S. A., Hasanova L.H., Mahammadov A.Z. 173

ACOUSTIC CHARACTERIZATION OF PHONEMES WITH COMPACT/ DIFFUSE FORMANT STRUCTURE AS A MEANS OF IDENTIFICATION IN PHONOSCOPIC RESEARCH
[1*]Aliyev L.P., [2]Gaziyeva N.G. 174

STRUCTURE AND PROPERTIES OF PVDF/ZnO-BASED NANOCOMPOSITES
Hacıyeva F.V., *Mehdiyeva S.Z., Eyvazova G.M. 175

STABILIZATION OF ZnS NANOPARTICLES BASED ON MODIFIED BUTADIENE RUBBER/EXPANDED PERLITE AND CARBON BLACK COMPOSITES: STRUCTURE, OPTICAL AND CONDUCTIVITY PROPERTIES
[1,2*]Edres N., [2]Buniyatzadeh I., [2]Alosmanov R., [2]Eyvazova G., [2]Mammadayarova S. 176

InN NANORIBBON MAGNETIC PROPERTIES
[*]Ismayilova N.A., Jahangirli Z.A. 177

STUDY OF THE SPECTRUM OF NOVA SCO 2023 DURING THE OUTBURST PERIOD
[1]Alisheva K.I., [1]Mikailov Kh. M., [1,2]Rustamov B.N., [1*]Alili A.H. 178

JOINT SURFACE IONIZATION OF CsCl MOLECULES AND Ba ATOMS ON THE SURFACE OF RHENEIUM COVERED WITH A GRAPHITE MONOLAYER
Orujov A.K. 179

ELECTRICAL PROPERTIES OF POROUS-Si/NANO-Cd0.4Zn0.6S HETEROJUNCTIONS
1*Mamedov H.M., 2Shah S.I., 1Mansimova F.B. 180

RAMAN STUDIES ON SI/PS NANOCOMPOSITE
Pashayev B.G., *Surxayli.A.E., Shirinova.H.A..... 181

DESIGN AND DEVELOPMENT OF ADVANCED MULTICOMPONENT BULK METALLIC GLASSY ALLOYS FOR TECHNOLOGICAL APPLICATIONS
[1*] Mekhrabov A.O., [2]Akdeniz M.V. 181

INNOVATIVE APPLICATIONS OF ADVANCED 2D MATERIALS

Bellucci S.

Enrico Fermi Institute of Nuclear Physics, Italy
bellucci@lnf.infn.it

We investigate electronic and plasmonic properties of Silicene nanostrips (SiNSs) with a minimum width of 100 nm using a semi-analytical model using the carrier velocity of silicene. Our results reveal that SiNSs with widths ranging from 100 to 500 nm exhibit small bandgaps, ranging from 30 to 6 meV, respectively. Furthermore, all the nanostrips analyzed in this study exhibit a √q-like plasmon dispersion within the THz regime (≤ 35 THz). By varying the experimental setup or the geometric factors of the nanostrips, the associated plasmon THz frequency can be manipulated, resulting in an increase or decrease in frequency or a shift to larger momentum values. Our study serves as a fundamental starting point and a source of inspiration for future experiments, providing a foundation for confirming the results presented here.

We then present an analysis of the electronic and plasmonic behavior of periodic planar distributions of sufficiently wide graphene nanoribbons, for which a thorough ab initio investigation is practically unfeasible. Our approach is based on a semi-analytical model whose only free parameter is the charge carrier velocity, which we estimate by density-functional theory calculations on graphene. By this approach, we show that the plasmon resonance energies of the scrutinized systems fall in the lower THz band, relevant for optoelectronic and photonic applications. We observe that the energies critically depend on the charge carrier concentration, ribbon width, electron relaxation rate, and in-plane transferred momentum angle, thus suggesting a tunability of the associated light-matter modes.

Several extrinsic conditions (for doped or gated nanoribbon arrays) are simulated to characterize the propagation and interplay of the bulk and edge plasmons, at far infrared to visible energies, and over a broad range of momentum transfers. Particular attention is paid to the interaction or overlap region of the two plasmons, explaining its sensitivity to induced Fermi level shifting, transferred momentum, ribbon type, and geometry, with the inclusion of many-body, GW-like effects. The lower-THz behavior of the bulk plasmon is explored, highlighting the limits of available non–ab initio approaches, suitable for stripes of graphene being tens of nanometers wide. Then, an effective model is derived from the ab initio framework, which reasonably accounts for the two-plasmon response of

the studied, ultranarrow nanoribbon systems, at small momentum transfers.

Lastly, we review the recent result of our group on the effective and efficient removal of cationic pollutants from aqueous solutions using eco-friendly prepared oxidized graphene. This adsorbent material has the advantage of a fast adsorption and keeps a good efficiency over a wide range of initial cationic pollutant concentrations and a broad range of pH values. Thus, we can propose the use of this adsorbent material, as a green adsorbent for wastewater decontamination.

PHYSICS OF DOUBLY HEAVY BARYONS

Aliyev T.
Middle East Technical University, Türkiye
taliev@metu.edu.tr

The study of the properties of doubly heavy baryons represents a promising area in particle physics. It can provide us with information about Cabibbo-Kobayashi-Maskawa (CKM) matrix elements and the low energy dynamics of QCD. They have a very rich phenomenology. The investigation of weak, electromagnetic, and strong decays has a vital importance for understanding the dynamics of doubly heavy baryons. The main ingredients of such studies are the spectroscopic parameters, the strong coupling constants, and the transition form factors. For calculations of these quantities, non-perturbative methods are needed. One of these methods is the QCD sum rules. In the present work, we review our studies on the properties of the doubly heavy baryons within the sum rules method, focusing mainly on the mass and strong coupling constants of the doubly heavy baryons. In addition, the radiative decays of doubly heavy baryons are estimated using the vector dominance model as well as weak radiative decays with FCNC. We also make few remarks on the semileptonic decays of the doubly heavy.

FUNDAMENTAL AND APPLIED PHYSICS WITH REACTOR NEUTRINOS

Yakushev E.
Joint Institute for Nuclear Research, Russia
yakushev@jinr.ru

Neutrinos continue to be a source of scientific discovery in nuclear, particle physics and cosmology. Over the last decades, various experiments based on different approaches and with different neutrino sources have led to two main conclusions: neutrinos have a non-zero mass and there is a significant mixing between individual neutrino mass states. Despite these major breakthroughs, further experimental studies based on new experimental techniques and using unexplored processes are urgently needed to go beyond the Standard Model, which, as we know from cosmology and particle physics, needs to be extended.

The neutrino physics is historically linked with nuclear reactors. It started with confirmation the existence of neutrinos in the reactor based experiment. Nuclear reactors are continued to be most powerful available artificial sources of antineutrinos. Given that neutrinos are only weakly coupled with other particles, a huge reactor antineutrino flux is often the only way to study the properties of neutrinos.

The talk will provide a general overview of some major neutrino experiments at reactors. The focus will be on experiments with the latest types of semiconductor, cryogenic and scintillation detectors. Some recent results obtained at experiments conducted with JINR (Dubna) participation will be discussed. The unprecedented percent level precision of reactor monitoring was achieved with using inverse beta processes induced by reactor antineutrinos. The fundamental task of neutrino detection at reactors is now has the new aim: detection and study of nuclear recoils at the almost zero energy range produced by coherent elastic neutrino nucleus scattering. The aim is in search for New physics at the highest precision.

COMPARATIVE ANALYSIS OF MEMBRANE PROPERTIES OF HUMAN LUNG CARCINOMA AND NORMAL CELLS: RELEVANCE FOR DRUG DELIVERY

[1*]Gasymov O.K., [2]Aliyev J.A.

[1]Institute of Biophysics, Ministry of Science and Education, Azerbaijan
[2]National Center of Oncology, Ministry of Health, Azerbaijan,
oktaygasimov@gmail.com

Cancer is the most challenging health problem, accounting for approximately 17% of deaths worldwide. The cancer cells in the disease progression develop new properties, like escaping apoptosis, continuous growth signals, tissue invasion, uncontrolled proliferation. Highly efficient methods, such as targeted drug therapy, still are not an option for widespread applications. Therefore, there is a need to improve the effectiveness of commonly used treatment options (radiation therapy, chemotherapy, and their combination). Lung cancer, particularly adenocarcinoma, is the most common type of cancer. The goal of the study is to reveal possible methodologies for more efficient conditions for chemotherapy attributable to the membrane properties. To resolve this aim, we studied and compared some membrane properties of human lung carcinoma and normal cells, such as membrane partitioning for relevant small molecules, membrane dynamics (fluidity), and interaction of the anti-cancer peptide and its lipopeptide analog (EQRPR and C16-EQRPR). Changes in lipid composition observed in cancer cells may influence its properties, like partitioning for small molecules and membrane dynamics. Partitioning of the spin probe 2,2,6,6 tetramethylpiperidine-1-oxyl (TEMPO) into the membranes of human lung normal and carcinoma cells was assessed by EPR spectroscopy to estimate the impact of the lipid compositions. Results indicate that compared to the healthy cells TEMPO incorporates into membranes of cancer cell more readily. Free energy changes for the transfer of TEMPO from the aqueous phase to the membranes in healthy and cancer cells are 3.1 ± 0.1 kcal/mol and 1.2 ± 0.1 kcal/mol, respectively.

The membrane surface probe C12SL (spin-labeled analog of lauric acid) indicates that the increased membrane dynamics in cancer cells could be a possible mechanism of enhanced partitioning of TEMPO. 5-doxyl stearic acid incorporated into the membrane of the human lung carcinoma and healthy cells reveals the existence of two lipid domains with distinct dynamics. The healthy cell membranes are characterized by rotational correlation times of 16.8 ns and 3.7 ns. In contrast, carcinoma cells show correlation times of 8.0 ns and 2.4 ns. Temperature and pH dependence of the dynamic parameters of the membranes of healthy and carcinoma cells can be used to identify the most efficient condition for drug delivery.

MAGNETOHYDRODYNAMIC KELVIN-HELMHOLTZ INSTABILITIES OF SUPERSONIC SHEAR LAYERS WITH FINITE INTERFACE THICKNESS AND HEAT FLUX IN ANISOTROPIC SPACE PLASMAS

[1*]Dzhalilov N.S., [2]Ismayilli R.

[1]Shamakhy Astrophysical Observatory named after N. Tusi, Azerbaijan
[2]Center for Mathematical Plasma-Astrophysics, Belgium
dnamig@gmail.com

The linear magnetohydrodynamic Kelvin-Helmholtz instability (KHI) in an anisotropic plasma is studied. The governing equations obtained as the 16 moments of Boltzmann-Vlasov kinetic equations, including the heat flow, are applied. In the case of tangential discontinuity between the supersonic flows along the magnetic field, the calculated growth rates as functions of the anisotropic plasma properties allow us to conclude that quasi-transverse modes grow faster. Then, dispersion equations for the KHI of quasi-transverse modes are derived, considering the finite width of the transition zone with different velocity profiles. For these modes, when the role of heat flow is not important, the plasma parameters are controlled so that the fundamental plasma instabilities (firehose and mirror) do not affect the KHI. The problem is solved analytically, which will be helpful in verifying numerical simulations. In contrast to the tangential discontinuity, the finite width of the transition layer confines KHI excitation as the wavenumber increases. In the general case of oblique propagation (when heat flux complicates the problem), the boundary value problem is solved to determine the spectral eigenvalues. In particular, it is observed that the fundamental plasma instabilities that arise in the transition zone between flows with a finite width can modify and considerably enhance the KHI.

THERMODYNAMIC SIGNATURES AND PHASE TRANSITIONS IN HIGH-ENERGY HADRONIC AND NUCLEAR COLLISIONS

[1*]Ajaz M., [2]Waqas M., [3]Alrebdi H.I., [1]Badshah M.

[1]Abdul Wali Khan University Mardan, Pakistan

[2]Hubei University of Automotive Technology, People's Republic of China

[3]Princess Nourah bint Abdulrahman University, Saudi Arabia

ajaz@awkum.edu.pk

Facilities like the Relativistic Heavy Ion Collider (RHIC) and the Large Hadron Collider (LHC) have multiple scientific objectives. One of these aims is to generate Quark-Gluon Plasma (QGP), a state of matter thought to mimic conditions just after the Big Bang. While high-energy heavy-ion collisions are a primary method for creating QGP, proton-proton collisions also offer valuable insights. These collisions serve as a reference point for heavy-ion studies and also help explore systems at the highest energy levels we can currently achieve.

In our research, we aim to understand specific changes in the momentum distributions of charged hadrons. We focus on variables such as the multiplicity and centrality of charged particles, and the energy involved in different types of collisions: proton-proton, proton-nucleus, and nucleus-nucleus.

To achieve this, we employ various statistical distribution functions. These functions effectively parameterize the pT spectra of hadrons, which are crucial for understanding the bulk properties of nuclear matter. The parameters we examine include temperature (T), a non-extensivity factor (q), thermal flow velocity (β), and a fitting constant related to the system volume.

Our data analysis strategy involves using simultaneous minimum chi-square fits. This method will help us extract essential parameters for understanding the different phases of nuclear matter, and it allows us to account for deviations from the traditional Boltzmann–Gibbs exponential distribution.

TRAVELLING OF SINE-GORDON SOLITONS IN NETWORK OF JOSEPHSON JUNCTION ARRAYS

[1,3*]Askerzade I.N., [2]Matrasulov D., [1]Salati M.

[1]Ankara University, Türkiye
[2]Turin Polytechnic University in Tashkent, Uzbekistan
[3]Institute of Physics, Ministry of Science and Education, Azerbaijan
imasker@eng.ankara.edu.tr

In this study we present soliton dynamics in Josephson junction array networks driven by external time-periodic field. The whole is modelled in terms of modified sine-Gordon equation containing time-periodic potential. By solving sine-Gordon equation numerically we explored soliton dynamics on each branch and transmission of sine-Gordon solitons through the junction's branching point. Driven, or modified sine-Gordon equation on a real line can be written as

$$\partial_t^2\psi(x,t) - \partial_x^2\psi(x,t) + \sin[\psi(x,t)] = \gamma + \lambda\partial_t\psi(x,t) + f\cos(\omega t),$$

where γ, f, ω are constants. Eq. described phase difference in a Josephson junction driven by external time-periodic (e.g., AC) field. Unlike to standard (integrable) sine-Gordon equation, it does not approve analytical soliton solutions. Therefore, one needs to solve it numerically. Current-voltage characteristics of the device is plotted using the obtained solution of the sine-Gordon equation.

EXTENDED LINEAR-SIGMA MODEL: MASS SPECTRUM OF CHARMED MESONS

[1*]Tawfik A., [2]Ahmadov A.

[1]Future University in Egypt
[2]Baku State University, Azerbaijan
ahmadovazar@yahoo.com

We derive analytical expressions for the masses of scalar, pseudoscalar, vector and axial-vector meson states. The effective Lagrangian in which four quark flavors (up, down, strange and charm) and scalar and pseudoscalar meson fields are integrated is constructed in the extended linear-sigma model (eLSM). The various eLSM parameters are determined, analytically and estimated, numerically. This allows for a precise calculation of the masses of twenty-nine meson state (sixteen non-charmed and thirteen charmed). Out calculations are compared the recent compilation of the particle data group

(PDG). We conclude that the eLSM calculations are in excellent agreement with the PDG. This suggests that the eLSM with its parameters is a suitable theoretical approach to determine the mass spectra of the various non-charmed and charmed meson states, especially at vanishing temperature.

THE SEARCH FOR A RARE PROCESS FOR HIGGS BOSON PRODUCTION BY APPLYING A NEW EVOLUTIONARY ALGORITHM WHICH CONSTRUCT A OPTIMIZED NEURAL NETWORK IN AN IRREGULAR HYPERPARAMETER SPACE

[1,2*]Huseynov N.A., [2]Boyko I.R., [2]Yeletskikh I.V., [2]Didenko A.R., [2]Koval O.A.

[1]Institute of Physics, Ministry of Science and Education, Azerbaijan
[2]Joint Institute for Nuclear Research (Dubna), Russia
nguseynov@jinr.ru

The Yukawa coupling of the Higgs boson to the top quark is a key parameter of the Standard Model (SM). It can be determined from the ratio of the top quark mass and Higgs field vacuumexpectation value, from the cross section of $gg \to H$ production through a top quark loop, from the cross sections of the processes $gg/qq \to ttH$, or from the cross sections of the processes $gq \to t(t)Hq$, which is a tree-level process at lowest order in perturbation theory. Comparison of these measurements has the potential to identify and disambiguate new physics effects that can modify the tHq production cross section relative to the SM expectation.

GEOGRAPHY OF OBSERVATION OF THE OWN REFLECTED RADIATION

Rustamov R.B.

Institute of Physics, Ministry of Science and Education, Azerbaijan
r_rustamov@hotmail.com

This is important to point out challenges of space science and technology developments in a former Soviet Union period. The number of sophisticated circumstances were the reason of complications of engagement of Republics into space technology applications.

It has been held the 24th IAC in 1973 in Baku capital of Azerbaijan. The Congress 1973 has created an excellent environment on establishment of entity related to the space science and technology activities.

There is no doubt that thanks to great efforts of the National Leader H. Aliyev Azerbaijan has become the World space science and technology family member.

Taking into account of the capacity of country it has been decided engagement of Azerbaijan for Earth study by use of advances of space technology.

This paper describes history of development of space technology in Azerbaijan as the country involved space technology as the pioneer in the region. It is considered obstacles and complications of space technology in the country when Azerbaijan was one of the parts of the former Soviet Union. There is no doubt that it was not easy to be engage into high technology application for countries of soviet empire where all significant issues were strongly under control of the soviet authority.

Today is important to point out how Azerbaijan could come to be member of space technology being part of the former Soviet Union. It is important what required circumstances have been impacted for space technology application in Azerbaijan.

This paper considers steps of achievements of space technology organization of Azerbaijan and development of the main space Agency of Azercosmos. For the time being activities of Azercosmos are carried out in five main directions supporting the socio-economic development of Azerbaijan;

- supporting national security;
- expanding commercial activities;
- supporting space R&D activities.

and representing the country in the international space arena.

EXPLORING THE CROSS SECTIONS OF DIRECT REACTIONS IN THE SU(5) REPRESENTATION

[1*]Abdulvahabova S.G., [2]Afandiyeva I.G., [2]Ahmedov R.A.

[1]Baku State University, Azerbaijan
[2]Azerbaijan State University of Oil and Industry, Azerbaijan
sajida.gafar@gmail.com

On the based SU(5) subgroup cross sections of direct reactions and characteristics 0^+ excited levels: probabilities multipole transitions were studied. This study demonstrated the sensitivity of transition probabilities to nuclear structure. The nature of 0^+ excited states is very complex; on

the one hand, they can be multiphonon, quasiparticle-phonon, and mixed residual states. It has been shown that in direct reactions 0^+ levels will be more strongly excited in deformed nuclei. This leads to the conclusion about the important role of the quadrupole-quadrupole interaction - this is the part of the interaction that is not reduced to the mean field. It is proposed to describe the collective vibrational degree of freedom by an algebra SU(5), which is formed by five components.

For a multipole transition, an expression is obtained for the cross section (p,t) of the direct reaction and the matrix element. The energy region under consideration lies below the meson production threshold and the momentum approximation is used. It is assumed that the amplitude of the interaction of nucleons of the incident nucleus with nucleons of the target nucleus is the same as in the case of collisionless nucleons.

The algebraic properties of collective variable lead to a quantum member, which implies in the boson representation the maximum number of phonons contained in the collective states. The proposed approach is applied to the transitional nuclei where the constants are determined by fitting the experimental spectra, the relative E2 transition probabilities and the cross section for the (p,t) transitions to the ground and excited 0^+ states. The proposed approach is applied to the ^{154}Sm, ^{156}Sm and ^{154}Gd transition nuclei, where the constants are determined by fitting the experimental spectra. Analise shows the relative transition probabilities E2 and cross sections for (p,t) transitions to the 0^+ ground state. The agreement between the experimental data and the theoretical description is good.

We expect on a qualitative basis that the application of subgroup SU(5) will open up new physical possibilities for the study of collective movements of the nucleus.

SEARCH FOR THE EXPERIMENTAL SIGNATURE OF THE STRINGS AT THE LHC

Suleymanov M.K.
Baku State University, Azerbaijan
mais.suleymanov@bsu.edu.az

This report reviews the results published by the author. It addresses experimental data from LHC experiments concerning the p_T distributions of particles in pp and Pb-Pb collisions, highlighting several p_T regions with distinct properties. These regions are characterized by the correlation length L_K^c and two fitting parameters, a_K^c and b_K^c, derived from exponential fitting. Notably, the upper

indices c indicates the event type, while the lower indices K denote the region number.

For nucleus-nucleus collisions, it was observed that the values of a_K^c and b_K^c. are highly dependent on the collision characteristics (medium effect) in the region of $p_T < 4 - 6\ GeV/c$ (Region I). These dependencies diminish in the second region, where $4 - 6\ GeV/c < p_T < 17 - 20\ GeV/c$, and nearly disappear in Region III, where $p_T > 17 - 20\ GeV/c$, except for centrality dependencies for the parameter a_K^c.

In central collisions, the ratio of a_K^c values for Pb-Pb to those for pp collisions, multiplied by the average number of participating nucleons, shows a minimum in the second region and becomes less than 1 for the most central events, indicating suppression.

The correlation lengths L_K^c increase with p_T, with the following ratios observed:

$$L_{III}^c : L_{II}^c \cong 5\ ;\ L_{II}^c : L_I^c \cong 3\ (\mathrm{Pb-Pb});$$
$$L_{III}^1 : L_{II}^1 \cong 5\ ;\ L_{II}^1 : L_I^1 \cong 5\ (\mathrm{pp})$$

The study found that the ratio of correlation lengths for η-mesons to π0-mesons produced in pp collisions at 8 TeV is approximately equal to the ratio of their masses (m_η to $m_{\pi 0}$, respectively): $< L_\eta > : < L_{\pi 0} > \cong m_\eta : m_{\pi 0}$. If the lengths L_K^c values are directly proportional to string tension, this result could be a compelling indicator of parton/string fragmentation dynamics. This explanation is proposed because, in string theory, the masses of elementary particles and their energies are determined by the intensity of string vibrations and the strangeness of string stretch, which are influenced by string tension.

Employing the expression $\alpha_S \cong \left[ln\left(q^2/\Lambda^2\right)\right]^{-1}$ (with Λ = 0.2 GeV/c), we find that $\alpha_S \cong 1$ for Region I, ~ 0.25 for Region II, and ~ 0.13 for Region III. The increase of α_S with decreasing p_T mirrors the QCD quark string relationship: $\frac{1}{r^2} \sim Q^2 = -q^2$, where r is the distance between quarks in a string. This result, coupled with the aforementioned ratio of lengths, suggests that fragmentation and hadronization of partons occur through string dynamics, with L_K^c values linked to string tension. We may conclude that the discerned p_T regions at LHC energies signify parton fragmentation and hadronization via parton strings: Region III is the domain of first-generation parton/string creation during collisions, producing the most energetic hadrons/partons/strings with the highest tension and minimal medium modification; Region II is characterized by the highest density of strings that have decayed from those in Region III.

The high density in Region II leads to string fusion and a collective phenomenon, resulting from new string formation in the most central Pb-Pb interactions. This may explain the anomalous behavior of the Nuclear Modification Factor in this region; Region I exhibits the maximum number of hadrons and a minimum number of strings.

FREQUENCY OF TRANSVERSE AND LONGITUDINAL THERMOMAGNETIC WAVES IN CERTAIN ANISOTROPIC CONDUCTING MEDIA

*Maharramova A.A., Hasanov E.R.
Baku State University, Azerbaijan
meherremovaaysel400@gmail.com

Theoretical and experimental study of physical phenomena in solids makes it possible to reveal the crystallographic internal structure and conductive properties of solids. The study of the physical properties of solids located in external electric and magnetic fields is based on the physical phenomena occurring in them. If a solid body is subject to a temperature gradient, in addition to an external electric and magnetic field, then a number of physical phenomena occur inside the solid body, which are called thermomagnetic phenomena. Many effects occur in solids if the magnetic field is perpendicular to both the electric field and the temperature gradient. The energy distribution of charge carriers in solids and their motion under the conditions of classical or wave mechanics do not always make it possible to compare theoretical studies of thermomagnetic effects with experimental values.

It mainly consists of studying the Nernst-Ettingshausen effect: If there is $\nabla_x T$ a temperature gradient in semiconductors and H_z a magnetic field acts on it $H_z \perp \nabla_x T$, an electric field E_y is created.

Experience shows that the magnitude of the effect varies in different semiconductors; on metals, and the scratch-free effect disappears. This makes a lot of sense in the case of cracks in semiconductors.

Basic equations of the problem. The total electric field in an isotropic solid has the form

$$\vec{E} = \varsigma\vec{j} + \varsigma'\left[\vec{j}\vec{H}\right] + \varsigma''\left(\vec{j}\vec{H}\right)\vec{H} + \Upsilon\frac{\partial T}{\partial x} + \Upsilon'\left[\vec{\nabla}T\vec{H}\right] + \Upsilon'\left(\vec{\nabla}T\vec{H}\right)\vec{H}. \qquad (1)$$

In anisotropic conducting media, all coefficients in equation (1) are tensors.

Then the equations for anisotropic conducting media will have the form:

$$\vec{E}_i = \varsigma_{ik}\vec{j}_k + \varsigma'_{ik}\left[\vec{j}\vec{H}\right]_k + \varsigma''_{ik}\left(\vec{j}\vec{H}\right)\vec{H}_k + \Upsilon_{ik}\frac{\partial T}{\partial x} + \Upsilon'_{ik}\left[\vec{\nabla}T\vec{H}\right]_k + \Upsilon'_{ik}\left(\vec{\nabla}T\vec{H}\right)\vec{H}_k, \qquad (2)$$

Υ_{ik} is the differential thermopower, and Υ'_{ik} is the Nernst-Ettinizhausen coefficients.

When $\vec{H}_0 = 0$ in the equations, the terms containing $\varsigma_{ik}, \varsigma''_{ik}, Y''_{ik}$, are equal to zero. Or

$$\omega = \omega_0 + i\gamma,\ \omega_0 = (\omega_{12}/4\varsigma)^{1/2},\ \gamma = (\omega_{12}/4\varsigma)^{1/2}. \quad (3)$$

For any orientation of the wave vector relative to the temperature gradient, the frequency and increment of excited thermomagnetic waves are the same

With longitudinal $\vec{k}||\vec{\nabla}T$ and transverse $\vec{k} \perp \vec{\nabla}T$ orientation of the wave vector relative to the temperature gradient, waves of a thermomagnetic nature are excited with different frequencies and increments.

SPECTRAL INVESTIGATIONS OF THE ALGOL-TYPE BINARY STAR U SAGITTAE

[1,2]Rustamov B.N., [1]Mikailov Kh.M., [1]Alisheva K.I., [2]Mammadova S.O., [2*]Aliyeva V.I.

[1]Baku State University, Azerbaijan

[2]Shamakhy Astrophysical Observatory named after N. Tusi, Azerbaijan

vusala.elizade@mail.ru

The results of spectral observations of the Algol-type binary star U Sagittae (U Sge) are presented. Spectral observations of the star U Sge were carried out at the Cassegrain focus of the 2-meter telescope of the Shamakhy Astrophysical Observatory named after N.Tusi, on the fiber echelle spectrograph ShaFES (Shamakhy Fiber Echelle Spectrograph), using a CCD matrix, with a spectral resolution R = 28000, in the wavelength region λλ 3900–7500 Å, in the years 2022-2023. The behavior of profiles: hydrogen lines of the Balmer series (Hα - Hδ), HeI 5876Å, as well as lines of resonance doublets - DNaI and KCaII, during the orbital period of the eclipsing binary system U Sge, is described. Radial velocities of the hydrogen lines (Hα - Hδ) and HeI 5876Å were measured. These lines are related to the main component of the U Sge binary system. Based on these measurements, radial velocity curves of the main component of the U Sge system were constructed. Orbital phases were calculated based on the ephemeris:

JD [primary minimum] = 2442207.8444 + 3.3806205E borrowed from [Tomkin J., 1978, Ap. J., 221, 608]. In Fig.1, the radial velocity curves of the primary and secondary components of the U Sge binary system are shown (see figure captions). At an orbital period, value of about 0.8 in the blue or about 0.3 in the red part of the line profiles, Hα in the spectrum of the U Sge system, absorption details appear. A similar picture was previously identified by us for the Algol-type binary star δ Lib. We preliminarily assume that this observational fact may indicate the presence of a third component in the system, and it is not excluded that this effect is related to

the so-called McLaughlin-Rossiter effect, which is observed in Algol-type binary systems.

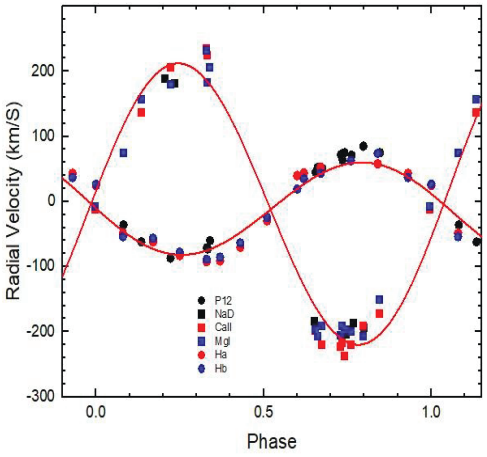

Fig. 1. Velocity curves for the primary and secondary components of the U Sge Algol type binary system. Primary component – full circles: dark – P_{12} (Tomkin J., 1978, Ap. J., 221, 608); red – Hα (this paper); blue – Hβ (this paper). Secondary component (Tomkin J., 1978, Ap. J., 221, 608) – full rectangles: dark – DNaI; red – CaII; blue – MgI.

AXIAL-VECTOR CHARGE RADIUS OF NUCLEONS IN THE SOFT-WALL MODEL OF HOLOGRAPHIC QCD AT FINITE TEMPERATURE

[1*]Nasibova N., [2]Mamedov Sh.

[1]Institute of Physics, Ministry of Science and Education, Azerbaijan
[2]Baku State University, Azerbaijan
n.nesibli88@gmail.com, sh.mamedov62@gmail.com

We investigate the dependence of the axial-vector transition form factor and charge radius of the nucleons on the temperature of the medium, using the AdS/QCD soft-wall model which is based on AdS/CFT duality. The dependencies of the axial-vector transition form factor and charge radius of nucleons on the square of the momentum transfer and the temperature are plotted. We observe that the value of the axial-vector transition form factor and the charge of nucleons radius decreases with increasing temperature.

Axial-vector transition form factor and charge radius at finite temperature. To obtain the axial vector radius of the nucleon, we obtained the axial vector transition form factor of nucleons at finite temperature. Using the relationship between the left and right profile functions of the

nucleons in the ground state, the axial-vector form factor should be obtained from the axial vector current of the nucleons. Then the axial vector radius of the nucleon at finite temperature is found by deriving the normalized axial vector form factor. Axial vector radius of nucleon at finite temperature has the following form [3]:

$$r_A^2(T) = -\frac{-6dG_A(Q^2,T)}{G_A(Q^2,0)\mathrm{d}Q^2}. \quad (1)$$

By using the Lagrangian terms for the interaction between axial-vector mesons and nucleons in general action it can be obtain $G_{AT}^{(i)}(Q,T)$ axial vector transition terms. We obtain the $G_{AT}^{(i)}(Q^2,T)$, which is the sum of the contributions of the minimal, magnetic type and Yukawa interaction of the transition axial form-factor of nucleons.

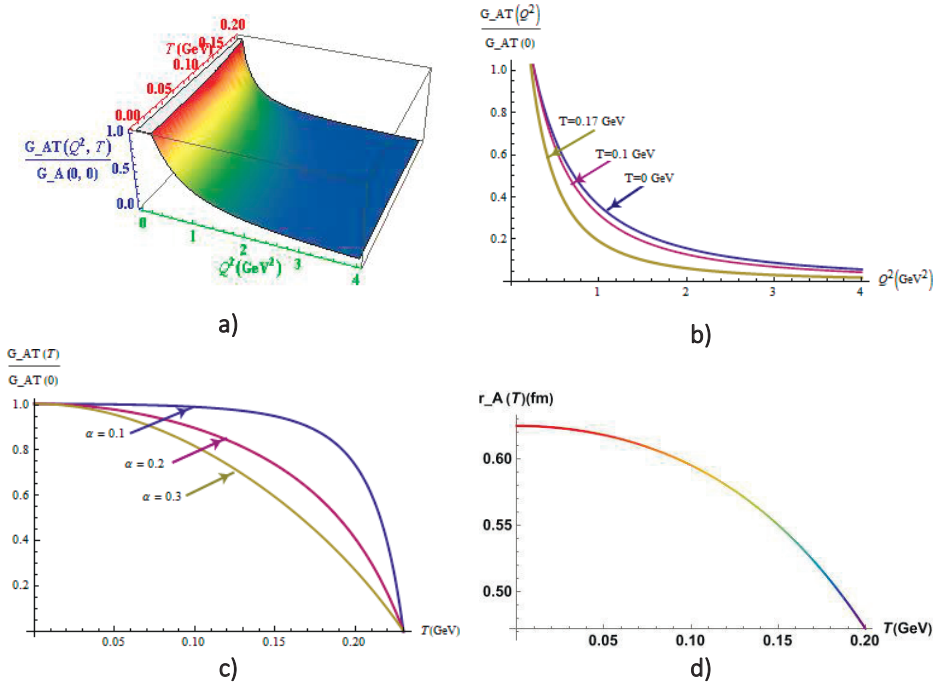

Fig. 1. a) The temperature dependencies of form factor and charge radius.

Numerical analysis shows that the axial vector transition form factor and radius of nucleon decreases on increasing temperature. This means in a hot medium, the β decay has less probability. This result may be used in neutrino experiments. Our result for the nucleon radius (0.626) is consistent with the experimental value (0.67) and other models' results (0.647).

METALLICITY OF THE STAR HR 4294(A5III)

[1,2]Samedov Z.A., [1]Rajabova S.Sh., [2]Rustem U.R., [2*]Hajiyeva G.M.

[1]Baku State University, Azerbaijan

[2]Shamakhy Astrophysical Observatory named after N. Tusi, Azerbaijan

zahir.01@mail.ru

The atmosphere of star HR 4294 (A5III) is investigated by the method of atmospheric model. Effective temperature and surface of gravity, microturbulence, and metallicity are determined. Knowing the effective temperature and surface of gravity the models of stellar atmospheres are calculated, and on the basis of these models, the evolutionary parameters of stars: masses, radii, luminosities, and ages are calculated. In astrophysics, microturbulence is considered a mechanism for the broadening of the spectral line. The equivalent width of the spectral line depends on microturbulence and to determine the chemical composition, it is necessary to know the microturbulent velocity. Therefore, it is necessary to know the microturbulent velocity in determining the chemical composition of stars. Metallicity is one of the main fundamental parameters of stars. According to the definition of this parameter, it is determined that the star and the Sun are formed from the same or different metallicity matter, the problem of the correctness of the provisions of the modern theory of chemical evolution of stars is solved.

The effective temperature of star HR 4294(A5III) T_{eff}=8300±100K and the surface of gravity logg=4.0±0.1 were determined based on a comparison of the observed and theoretically calculated values of the photometric quantities [c_1], Q, β, and the use of parallax method. The determination of the microturbulent velocity by the model method is based on the study of equivalent widths in a wide range of spectral lines of FeII of star HR 4294(A5III) and the iron abundance is determined: ξ_t=2.2±0.1км/s, logε(Fe)= 7.40±0.12. The metallicity was determined in the atmosphere of the star HR 4294(A5III): [Fe/H]= -0.07. As is shown the metallicity of the studied stars and the Sun is practically the same. This result is important for making corrections in the chemical evolution models of the Galaxy.

INVESTIGATING THE STRUCTURAL AND OPTICAL PROPERTIES OF $Cu_xCo_{3-x}O_4$ NANOPARTICLES SYNTHESIZED BY SONOCHEMICAL METHOD

*Mammadyarova S.J., Muradov M.B., Eyvazova G.M., Balayeva O.O.
Baku State University, Azerbaijan
sevinc.memmedyarova@inbox.ru

Among transition metal oxides, cobalt oxide nanoparticles (Co_3O_4 NPs) have gained much attention due to their uncommon physical and chemical properties. They are widely used as a gas sensor, pH sensor, catalyst, anode material in Li-ion rechargeable batteries, supercapacitors, electrochemical sensors, photocatalyst, solar absorbing and electrochromic material. It is reported that the incorporation of metal dopants is an effective method for improving the properties of oxide NPs such as electrical conductivity and catalytic activity. Up to date, several metals were used to modify the Co_3O_4 NPs including Fe, Mn, Cu, Ni, Cr, Mo, Ag, Pd, Au and etc. In the present study, $Cu_xCo_{3-x}O_4$ (x=0, 0.02, 0.04, 0.06, 0.1) NPs have been synthesized by the sonochemical method and subsequent calcination at different high temperatures (500°C and 600°C). The purpose of choosing copper in our work is that the ionic radius of Cu^{2+} (0.71 Å) is near to the ionic radius of Co^{2+} (0.72 Å) and therefore Cu^{2+} ions can easily enter into the Co_3O_4 matrix. The synthesized NPs were further characterized using X-ray diffraction, UV-vis spectroscopy, FTIR spectroscopy, Raman spectroscopy and transmission electron microscopy. According to the XRD results, the size of Co_3O_4 NPs exhibits irregular changes as the concentration of Cu increases. No peaks associated with copper or copper oxide phases were observed in the diffractograms of doped samples and it indicates that Cu is successfully substituted in the Co_3O_4 lattice. The band gap value of undoped Co_3O_4 NPs annealed at 500°C initially rises from 1.58 eV and 3.33 eV to 1.70 eV and 3.43 eV with a 2% Cu doping content, but subsequently decreases with higher Cu content. The increase in the band gap of $Cu_{0.02}Co_{2.98}O_4$ NPs can be attributed to the Moss-Burstein effect and the decrease of band gap at higher dopant concentrations can be explained with crystal defect. For samples annealed at 600°C, the band gap value increases with decreasing of nanoparticle size according to quantum size confinement. Based on the TEM measurements, $Cu_{0.1}Co_{2.9}O_4$ NPs annealed at 500°C exhibit spherical-like, hexagonal-like, rhombohedral-like and irregularly structured morphology and the size of NPs is in the range

of 15.78 nm-78.31 nm. The characteristic peaks appeared at 662 cm^{-1} and 572 cm^{-1} in the FTIR spectra of $Cu_{0.1}Co_{2.9}O_4$ NPs annealed at 500°C. So, this result confirms the formation of Co_3O_4 with spinel structure. The absence of a peak related to Cu-O bond in the spectrum of Cu-doped Co_3O_4 NPs can be explained by the overlapping of Cu-O peak with Co-O peak because their vibration wavelengths are very close. Three peaks at 184, 464 and 666 cm^{-1} were observed in the Raman spectra of undoped Co_3O_4 NPs annealed at 500°C and these peaks are attributed to the F_{2g}, E_g and A_{1g} modes, respectively. The strong band at 666 cm^{-1} (A_{1g} mode) is assigned to the characteristics of the octahedral sites, while F_{2g} and E_g modes are correspond to the combined vibrations of the tetrahedral site and octahedral oxygen motions. The Raman peaks at 513.19 and 675.68 cm^{-1} were observed for $Cu_{0.02}Co_{2.98}O_4$ NPs and the Raman peaks at 512.13 and 674.66 cm^{-1} were observed for $Cu_{0.1}Co_{2.9}O_4$ NPs. A slight shift of the peak observed at A_{1g} mode to higher wavenumbers occurred after doping.

DOUBLE QUADRATIC PHOTODETECTION BASED GAAS/ALGAAS STEPPED QUANTUM WELL IN A TERAHERTZ AND FAR INFRARED RANGE

[1*]Salhi W., [1]Rajira A., [1]Samyh A., [2]Akabli H., [1]Abounadi A., [1]Almaggoussi A.
[1]Cadi Ayyad University, Morocco
[2]Hassan first University, Morocco
salhiwafaa95@gmail.com

We have calculated the electronic states for the GaAs/AlGaAs stepped quantum well. The results show a singular behavior of a confined energy versus the step widthL_{w2}. As a consequence, there is at least, one crossing between two different transitions that occurs for many geometries, which may enhance the optical absorption in unipolar optoelectronic devices. We have, then, evaluated the response to a electromagnetic radiation, of a structure where a double two photon absorption (TPA) may occur in the THz/FIR domain, through the calculation of a intersubband absorption coefficient.

The first TPA corresponds to the E_{12} and E_{24}transitions crossing at 70meV (17THz) and the second to the crossing of E_{23} and E_{34} transitions at 35meV (8.5THz).

DLTS SPECTROSCOPY OF RADIATION DEFECTS IN SILICON WITH PLATINUM IMPURITY

Utamuradova Sh., *Rakhmanov D.
National University of Uzbekistan, Uzbekistan
dilmurod-1991@bk.ru

It is known that complex formation processes in irradiated semiconductors are determined by the concentration ratios of certain defects, their charge state and the defect structure of the crystal as a whole. Parameters of semiconductor devices, such as speed, forward voltages and reverse currents, quantum efficiency of LEDs and lasers, and gain of transistors are highly dependent on the presence of deep-level impurities (DL). The purpose of this work is to study radiation defect formation in single-crystal n-Si<Pt> using DLTS spectroscopy.

The objects under study were n-type silicon wafers measuring 1.5 x 6 x 13 mm with a resistivity of 40 Ohm cm (KEF-40). The wafers were cut from silicon ingots grown using the Czochralski method. Doping of silicon with platinum was carried out by the diffusion method from a layer of metal platinum deposited on the silicon surface in evacuated quartz ampoules at a temperature of 1200 °C for 2 hours.

The diffusion introduction of platinum atoms into n-Si leads to the formation of two deep levels in the upper half of the n-Si<Pt> band gap: Ec-0.20 eV and Ec-0.25 eV (see Fig. 1).

Analysis of the measured DLTS spectra in doped and control samples showed that only one level, Ec-0.25 eV, is associated with platinum atoms in silicon, and the efficiency of the formation of this deep level depends on the technological modes of introducing Pt into n-Si - temperature and diffusion time. The level of Ec-0.20 eV is also observed in the control heat-treated (without Pt) samples, but its concentration is half an order of magnitude higher than in the doped samples (Fig. 1, curve 2).

From a comparison of the measured DLTS spectra it follows that as a result of irradiation both in the control n-Si samples (Fig. 2, curve 3) and in the n-Si<Pt> samples (Fig. 2, curve 4), new levels with ionization energies Ec-0.17 eV and Ec-0.43 eV. The values of the parameters of this deep level refer to known radiation defects - vacancy-oxygen complexes (A-centers) and vacancy-phosphorus complexes (E-centers).

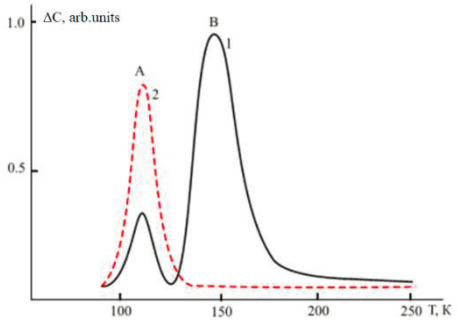

Fig. 1. Typical DLTS spectra of unirradiated n-Si<Pt> samples (curve 1, peaks A and B), control n-Si (curve 2, peak A).

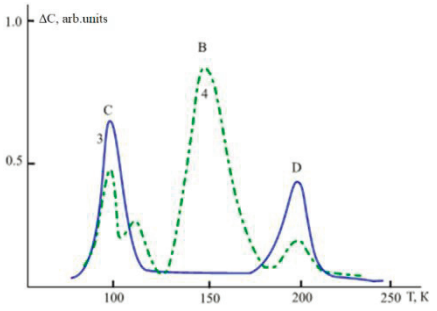

Fig. 2. Typical DLTS spectra of irradiated n-Si (curve 3, peaks C and D) and n-Si<Pt> (curve 4, peaks A, B, C and D).

From the results obtained it follows that the presence of platinum impurities in the silicon lattice leads to a slowdown in the formation of radiation defects: the concentrations of A- and E-centers in n-Si<Pt> samples are 2-3 times lower than in control samples. Moreover, the higher the concentration of platinum, the lower the concentration of radiation defects.

TWO-DIMENSIONAL ENERGY STRUCTURE OF SCHOTTKY DIODES

*Mamedov R.K., Aslanova A.R.
Baku State University, Azerbaijan
rasimaz50@yahoo.com

Metal-semiconductor contacts (MSC), which have rectifying and ohmic properties, are important physical elements of simple and complex discrete semiconductor devices and integrated circuits of modern electronic devices. Electronic processes occurring in ideal MSCs with an unlimited homogeneous contact surface (interface) are well described by the fundamental one-dimensional energy structure developed by Schottky. The results of numerous experimental studies show that some features of the electrophysical properties of real rectifying MSCs with a limited contact surface (Schottky diodes (SD), created on the basis of various contacting metals and semiconductors are difficult to add up within the Schottky model. In particular, the dependence of the potential barrier height on the applied voltage of real SD turns out to be stronger than it follows from the Schottky model, i.e. the ideality factor of the current-voltage characteristics of real SD is much greater than unity.

Recently, the establishment of the phenomenon of the appearance of an additional electric field (AEF) in the edge region of the limited contact surface of real SDs shows that complex electronic processes occurring in them can be described by a two-dimensional energy structure. This report presents the features of our developed two-dimensional energy structure of the SD with the corresponding parameters, schematically shown in Fig. 1.

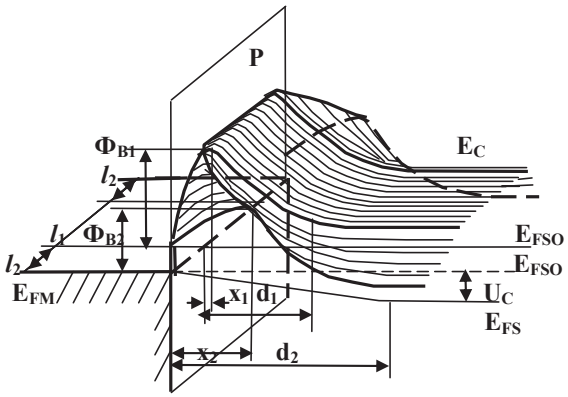

Fig. 1. Schematic two-dimensional energy structure of real SD

AEF in the SD, which arises due to the potential difference between the interface surface and the adjacent free surfaces of the semiconductor and metal, exists in almost all real MSCs. The AEF tension is directed from the edge part of the contact surface of the metal to the free surfaces of the contacting materials. The general contact surface of the SD consists of an inner part with a high potential barrier height Φ_{B1} and an edge part with a low potential barrier height Φ_{B2}, where $\Phi_{B1} > \Phi_{B2}$. The potential barrier has a maximum value of Φ_{B1} at a distance x_1 from the interface in the inner part of the contact and decreases along the direction to the periphery in the edge part of the contact to a minimum value of Φ_{B2} at a distance x_2 from the interface. Under the influence of the AEF a redistribution of charge carriers occurs in the peripheral contact area and a voltage drop ($-U_C$) occurs.

SELF-POWERED TRANSMISSION LINE MONITORING SENSORS BASED ON TRIBOELECTRIC NANOGENERATORS WITH MAGNETIC NANOPARTICLES /NYLON NANOCOMPOSITE FILMS

*Gulahmadov O.G., Muradov M.B., Mamedov H.M., Qahramanli L.R., Jiseok K.
Baku State University, Azerbaijan
ogulahmadov@bsu.edu.az

A triboelectric nanogenerator (TENG) is an energy harvesting device that uses the triboelectric phenomenon to convert mechanical energy into electrical energy. When two different materials come into contact and then separate, the triboelectric effect causes the creation of electric charges. The triboelectric material acquires or loses electrons when the electrode and triboelectric material come into contact and are then removed, generating an electric potential difference or voltage between the two electrodes. TENGs have several advantages, such as their simple design, low weight, and potential for scalable fabrication.

Monitoring transmission lines is of utmost importance to ensure the safe and reliable operation of the power grid. Transmission lines are the backbone of the power grid and are responsible for transporting electricity over long distances from power plants to distribution centers. However, transmission lines are also susceptible to serious failures such as short-circuits, overloading, and even the occurrence of insulator damage which can lead to issues such as blackouts or even fire hazards. Additionally, transmission lines are often exposed to harsh environmental conditions that can lead to degradation over time. Therefore, efficient monitoring systems using innovative technologies, such as self-powered sensors based on TENGs, play a crucial role in maintaining transmission line infrastructure and preventing dangerous and costly failures.

In this study, we propose a novel approach for self-powered transmission line monitoring sensors based on triboelectric nanogenerators (TENGs) with magnetic Fe3O4 nanoparticles/nylon nanocomposite films. We leverage vibrations and the magnetic field generated by the transmission line to induce movement in the nanocomposite film, resulting in the self-operation of the TENGs. The self-powered sensors not only gather valuable data from the transmission line but also harness the energy associated with the line's magnetic field to continuously power themselves.

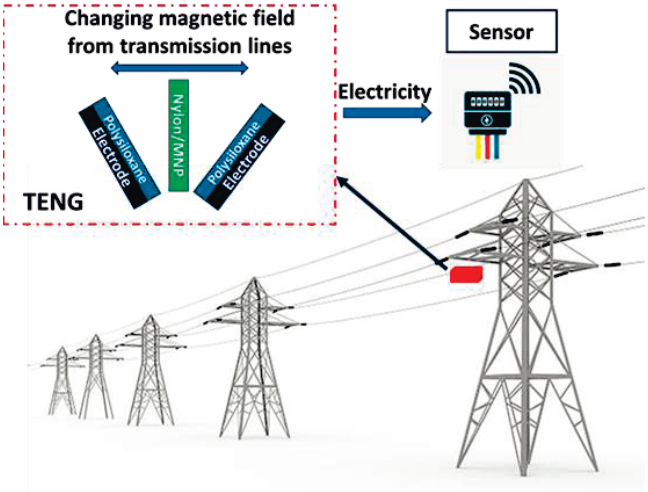

Our research opens up exciting possibilities for sustainable and reliable self-powered transmission line monitoring. By harnessing the energy from the transmission line's magnetic field, our TENG-based sensors offer a cost-effective and environmentally friendly solution. This approach has immense potential to reduce maintenance costs and enhance the overall efficiency and reliability of transmission line systems.

ACOUSTIC WEYL METAMATERIALS BASED SPACE-TIME CRYSTALS WITH TOPOLOGICAL STATES

[1]Ozer Z., [2,3*]Mamedov A.M., [2]Ozbay E.

[1]Mersin University, Türkiye
[2]Bilkent University, Türkiye
[3]Baku State University, Azerbaijan
mamedov46@gmail.com

Time crystals are time-periodic self-organized structures postulated by Frank Wilczek. While the original concept was strongly criticized, it stimulated at the same time an intensive research leading to propositions and experimental verifications of discrete (or Floquet) time crystals – the structures that appear in the time domain due to spontaneous breaking of discrete time translation symmetry. The struggle to observe discrete time crystals is reviewed here together with propositions that generalize this concept introducing condensed matter like physics in the time domain. We shall also revisit the original Wilczek's idea and review strategies aimed

at spontaneous breaking of continuous time translation symmetry. On the other hand, I t is well known that an interface created by two topologically distinct structures could host nontrivial edge states that are immune to defects. In this investigation, we introduce a 1- and 2D space-time phononic crystal and study the associated anomalous topological edge states when the phononic crystal's density is modulated both in space and time. While preserving the key topological feature of the system, the time modulation also duplicates the edge state mode across the spectrum, both inside and outside the band gap. It is shown that, in contrast to conventional topological edge states which are excited by frequencies in the Bragg regime, the time-modulation-induced frequency conversion can be leveraged to access topological edge states at a deep subwavelength scale. This feature could open another route for designing miniature devices that are based on topological physics. We also investigated the situation when the breakdown this barrier by imposing both space and time modulation (STM) on the medium properties. The STM could enable the engineering of topological phases in the time domain which provides an extra degree of freedom and therefore richer physics. There are two major findings in this study: (1) the emergence of anomalous topological edge states in the bulk band; and (2) the possibility to excite the edge state in the Bragg regime using ultralow frequencies whose wavelengths could be orders of magnitude greater than the periodicity of the PC. These features could bring about different designs of miniature devices based on topological phases for unconventional wave manipulation, excitation, and detection. Although the current study focuses on 1D acoustic systems, the theory developed here can readily be extended to higher dimensions and other wave-based systems. In conclusion, we propose to enrich the functionalities of topological devices via time modulation, which gives rise to the duplication of topological edge states across the entire spectrum. This feature can be used to achieve deep subwavelength manipulation of the edge state in the Bragg regime, which could be proven useful for designing miniature topological devices for waveguiding, sensing, and excitation, among other intriguing functionalities.

CONTROLLING THE UNCONTROLLABLE: QUANTUM CONTROL OF OPEN SYSTEM DYNAMICS

[1,2*]Kallush Sh., [1]Dann R., [1]Kosloff R.

[1]Holon Academic Institute of Technology, Israel
[2]Herber University of Jerusalem, Israel
ronnie@fh.huji.ac.il

Control of open quantum systems is essential for the realization of contemporary quantum science and technology. We demonstrate such control by employing a thermodynamically consistent framework, taking into account the fact that the drive can modify the systems interaction with the environment. Such an effect is incorporated within the dynamical equation, leading to control-dependent dissipation. This relation serves as the key element for open system control. The control paradigm is displayed by analyzing entropy changing state-to-state transformations, such as heating and cooling. The difficult task of controlling quantum gates is achieved for non-unitary reset maps with complete memory loss. In addition, we identify a novel mechanism for controlling unitary gates by actively removing entropy from the system to the environment. We demonstrate a universal set of single and double qubit unitary gates under dissipation.

SYNTHESIS OF AgNWs/PVA NANOCOMPOSITE AND EXAMINATION OF THE IMPACT OF SULFIDATION ON ITS STRUCTURAL CHARACTERISTICS

*Addayeva Z.R., Muradov M.B., Eyvazova G.M., Mammadyarova S.J., Baghirov M.A.

Baku State University, Azerbaijan
zeynabramazan5399@gmail.com

In recent times, there has been growing interest in the utilization of composites composed of Silver Nanowires (AgNWs) and polyvinyl alcohol (PVA). Consequently, AgNWs/PVA composites have been applied in various devices, including transparent conductive films, flexible electronics, sensors, light-emitting devices, etc., leveraging their lightweight, flexible electrical, and optical properties. The effect of sulfidation on the structure of AgNWs/PVA composites has been investigated in the conducted study.

In the conducted research, AgNWs were synthesized through the modified polyol method. AgNWs/PVA composites were then prepared by mixing the synthesized AgNWs with PVA at a concentration of 1.5 wt%. Samples were subjected to the influence of hydrogen sulfide (H_2S) gas obtained through the reaction $Na_2S+2HCl \rightarrow 2NaCl+H_2S\uparrow$. Three samples were sulfided by varying the amount of Na_2S used in obtaining H_2S gas, denoted as AgNWs/PVA-1, AgNWs/PVA-2, and AgNWs/PVA-3 according to the Na_2S quantities of 4, 6, and 8 q.

Figure 1(a) illustrates the X-ray diffraction patterns of AgNWs/PVA samples. The characteristic peak for PVA is observed at $2\theta=19.31°$, corresponding to the (101) index. Peaks at $2\theta=38.33°$, 44.51°, 64.63°, and 77.58°, corresponding to (111), (200), (220), and (311) planes, are attributed to AgNWs (JCPDS card no. 04-0783). Figure 1(b), c, and d depict the XRD peaks of AgNWs/PVA-1, AgNWs/PVA-2, and AgNWs/PVA-3, respectively. As evident from the spectra, the crystallinity degree of PVA in samples exposed to the influence of H_2S gas decreases, leading to amorphization. Additionally, after sulfidation, a decrease in the intensity of the peak corresponding to AgNWs (111) index is observed, and a new peak appears at $2\theta=32.34°$, associated with the sulfidation of AgNWs and the formation of Ag_2S (JCPDS card no. 14-0072). However, the complete absence of shifts in the peaks attributed to AgNWs suggests that AgNWs are only surface-sulfided and not completely sulfided. The quantity of Ag_2S formed increases with an increase in the amount of H_2S gas and the duration of exposure, as evident from the spectrum.

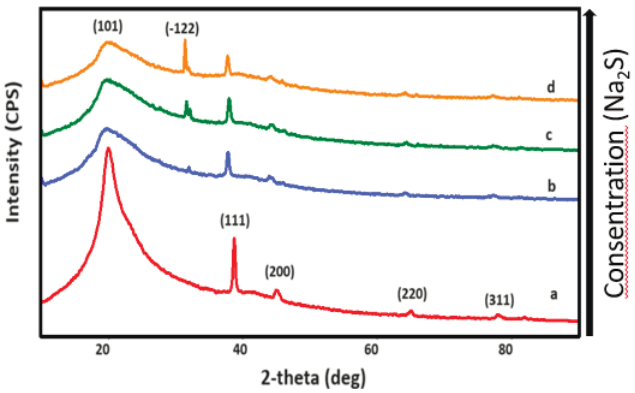

Fig. 1. XRD diffractogram for a) AgNWs/PVA, b) AgNWs/PVA-1, c) AgNWs/PVA-2, d) AgNWs/PVA-3

THE USE OF MULTI-QUANTUM ABSORPTION FOR THE STUDY OF SEMICONDUCTOR MULTILAYER STRUCTURES

*Salmanov V.M., Huseynov A.G., Mamedov R.M., Hasanova L.G., Mahammadov A.Z., Ahmadova F.Sh., Mammadova T.A.
Baku State University, Azerbaijan
vagif_salmanov@yahoo.com

Determination of the main parameters of multilayer semiconductor structures is one of the urgent tasks of optoelectronics. The methods of X-ray spectral microanalysis currently applied to such structures and the registration of photoluminescence of the layers of the structure using layer-by-layer bleed have significant drawbacks, consisting in the violation of the integrity of the samples, the requirement of their careful preparation and significant time spent on measurements. In This paper proposes a method for studying semiconductor multilayer structures based on the analysis of absorption and photoluminescence spectra under two and three-quantum excitation by laser radiation.

Multilayer structures were obtained by sequential deposition of InSe, GaSe and GaS crystals on a glass substrate by the Modified Chemical Bath Deposition method. A pulsed Nd:YAG laser with built-in 2nd and 3rd harmonic generators, designed to generate radiation with a wavelength of 1064, 532 and 335 nm, was used as a radiation source. The duration of the laser pulse was 10 ns with a maximum power of ~ 12 MW/cm^2. The optical absorption and luminescence spectra of multilayer structures were studied using an automatic monochromator M833 with double dispersion, with computer control and a detector that registers radiation in the wavelength range of 350-2000 nm.

GaS thin films have a band gap of E_g=2.53 eV, so the radiation of the 2nd harmonic of the Nd:YAG laser of ($\hbar\omega$=2.34 eV) should lead to a two-quantum, and the radiation of the 1st harmonic ($\hbar\omega$=1.17 eV) to three-quantum absorption. Unlike GaS, GaSe thin films have a locked band width of 2.02 eV, excitation by the 1st harmonic of a neodymium laser can lead to two-quantum absorption. The band gap InSe is in the near-infrared region of the spectrum of (E_g=1.10 eV), laser light with $\hbar\omega$=1.17 eV energy can lead to single-photon absorption.

Our experimental results showed that the observed maxima in the photoluminescence spectra (415 nm, 484 nm, 607 nm, 760 nm and 1085 nm) of the multilayer structure are due to radiative recombination at the edge of the fundamental absorption. The estimates show that the ratio of the two-quantum coefficient to the three-quantum absorption coefficient

is $3x10^4$, which is in good agreement with the experimental results. In our opinion, the results obtained by us can find a number of applications in the manufacture of optoelectronic devices based on semiconductor layers with a variable band gap E_g, for which knowledge of such characteristics as the composition and, accordingly, the value of E_g, the thickness of the layers, the concentration of deep and fine impurities is very important.

ELECTRONIC BAND STRUCTURE OF $Cd_{1-x}Fe_xSe$

[1,2*]Mehrabova M.A., [3,4]Allahyarov E.A., [5]Hasanov N.H., [6]Gasimova N.R.

[1]Azerbaijan Technical University, Azerbaijan
[2]Institute of Radiation Problems, Ministry of Science and Education, Azerbaijan
[3]Heinrich-Heine University Dusseldorf, Germany
[4]Macromolecular Science, CWRU Cleveland, USA
[5]Baku State University, Azerbaijan
[6]Azerbaijan University of Architecture and Construction, Azerbaijan
metanet.mehrabova@aztu.edu.az

In the present paper theoretically investigated electron band structure of $Cd_{1-x}Fe_xSe$ by DFT method using ab initio calculations. The calculations are based on the first-principles pseudopotential method within the density functional theory (DFT) and the Local Spin Density Approximation (LSDA) using the Tight Tier basis set. All calculations are performed by using Atomistix Toolkit (ATK) program.

$Cd_{1-x}Fe_xSe$ supercell of 8 and 64 atoms were constructed. It was used Hubbard U potential U_{Fe} = 2.42 eV for 3d states for Fe atoms. After the construction of $Cd_{1-x}Fe_xSe$ (x = 0; 6.25 %; 25 %) supercells, atom relaxation and optimization of the crystal structure were carried out to eliminate forces and minimize stresses. The equilibrium lattice parameters have been computed by minimizing the crystal total energy calculated for different values of lattice constant.

Firstly, electron band structure (EBS) was calculated for CdSe semiconductor compound. The calculated band gap was 1.73 eV. The electron band structure of $Cd_{1-x}Fe_xSe$ SMSC is determined from the projected density of states (PDOS). The analysis of graphs shows that in the valence band, the electron band structure of $Cd_{1-x}Fe_xSe$ consists of three parts: (1) the upper part of the valence band is mainly formed by *p*-orbitals of Se and Cd atoms, *s*-orbitals of Cd and Fe atoms with some contribution of *d*-orbitals of Fe atoms; (2) the middle part is formed by *d*-orbitals of Cd atoms, which are 7 eV lower than the valence band maximum (3) the lower part is formed by *s*-orbitals of Se and Fe atoms, and *p*-orbitals of Fe atoms

which are located 18 eV lower than the valence band maxim.

The bottom of the conductivity band is formed by *s*-and *p*-orbitals of Fe atoms and *p*-orbitals of Cd atoms, *d*-orbitals of Se atoms. EBS and density of states (DOS) for $Cd_{1-x}Fe_xSe$, x=0.25 were calculated, and band gap, the total energy has been defined as E_g= 1.92 eV, E_t=-6308.42730 eV respectively. EBS and density of states (DOS) for $Cd_{1-x}Fe_xSe$, x=0.06 were calculated and the band gap, DOS, total energy has been defined in antiferromagnetic (AFM) and ferromagnetic (FM) phases.

The band gap for the $Cd_{1-x}Fe_xSe$, x=0.06 in ferromagnetic phase is equal to E_g = 1.77 eV and total energy is equal to E_t = -60818.04032 eV. The band gap for the $Cd_{1-x}Fe_xSe$, x=0.06 in antiferromagnetic phase is equal to E_g = 1.78 eV and total energy is equal to E_t = -60818.03595 eV.

The calculated band gap much closer to literature data and our experimental results. It was defined that total energy in AFM phase more than in FM phase E_t (AFM) › E_t (FM), therefore AFM phase considered more stabile. Band gap in AFM more than in FM phase E_g(AFM) › E_g (FM).

CdS NANOPARTICLES SYNTHESIZED BY LASER ABLATION

Jafarov M.A., *Salmanov V.M., Huseynov A.G., Mamedov R.M., Abasova A.Z., Jahangirova S.A., Ahmadova F.Sh., Mammadova T.A.

Baku State University, Azerbaijan

vagif_salmanov@yahoo.com

Semiconductor nanoparticles have recently attracted attention due to their unique physical and chemical properties. Cadmium sulfide (CdS) is a technologically useful material due to its wide bandgap of $2.42\ eV$, making it useful in a wide range of applications such as; light-emitting diodes, single electro- and field-effect transistors, photo sensors, window materials, solar cells. CdS nanoparticles were synthesized via a many methods such as a sol-gel template, Solvo-thermal route, hydrothermal, chemical method and laser ablation.

In this work, CdS nanoparticles were synthesized by laser ablation of a solid target in a liquid medium. Special pure Cd (99%) and a solution of $(NH_2)_2CS$ were used as the initial raw materials. The reaction occurred according to the following formula:

$$Cd + (NH_2)_2CS + H_2O \rightarrow CdS + (NH_2)_2CO + H_2$$

Immediately after irradiation with a laser pulse, CdS nanoparticles were formed. The ablation process was carried out with laser radiation

with a wavelength of $\lambda = 1064\ nm$, with a pulse energy of $135\ mJ$ and an ablation time of $\sim 10\ min$. The emission intensity was varied using calibrated neutral light filters. The optical absorption and luminescence spectra of the $GaSe$ nanoparticle were studied using an M833 automatic monochromator with dual dispersion (spectral resolution $\sim 0.024\ nm$ at a wavelength of $600\ nm$), with computer control and a detector that records radiation in the wavelength range waves $350 - 2000\ nm$.

Based on the X-ray diffraction patterns of nanoparticles from droplets of a CdS colloidal solution dried on a clean glass substrate, the sizes of the nanoparticles were calculated using the Scherer formula. Estimates show that the average size of CdS nanoparticles is $\sim 27\ nm$. XRD patterns show that the synthesized CdS nanoparticles are nancrystalline and have a hexagonal wurtzite structure.

The luminescence spectrum of CdS nanoparticles excited by the 2nd harmonic of an Nd:YAG laser ($\hbar\omega = 2.34\ eV$) has a maximum at a wavelength of $375\ nm$ ($3.30\ eV$). An increase in the laser light power by 1.5 times does not affect the position of the spectrum, but leads to an increase in the radiation intensity by ~2 times. In our opinion, the observed luminescence is due to radiative recombination of free excitons. Knowing of the energy of free excitons in CdS ($E_{f.ex} \sim 29\ meV$), we can determine the band gap of nanoparticles $E_g = h\nu + E_{f.ex}$, which turned out to be equal to $3.33\ eV$. This value turned out to be $0.91\ eV$ greater than the band gap of the bulk material.

STATE OF THE ART IN CANCER THERAPY: COMBINED THERAPY AND THE MAIN FACTORS LIMITING OR ENHANCING THE EFFICACY OF PROTON THERAPY

[1]*Chirakadze A., [1]Mitagvaria N., [1]Chubinidze G., [1]Dvali N., [1]Khuskivadze N., [2]Shanidze R., [2]Abuladze M., [3]Palavandishvili G.

[1]Caucasus International University, Georgia
[2]Kutaisi International University, Georgia
[3]Georgian Technical University
achirakadze@gtu.ge, achikochirakadze@gmail.com

At the beginning of this century a kind of hierarchy of cancer treatment methods had been developed:

a) the universally recognized treatments: Surgery, Chemotherapy, Radiotherapy;

b) Targeted therapy, gene expression modulators, immunotherapy, angiogenesis inhibitors, hormone therapy, etc., mainly recognized as more specific, less common additional ancillary therapies;

c) All other modalities (hyperthermia, photodynamic therapy, palliative therapy, supportive therapy, stem cell therapy, other modalities of adjuvant therapy, etc.) which are are considered as less important means of treatment.

The most advanced modern cancer treatment modality today is the hadron (namely, proton and heavy ion therapy). Due the super-linear growth of the number of particle (especially, proton) therapy centers, many researchers forecasted a very high number of patients treated by proton therapy before 2026. However, the real overall spread of hadron therapy was much slower due to its very high cost, research intensity and requirements for medical and engineering staff. Therefore, a significant increase of the effectiveness and safety of proton therapy is an acute need.

A detailed analysis of research data from the last five years have clearly shown that the most important limiting phenomena are as follows: the high proton irradiation doses required for the confident significant effect; the spread of proton radiation into the healthy tissues; Inaccuracy in target positioning or target displacements; additional leakage of radiation through the diffusers (pre-scatterers), collimators, ridge filters, modulators, bolus, etc.; the secondary neutron radiation in tissues; leakage of radiation scattered by the treatment part (gantry) and prompt gamma-quants produced either in the machine and the patient tissues. The most promising new solutions that can increase the treatment efficacy and crucially reduce the side effects are proposed and discussed. The presented research substantiates the authors' concept of the strongly localized combined multicomponent treatment of cancer (including proton radiotherapy, chemotherapy, Curie temperature controlled magnetic hyperthermia and boron-neutron/boron-proton capture nuclear reactions using boron nitride nanosheets, metal, metal oxide nanoparticles and anticancer drug mixtures) as the most promising adjunct modality for enhancing the proton therapy.

ALKALI METAL SALT SOLUTION BASED SYNERGISTIC CANCER THERAPY COMBINED WITH ANTICANCER METAL OXIDE NANOPARTICLES: ACUTE TOXICITY STUDY

[1*]Chubinidze G., [1]Mitagvaria N., [1]Chirakadze A., [1]Dvali N., [1]Khuskivadze N., [1]Chichua T., [2]Chikadze N., [3]Khomeriki I., [3]Buachidze Z., [4]Abuladze M.

[1]Caucasus International University, Georgia
[2]Tbilisi State University, Georgia
[3]Georgian Technical University, Georgia
[4]Kutaisi International University, Georgia
chubinidzegeorge@gmail.com

In 112 of the 183 monitored countries before the age of 70 years cancer currently is the first or second leading cause of death and the third or fourth cause in the rest of the world, Cesium and Rubidium, the heaviest alkali metals occurring in nature in stable form, are putative cancer treatment compounds. Cesium chloride-based preparations are among the most widely used alternate antitumor modalities in the United States, although the over-the-counter use can cause undesirable, dangerous and even lethal side effects. Many researchers, taking into account the rather conflicting data from various studies, are of the opinion that this issue should be studied more intensively. Special attention should be paid to the study of acute and chronic toxicity (as one of the main characteristics of the medical drugs) of cesium and rubidium preparations, to their interaction with other antitumor modalities and to their bio-kinetics in bird embryos and laboratory animals, as well as in the human body. On the other hand, metal and metal oxide nanoparticles have proven their pronounced anticancer activity and also are considered as promising materials for synergistic anticancer combinations. The general purpose of the reported research was an in vivo study of the acute toxicity to chick embryos of the seven putative anticancer combinations (rubidium chloride, cesium carbonate and rubidium carbonate water, and DMSO and standard saline solutions combined with dispersed silver and copper oxide nanoparticles in comparison to the solutions with dispersed SPIONs). The data of the presented research clearly show that chlorides are noticeably safer than carbonates, while rubidium salts are noticeably more toxic, than cesium salts. DMSO dispersed zinc oxide is only 1.2-1.5 times more toxic than the saline solution dispersed iron oxide and, taking into account the high anticancer activity of DMSO, this dispersion can be considered as a promising synergistic component for the anticancer drugs. Testing of the behavioral and

physiological characteristics confirmed the results of testing of the acute toxicity, showing the same raking of safety of the combinations. The reported study shows that all the tested combinations are highly safe at the exposure doses lover than 0.2-0.4 mg/g. The results obtained by both novel methods are in good correlation with each other.

BAND STRUCTURE, DIELECTRIC FUNCTION AND REFLECTION COEFFICIENT OF CHAIN $TlGaTe_2$

[1]Abdullayev A.P., [1*]Gafarova D.M., [1]Musazade I.V., [2]Ismayılov T.I.
[1]Azerbaijan University of Architecture and Construction, Azerbaijan
[2]Military Institute named after H. Aliyev, Azerbaijan
Dgafarova14@gmail.com

$TlGaTe_2$ has the TlSe-type (B37) quasi-one-dimensional chain structure and possesses a large Seebeck coefficient.

Band structure has been calculated for $TlGaTe_2$ by pseudo-potential method using non-local ionic pseudo-potentials built up in the scheme suggested by Bachelet-Hamann-Schluter.

Screening and exchange-correlation effects have been treated within Hubbard-Sham model with selected parameters of the charge distribution around each particular ion. We have used ~1800 plane waves (16 Rydberg cut off energy) in decomposition of the wave function.

As follows from the calculated band structure the top of the valence band is located in the symmetry point T(0.5; -0.5; 0.5) on the surface of the Brillouin zone (BZ) and belong to the irreducible representation T_3. the bottom of the conduction band is located in the symmetry line D(k; k; 0.5-k) on the surface of the BZ between symmetry point N(0; 0; 0.5) and P(0.25; 0.25; 0.25) and belongs to the irreducible representation D_1. the minimal energy gap for direct transitions which possess T_3-T_4 symmetry and forbidden in dipole approximation takes place in the T point.

Comparison with the previous band structure calculations for $TlGaTe_2$ by the empirical pseudo-potential method and method and the liner acigmented plane-wave method shows that the symmetry of the electron states at band gap is the save.

On an energetic scale the valence bands can be conditionally sorted into three groups. Group theory study shows, that the lowest group with four bands around -12eV is of the anion origin and results from 5s- states

of Te. Another group with four bands between –6 and –4 eV is largely formed by 6s- states of Tl and 4s states of Ga. The main origin of the highest group with ten bands in the range –4 to 0 eV is p-states of the anion as well as atoms of the third group.

Above theoretical assignment of the valence band states of $TlGaTe_2$ agrees with experimental data on electron photoemission.

Imaginary part of the dielectric function for e||c and e⊥c configuration of the incident radiation, where c is the optical axes, has been calculated for energies up to 12 eV. Real part for the same configurations has been obtained after extrapolations of the imaginary part to higher energies and subsequent Kramers-Kronig transformation.

The resultant complex dielectric function has been used for determination of the reflection coefficient.

We also have been measured the reflection spectra in the energy range 1.78-3.11 eV at 240, 200, 100, 150K temperatures. There is a satisfactory consent between calculated and measured results.

ELECTRONIC AND MAGNETIC PROPERTIES OF AG-DOPED (6,0) SINGLE-WALLED ZnO NANOTUBES

[1*]Jafarova V.N., [2]Mamedov N.T.

[1]Azerbaijan State Oil and Industry University, Azerbaijan
[2]Institute of Physics, Ministry of Science and Education, Azerbaijan
vusale.cafarova@asoiu.edu.az

ZnO is one of the most significant II-VI semiconductors and has attracted the research interest of many research groups because its large exciton binding energy (60 meV) and a wide direct energy band gap (3.37 eV). ZnO has promising material for numerous applications in the fields of optoelectronics and spin-based devices. ZnO nanocrystalline compounds are attractive due to their fantastic physical properties, such as electronic, optical, and magnetic. Doping with transition metal elements is one of the most effective methods to obtain magnetic materials. The Ag-doped ZnO system is of great interest due to its suitability for doping and the existence of a ferromagnetic (FM) phase at room temperature. It was shown that Ag-doped ZnO exhibited room-temperature ferromagnetism and half-metallic behavior.

In this work, we studied the electronic and magnetic properties of defected single-wall (6,0) chiral ZnO nanotubes using DFT method. For the

Ag-doped ZnO NTs, the energy gap decreases with the impurity concentration. The obtained total magnetic moment for SWZnONT systems is equal to 1.001 μ_B. The main contribution to magnetization of systems comes from 3 O atoms (~0.77 μ_B), which are chemically bonded (CB) with Ag. The insignificant positive contribution to the magnetization of systems comes from other host oxygen atoms and the negligible negative contribution from host zinc atoms. The local magnetic moment of an impurity atom is ~0.2 μ_B and ~0.23 μ_B in *d*-states. The total energy calculations for these systems show the stability of the ferromagnetic phase. In the case of Ag doping and with Zn vacancy, the wide energy gap decrease and the total magnetic moment of this system increase by ~2 μ_B compared with the free vacancy case. From first-principles calculations, show that Ag-doped ZnO NT systems are semi-magnetic ferromagnetic materials, and it is a promising candidate for spintronics device applications.

DEVELOPMENT OF SELECTIVE INHIBITORS FOR THE TUMOR-ASSOCIATED CARBONIC ANHYDRASES

[1*]Akdemir A., [2]Demir-Yazıcı K., [2]Trawally M., [2]Guzel-Akdemir O.

[1]Istinye University, Türkiye
[2]Istanbul University, Türkiye
atilla.akdemir@istinye.edu.tr

Carbonic Anhydrases (CA) are structurally diverse metalloenzymes that are involved in a simple but physiologically crucial chemical reaction, which is the interconversion of carbon dioxide and bicarbonate ions. Nevertheless, the enzymes play important roles in (patho)physiology, such as the virulence of infectious agents and cancer. Especially, the human CA isozymes IX and XII (hCA IX / hCA XII) are involved in the protection of cancer cells against their acidic microenvironment, which they create due to the Warburg effect. In contract, hCA I and II are widely distributed in the human body and are mainly involved in the maintenance of physiological conditions. As such, the are considered off-targets.

Here we describe the development of selective inhibitors of the tumor-associated hCA IX and XII isozymes, based on an unselective but potent hCA enzyme inhibitor. Using in silico combinatorial chemistry, more than 100.000 analogs were created that differ in the location of the sulfonamide group and contain additional functional groups at selected position on the molecule.

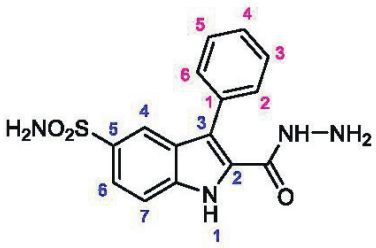

Virtual screenings were performed using an ensemble docking protocol with subsequent rescorings to identify molecules that were expected to bind with hCA IX and/or hCA XII. Afterwards, these identified compounds were subject to a virtual screening with the same protocol, but against hCA I and II cocrystal structures. Subsequently, all compounds expected to bind to hCA IX and/or hCA XII, but not to hCA I or hCA II were selected for MD simulations to investigate their potential binding to hCA IX and/or hCA XII.

Finally, the compounds expected to bind selectively and potently to the tumor-associated hCA enzymes were synthesized and subsequently tested in hCA I, II, IX and XII enzyme inhibition assays.

Using the described methodology, 57 compounds belonging to three different scaffolds have been synthesized. The majority of these compounds show intermediate to strong inhibition of hCA IX and/or XII compared to the widely distributed off-targets hCA I and II.

ACOUSTIC METAMATERIALS FOR AERONAUTIC APPLICATIONS: A REVIEW

[1,2*]Mamedov A.M., [1]Ekmel Ozbay

[1]Bilkent University, Türkiye

[2]Baku State University, Azerbaijan

mamedov46@gmail.com

Acoustic metamaterials have emerged as a groundbreaking technology with the potential to revolutionize the aeronautics industry. These specially designed materials manipulate sound waves in unconventional ways, enabling the development of lightweight, efficient, and high-performance solutions for noise control, vibration reduction, and improved aeronautic systems. This investigation provides an overview of acoustic metamaterials and their promising applications in aeronautics. The review includes the next sections:

Introduction

Acoustic metamaterials, a subset of metamaterials, offer innovative solutions to address these issues. These materials are engineered to have unique properties that enable precise control over sound waves.

Basics of Acoustic Metamaterials

Acoustic metamaterials are structured composites designed to manipulate sound propagation in unconventional ways. They consist of carefully engineered unit cells that can interact with sound waves and modify their behavior. These unit cells are typically much smaller than the wavelength of the acoustic waves, which allows for precise control over the propagation of sound.

Applications in Aeronautics

Noise Control, Vibration Damping (vibrations in aircraft structures, metamaterial-based vibration dampers can be designed to absorb and dissipate energy, reducing the impact of vibrations on the airframe), Engine Noise Reduction (Acoustic metamaterials can be incorporated into the design of engine components to minimize noise emissions without compromising performance), Sonar and Radar Stealth (In addition to aeronautics, acoustic metamaterials have applications in military aircraft. Metamaterials can be used to design stealth technologies that absorb or redirect incoming sonar or radar waves, making aircraft less detectable by enemy systems), Challenges and Future Prospects (While acoustic metamaterials offer promising solutions for aeronautic applications, several challenges remain, including the development of cost-effective manufacturing techniques and the integration of these materials into existing aircraft designs. The future of aeronautics will likely involve ongoing research and development to optimize the use of acoustic metamaterials for noise control, vibration reduction, and overall system improvement).

Conclusion

Acoustic metamaterials have opened up exciting possibilities for the aeronautics industry. These engineered materials have the potential to enhance passenger comfort, reduce noise pollution, and improve the efficiency and environmental impact of aircraft. As research in this field continues, we can expect to see more innovative applications of acoustic metamaterials in the aerospace industry, leading to quieter, more efficient, and more environmentally friendly air travel.

JANUS MATERIALS: INDIRECT (Λ-Γ)-TO-INDIRECT (K-Γ) CROSSOVER IN FEW MONOLAYER MoS_2

[1,2]Mamedov N.T.
[1]Baku State University, Azerbaijan
[2]Institute of Physics, Ministry of Science and Education, Azerbaijan

The main trend in contemporary condensed matter physics is related to the development of quantum materials enabled to provide revolutionary breakthroughs in technologies vitally important on a global scale. One of such materials, molybdenum disulfide (MoS_2) exhibits tunable band gap properties and is considered a semiconducting alternative to metallic graphene. Successful development of single- and few-layer MoS_2 phototransistors, photodetectors, solar cells, biosensors and many other devises with promising parameters favors such positioning of MoS_2 and moves the primary focus onto its ultrathin varieties.

MoS_2 is often referred to as Janus material, because of an indirect - to - direct crossover in its one monolayer. However, little progress is made so far regarding the information about evolution or transformation of the indirect band gap in MoS_2 containing more than one layer but still having thickness at the nanoscale. The present work provides a new platform for studying thickness-dependent band gap of such ultrathin MoS_2 varieties; theoretical consideration, together with direct experimental evidence for indirect (Λ – Γ) - to - indirect (K - Γ) crossover upon thinning MoS_2 thickness down to a few layers is given.

REPULSION DRIVEN METALLIC PHASE IN THE GROUND STATE OF THE HALF-FILLED T-T' IONIC HUBBARD CHAIN

[1]Rossini G.L., [2]Japaridze G.I.
[1]Universidad Nacional de La Plata, Argentina
[2]Ilia State University, Tbilisi, Georgia

An unusual metallic phase is argued to develop in the one dimensional ionic Hubbard model, at half-filling and zero magnetization, at intermediate electron-electron repulsion U when second neighbors hopping is allowed and tuned close to a topological Lifshitz transition (connected with a change of the Fermi surface in the non-interacting system). The metallic state lies between a band insulator phase at low repulsion and a correlated (Mott-like) insulator phase at high repulsion. In approaching the later, the

model supports short range antiferromagnetic order and spontaneous dimerization of both bond charge and nearest neighbors antiferromagnetic correlations. A combi- nation of mean field and effective field theory (bosonization) provides an analytical understanding of the physical processes underlying the argued phase transitions. The ground and low energy ex- cited states of finite length chains are explored by density-matrix renormalization-group (DMRG) calculations, providing numerical evidence for the intermediate gapless phase. Such finite systems are attainable by cold atoms in optical lattices for a wide range of the parameter U.

MONTE CARLO PREDICTIONS FOR AND ϕ(1020)° and K* (892)° MESONS PRODUCTION AT LHC ENERGIES IN HADRON-HADRON AND HEAVY ION COLLISIONS

Yasir A.S.

COMSATS University Islamabad, Pakistan
yasir_ali@comsats.edu.pk

In this analysis the results on the study of the K* (892)° and ϕ(1020)° mesons production in proton-proton collisions at $\sqrt{s}$=7, 13 and 5.02 TeV, and in heavy ion (Pb+Pb) collisions at $\sqrt{s}$=5.02 TeV are presented. Transverse momentum (p_T) distributions of ϕ (1020)° and K* (892)° mesons are reported in the ranges of of $0 < p_T < 9$ and $0 < p_T < 6$ GeV/c, respectively at $\sqrt{s}$=7 and 13 TeV.

The yields of K* (892)° and ϕ(1020)° mesons are presented in proton-proton and Pb–Pb collisions at $\sqrt{s}$=5.02 TeV in the rapidity interval of $|y| < 0.5$ and in the transverse momentum range of $0 < p_T < 20$ GeV/c. EPOS-LHC, EPOS−1.99 and PYTHIA8 simulation codes are used to produce the required simulated distributions.

Nuclear modification factor R_{AA} is also plotted at $\sqrt{s}$=5.02 TeV. The simulated distributions are compared with the ALICE experimental data. PYTHIA8 gives good estimate of the ALICE as compared to EPOS-LHC and EPOS 1.99. It seems that PYTHIA8 CR mode 2 best describes the ALICE both at $\sqrt{s}$=7 and 5.02 TeV. EPOS-LHC predictions are consistent with ALICE data for ϕ(1020)° at 5.02 TeV energy as obvious from $R_{AA.}$ Another good quantitative analysis is provided by data to model rato.

IR LASER-INDUCED ABLATIVE DEPOSITION OF POLYMER BASED COMPOSITES

Gilev J.B.

Ss. Cyril and Methodius University in Skopje, Macedonia

IR laser-induced ablation of polymer composites is attracting particular attention due to the specific application of the resulting thin films. This technique is promising in terms of the fabrication of polymers containing polar groups that can serve as protective layers to different nano-bodies (metals, metal chalcogenide's, conductive polymer nanocomposites carbon-based nanofillers, such as graphene, carbon nanotubes and carbon nanoribbons. This specific process occurs within a temperature jump and is controlled by kinetic rather than thermodynamic polymer degradation. It is feasible through multiple-photon absorption of energy-poor infrared photons, which leads to high vibrational excitation density in the polymer and high heating and cooling rates (respectively, ~$10^{6–11}$ and ~$10^{3–6}Ks^{–1}$). We have examined IR laser-induced ablative deposition with poly(vinyl acetate) (PVAc), poly(vinyl chloride) (PVC), poly(vinyl chloride-co-vinyl acetate) P(VC/VAc), poly(vinyl acetate) loaded with Fe and Cu particles, poly(ethylene-co-acrylic acid)zinc salt (PEAZn), poly(phenylene ether-sulfone) (PES) to establish its specific features and differences from conventional pyrolysis.

It was of interest to us to continue our previous effort on pulsed laser ablation of polymer composites and we focused on composites from different type of carbon nanofillers incorporated into acrylic/methacrylic matrices. Therefore, graphene nanoribbons, and mixture of graphene nanoplatelets were used. Graphene nanoribbons (GNR) are narrow strips of graphene in one dimensional morphology with extraordinary properties, owing to the large edges that offer numerous interfacial contact area to the polymer phase in the composite materials. Consequently, minor amount of GNR incorporated within polymer matrix, will not only reinforced mechanically and thermally the composite materials, but will significantly expand their application potential, giving added value to the cheap polymeric material. Herein, the quartz crystal microbalance (QCM) gas sensing of the nanocomposites was investigated.

Polymerization in dispersed media was used as a green synthesis method to produce for first time waterborne polymer/GNR nanocomposites. The lack of aggregation during structuring of GNRs within the

polymer matrix and the established covalent bonding between the polymer and GNRs phases were responsible for the observed strong mechanical and thermal reinforcement of the nanocomposites. By exposure of the nanocomposites to low concentrations of toxic gases (in a concentration range of 70-1000 ppm), it was found that the sensors are characterized by a large sensor response in short time, at room temperature and with very good reproducibility in three investigated cycles of gas adsorption and desorption. The excellent performance was attributed to the large functional interface created between the GNRs and the polymer that offer numerous adsorption sites, along with the composite morphology that provide availability of these sites to the gasses. The sensors have shown selectivity towards NH_3 rather than N_2O and CO, likely, because the former interacted with the composite materials by joint Wan der Waals forces and hydrogen bonding, whereas the last two gasses interact exclusively by the van der Waals interactions.

EARTH-ABUNDANT COMPOUND SEMICONDUCTORS FOR SOLAR ENERGY CONVERSION

[1,2*]Schorr S.

[1]Helmholtz-Zentrum Berlin fuer Materialien und Energie, Germany
[2]Freie Universitet Berlin, Institute of Geological Sciences, Germany
susan.schorr@helmholtz-berlin.de

The need of handling eco-friendly and cheap compound semiconductors in thin film photovoltaics (PV) has constantly pushed the research towards more environmental friendly materials, such as Kesterite-type compound semiconductors Cu_2ZnSnS_4(CZTS), $Cu_2ZnSnSe_4$(CZTSe) and $Cu_2ZnSn(S, Se)_4$ (CZTSSe). They present the only critical raw material (CRM) free thin film PV technology with tunable band gap energy and excellent long-term stability. The current record efficiency for CZTSSe solar cells of 14.9 % highlights the great potential of this abundant chalcogenides to support a sustainable energy transition.

In record devices these absorber materials generally show a non-stoichiometric composition which is possible due to a remarkable flexibility of their crystal structure. This ability to accept deviations from stoichiometry is correlated to the formation of intrinsic point defects. The formation of such defects, like vacancies, ant-sites and interstitials, is driven thermodynamically by minimizing the Gibbs free energy of the crystal. The key

issue for kesterite solar cells is the large open-circuit voltage deficit which is caused by three main factors: (i) a non-homogeneous absorber composition resulting in bandgap fluctuations and formation of secondary phases, (ii) structural disorder like Cu-Zn disorder or intrinsic point defects causing strong band tailing and (iii) the multi-element composition and the variable valence of Sn resulting in complicated defect properties.

The presentation will discuss the potential of point defect engineering to optimize the key factors limiting the open circuit voltage of the potential solar cell. Based on the off-stoichiometry type model correlating chemical composition and occurring intrinsic point defects in these quaternary compound semiconductors, a compositional region for high efficient devices can be revealed. Changing the degree of Cu-Zn disorder varies the band gap energy as well as the value of PL_{max}. The Cu-Zn disorder can be influenced by a thermal annealing process nowadays technologically applied as post-deposition treatment. Cu-Zn disorder can even be avoided by changing the crystal structure by alloying CZTSe with Ag.

The presentation is based on our systematic experimental studies of quaternary compound semiconductors applying advanced analytical methods like neutron and synchrotron X-ray diffraction, photoluminescence and UV-Vis spectroscopy.

KNOCKING OUT OF NEUTRON BY THE PROTON FROM NUCLEUS

*Abdulvahabova S.G., Bayramova T.O.
Baku State University, Azerbaijan
sajida.gafar@gmail.com

The study of the cross sections of the knocking out nucleons provides important information about the asymptotic behavior of the scattering amplitude. During the interaction of the incident particle with nucleus, its function is distorted. In this case, we are talking about those components of the wave function for which the probability of interaction with the target is small, i.e. during the collision, only a small part of the target is excited (an elastic collision with only one of its constituent particles). To do this, it is necessary to use the "point" component of the wave function of the incident particle.

In this paper, we consider processes knocking out of neutron by the proton in the eikonal approximation with distorted waves. The high-energy or eikonal approximation is broad and consistent for describing

scattering in complex groups, like scattering in some optical continuum. In this approximation, after the closure of the power, there is a closure of the projection of the k-direction momentum: pk = const. This means that the movement in the transverse directions is completely neglected. In addition, in this approximation, restrictions on any masses and coordinates of particles are not collected, while both the final radius and the recoil are calculated exactly. In the eikonal approximation, the cross section of any process of interaction of a nucleon with a nucleus is expressed in terms of the amplitude of the scattering of a nucleon by an individual nucleon. It is also assumed that the scattering of a nucleon by any nucleon of the target nucleus is not affected by the presence of other nucleons in the nucleus. Therefore, the high-energy approximation can be used for angular distributions of scattered particles.

It is assumed that the neutron is emitted at the same point where it interacts with the proton. The need to introduce a finite interaction radius for calculating exchange processes is more or less acceptable for calculating direct processes in reactions with the transfer of one particle. A characteristic feature of the approximation used is the division of its methodological basis into two main parts. The first part relates to the theory of nuclear reactions, since it consists in choosing an approximation for the effective cross section that determines the reaction mechanism. The second part relates to the theory of nuclear structure, which contains information about the spectrum of the final nucleus.

SPECTRAL OBSERVATIONS OF THE SYMBIOTIC STAR AG PEGASI

[1]Mikailov Kh.M., [2*]Rustamova A.B., [1,2]Rustamov B.N., [2]Alekberov I.A.
[1]Baku State University, Azerbaijan
[2]Shamakhy Astrophysical Observatory named after N. Tusi, Azerbaijan
aysel.rustemova@yahoo.com

The results of spectral observations of the symbiotic star AG Pegasi (AG Peg) conducted at the Cassegrain focus of the 2-meter telescope of the Shamakhy Astrophysical Observatory named after N.Tusi by using the Shamakhy Fiber Echelle Spectrograph (ShAFES) are presented. The spectra of the star AG Peg were obtained with a spectral resolution of R = 28000 during the period of 2016-2019, in the wavelength range λ = 3900–7700 Å. Using the photometric database of variable stars AAVSO (American

Association of Variable Star Observers), the light curve of the star AG Peg was constructed for the period of our spectral observations. Based on the AAVSO data for the period 1954-2022, a periodicity in the star's brightness changes was identified, with a period of about 815 days. The behavior of selected spectral lines in different phases of the orbital period of the AG Peg binary system is described. For the analysis, we chose: emission lines Hα, Hβ, HeI λ 5876 Å, and HeII λ 4686Å, as well as about 30 selected absorption lines of metals, in the spectrum region: 5000-8000 Å. Profiles of the considered emission lines show strong variability, with a complex structure - single-peaked, double-peaked, and intermediate between them, and their variability, in general, does not show dependence on the orbital period of the AG Peg binary system. The figure presents the dependencies on the orbital period parameters of the AG Peg system: on the top panel is the light curve in the R-magnitude; on the panels below are the radial velocities of the absorption lines; on the two lower panels are the ratios of the equivalent widths of the HeII λ 4686Å lines to Hβ, and the temperature of the hot component of the system, calculated by the ratio of the equivalent widths of the HeII λ 4686Å lines to Hβ. As seen from the figure, the change in the considered parameters of the symbiotic star AG Peg satisfactorily agrees with the period we found for the star's brightness change.

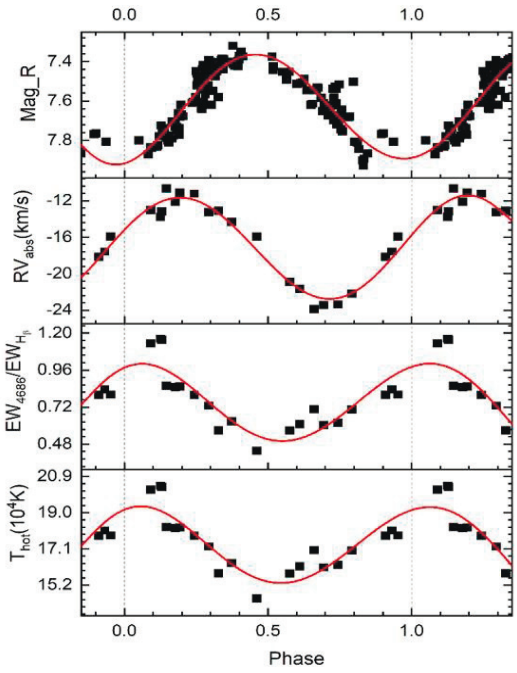

Fig. 1. Dependencies of the orbital period on the parameters of the AG Peg system (see text).

STUDY OF THE ASSOCIATIVE PRODUCTION OF THE HIGGS BOSON WITH THE Z-BOSON USING MVA METHODS

Ahmadov F.N.
Institute of Physics, Ministry of Science and Education, Azerbaijan
Joint Institute for Nuclear Research, Russia
fahmadov@jinr.ru

After the discovery of the Higgs boson in experiments at the LHC, its mass was measured to be 125 GeV. With such a mass, the probability of its decay into bb is greater than the sum of the probabilities of all other decay channels. Therefore, this channel makes a great contribution to the study of the Higgs boson.

To study the Higgs boson in the bb decay channel, a more suitable production channel is associative production with a vector boson. Since the decay of the Higgs boson into a pair of b-quarks was observed for the first time in this production channel. Therefore, we can say with confidence that the VH(bb) (V is Z or W) process is one of the most important channels for studying the properties of the Higgs boson.

Theoretical and experimental data can be analyzed using different methods. Currently, a more promising method is the Multivariate Analysis method (MVA). The MVA method itself is divided into a large number of submethods or algorithms. Two of them that are widely used in high energy physics are Neural Networks (NN) and Boosted Decision Tree (BDT). In the work, these methods were used to separate the signal from the background and the results obtained from them were compared.

The list of input variables for BDT or NN is similar to those used in the analysis in the ATLAT experiment. Up to 0.4 million signals and the same number of background events were used for training. The settings used in the ATLAS analysis, which has the best performance, were chosen to tune the BDT hyperparameters. Various number of events (2K, 5K, 10K, 0.1M, 0.2M and 0.4M) are trained and different settings for NN are obtained, providing performance that exceeds that of BDT. It turns out that for any number of training events, it is possible to find corresponding NN settings with better performance than BDT. The only problem with NN training is that it is computationally intensive compared to BDT.

TEMPERATURES OF THE CENTRAL STARS OF PLANETARY NEBULAE NGC 2392, NGC 1535, NGC 3242, IC 418

*Alili A.H., Alisheva K.I., Mikailov Kh.M.
Baku State University, Azerbaijan
aliliaynura@bsu.edu.azı; kamalaalisheva@bsu.edu.az

Central stars of PN (CSPN) are difficult to study because of their faintness in the visible (due to their high temperature) and the contamination of their spectra by nebular emissions. CSPN undergo considerable changes in temperature over their short lifetimes. The temperatures of the CSPN are considered an important quantity that directly characterizes their evolution. In this study, according to the HeII line calculated the Zanstra temperatures of the central stars of 4 planetary nebulae. For this purpose, by processing the spectra of these nebulae taken from the European Southern Observatory's archive from the observation, was determined the flux in the He_4686 radiation line – F (4686). Then considering absorption in the interstellar medium was calculated according to the following known $F(4686)_{theor.}$ formula

$$lg\frac{F(4686)_{theor.}}{F(4686)_{observ.}} = 1{,}52E_{B-V} \qquad (1)$$

here E_{B-V} is an excess of color. Then the temperatures of the central stars according to the HeII line according to the Zanstra method calculated by the following known expression:

$$F(4686)/F_{\lambda(vis)} = 8{,}49\cdot10^{-11}T^3G_4(T)\left[e^{26650/T}-1\right]\,[\text{Å}] \qquad (2)$$

$F_{\lambda(5450)} - m_v$ visual is a flood of radiation in the visible region of the spectrum determined by star size:

$$F_\lambda = 3{,}68\cdot10^{-9}\cdot10^{-m_v/2{,}5}\,\left[erg/\left(cm^2\cdot s\cdot\text{Å}\right)\right].$$

(2) included in the expression $G_4(T)$ is calculated as following:

$$G_4(T) = \int_{h\nu_4/kT}^{\infty} x^2(e^x-1)^{-1}\,dx. \qquad (3)$$

ν_4 – It is the limit of the main series of HeII, the energy of this quantum is sufficient to ionize a single layer of ionized helium. In (3) – replaced the integral with the sum, in (2) taking into account the temperature was determined by the method of successive approximation. Archieved results are given in table 1. In column 4 of the table has given the magnitudes of the nebulae, in the 5 columns are given the values of the temperatures

that we calculated, and at the last column shows the grades received by other authors.

Table 1.

PN	$\mathbf{F(4686),\times 10^{-11}}$	E(B-V)	V	$F(4686)_{theor.}/\mathbf{F_\lambda}$	T(HeII)	T
NGC 2392	46,5	0,09	9,68	993,675	87184	78000
NGC 1535	0,48	0,02	12,82	179,529	70627	76000
NGC 3242	6,17	0,05	12,15	1252,450	90014	90000
IC 418	0,14	0,2	9,01	1,718	46356	38000

PROMPT PHOTON PRODUCTION IN BREMSSTRAHLUNG AT NICA ENERGIES

[1*]Alizada M.R., [1]Ahmadov A.I., [2]Arbuzov A.B.

[1]Baku State University, Azerbaijan
[2]Joint Institute for Nuclear Research, Russia
mohsunalizade@gmail.com

With energy ranging from 1.5 *GeV* to several 1 *GeV*, prompt photons from proton-proton collisions provide data on the development of the quark-gluon phase, the distribution of partons in nucleons, and the testing of perturbative QCD (pQCD). Prompt photons are produced by the hard scattering of partons in protons, as well as by Compton scattering of quark-gluon, annihilation of quark-antiquark pair, bremsstrahlung of quarks, and other processes. At LHC energies, pQCD in leading order (LO) and next-to-leading order (NLO), is used to characterize these processes

The differential cross-section of bremsstrahlung $qq \to qq\gamma$ has been determined without and taking into account of longitudinal polarization of colliding particles. The dependence of differential cross section of bremsstrahlung process on the energy of the colliding particles $\sqrt{s}$, the transverse momentum p_T, the cosine of the scattering angle *Cos(ϑ)*, the rapidity *y* of photon and x_T has been investigated. Double spin asymmetry of process of bremsstrahlung has been studied. The contributions of Compton quark-gluon scattering, annihilation of quark-antiquark pair, and bremsstrahlung to prompt photon production has been compared.

The dependencies of process of bremsstrahlung on on the energy of the colliding particles $\sqrt{s}$, the transverse momentum p_T, the cosine of the scattering angle *cos(ϑ)*, the rapidity *y* of photon and x_T less than the dependencies of processes of Compton scattering of quark-gluon and

annihialtion of quark-antiquark pair on on the energy of the colliding particles $\sqrt{s}$, the transverse momentum p_T, the cosine of the scattering angle $Cos(\vartheta)$, the rapidity y of photon and x_T.

The contribution of bremsstrahlung to the total differential cross-section of the process of production of the prompt photon is 0.03% of the total differential cross-section. The contribution of Compton scattering quark-gluon, and annihilation of quark-antiquark pair to the total differential cross-section of the process of production of the prompt photon is large and make up more than 50% and 40%, correspondingly of the total differential cross-section.

Polarization of the colliding particle little affects the bremsstrahlung process and strong affects the annihilation of quark-antiquark pair process. Effect of polarization to annihilation and bremsstrahlung process is different.

The double spin asymmetry A_{LL} of process decreases at $\lambda_1\lambda_2<0$ and increases at $\lambda_1\lambda_2>0$ with increasing value of transverse momentum p_T and reaches the plateau.

$f_2(1270)$ TENSOR MESON COUPLING CONSTANT FROM THE HARD-WALL AdS/QCD

[1*]Hashimli Z.I., [1,2,3]Mamedov S.A.

[1]Institute of Physics, Ministry of Science and Education, Azerbaijan
[2]Baku State University, Azerbaijan
[3]Khazar University, Azerbaijan
z.hashimli21@gmail.com

Using the AdS/QCD hard-wall model, we study the $f_2(1270)$ tensor meson-nucleon-nucleon coupling ($g_{f_2\mathrm{NN}}$).

The extension of the Lagrangian in $5D$ space-time is the interaction Lagrangian between the fermionic fields N and the bulk tensor h_{MN}. To achieve this, we need to build the second term in [1] in a hermitian way and substitute the covariant derivatives of the nucleon field for the partial derivative

$$L^{5D}_{f_2NN} = 2i\bar{\psi}\left(\Gamma^M\overleftrightarrow{\nabla}^N + \Gamma^N\overleftrightarrow{\nabla}^M\right)\psi h_{MN} +$$
$$+4(\psi^+\Gamma^0\nabla^M\nabla^N\psi + (\psi^+\Gamma^0\nabla^M\nabla^N\psi)^+)h_{MN}.$$

Eventually, the following interaction Lagrangian allows us to

formulate the 5D action $S^{5D} = \int d^5x\, L^{5D}_{f_2NN}$. We use the Fourier transforms of the nucleon and tensor fields for expressing the action in momentum space after decomposing these fields down into Kaluza-Klein modes.

We determine the coupling constants $g^{(1)}_{f_2NN}$ and $g^{(2)}_{f_2NN}$ for the interaction between the tensor meson and the ground state nucleon by comparing the equation with four-dimensional action. We found the following integral representations for these couplings in the HW model:

$$g^{(1)HW}_{f_2NN} = \frac{M_n}{2}\int_0^{z_m} dz\,\frac{1}{z^4}\left(\left(F_L^{HW}(z)\right)^2 + \left(F_R^{HW}(z)\right)^2\right)h^{HW}(z) = 1.06$$

$$g^{(2)HW}_{f_2NN} = \frac{M_n^2}{2}\int_0^{z_m} dz\,\frac{1}{z^5}\left(\left(F_L^{HW}(z)\right)^2 - \left(F_R^{HW}(z)\right)^2\right)h^{HW}(z) = 0.23.$$

The profile functions of the tensor meson [2] and the fermion field [3] in left- and right-chirality are represented by $h^{HW}(z), F_L^{HW}(z)$ and $F_R^{HW}(z)$.

ON THE DIRECT CORRESPONDENCE BETWEEN THE TRIGONOMETRIC PÖSCHL-TELLER POTENTIAL WALL AND THE QUANTUM SINGULAR OSCILLATOR WITH THE POSITION-DEPENDENT MASS

Nagiyev Sh.M., *Jafarov E.I.

Institute of Physics, Ministry of Science and Education, Azerbaijan
shakir.m.nagiyev@gmail.com

The position-dependent mass concept is one of the successfully developed directions of modern quantum mechanics during the last decades. Their main attractivity is due to two important reasons: the first reason is that they have a huge number of applications for an explanation of the electronic structures of the various solid-state heterostructures thanks to the possibility of introducing the confinement effect successfully through the position-dependent mass; the second reason is related with the certain analytical expressions of the mass varying with position, which leads to the exact solutions of the corresponding Schrödinger equation. All obtained analytical solutions of the Schrödinger equation can reproduce correctly the known similar quantum mechanical systems if one manages to remove the confinement effect and return the position-dependent mass to its constant or homogeneous analogue.

Recently, we have developed the quantum singular oscillator model with the position-dependent mass. It is well known that the singular oscillator has exact solutions in the framework of non-relativistic quantum mechanics. Its wavefunctions of the stationary states are expressed through the generalized Laguerre polynomials and the energy spectrum exhibits close similarity with the non-relativistic quantum harmonic oscillator – it is equidistant and consists of an infinite number of energy levels. At the same time, the trigonometric Pöschl-Teller potential well is also one of the exactly solvable problems of the one-dimensional non-relativistic quantum mechanics. It also has an energy spectrum with similar behavior to the non-relativistic quantum harmonic oscillator energy spectrum, whereas, its wavefunctions of the stationary states are expressed through the Jacobi polynomials. In this presentation, we are going to show that the quantum singular oscillator with certain analytical position dependencies on its mass and the trigonometric Pöschl-Teller potential well problem of the non-relativistic quantum mechanics can be directly connected through the elegant mathematical transform tool between both of their exact solutions.

COULD QUARK STARS BE A SOURCE OF ULTRA-HIGH ENERGY COSMIC RAYS?

Suleymanov M.K.

Baku State University, Azerbaijan

Cosmic rays are vital carriers of information about the creation and evolution of the Universe. However, the origin of cosmic rays with ultra-high energies (>10^{17} eV), whether galactic or extragalactic, remains a mystery. In our paper, we investigate whether dense quark matter—quark-gluon plasma, potentially formed in the centers of neutron stars or Quark Stars (QS), could be a source of these ultra-high-energy cosmic rays. These stars typically emerge from supernova explosions. QS, in particular, are more likely candidates for being the source of ultra-high-energy cosmic rays, although for a long time, they remained unobserved. Only 2-3 experimental observations have been mentioned, none of which were confirmed. However, a recent study proposed that the low-mass companion of the black hole in GW190814 might be a strange quark star. This hypothesis fits within the 'two-families' scenario, where neutron stars and strange quark stars coexist. In this scenario, strange QS can achieve the mass range

indicated by GW190814, M∼(2.5–2.67) M⊙, due to a high adiabatic index, without requiring a velocity of sound near the causal limit. In contrast, neutron stars (or hyperonic stars in the two-families scenario) can meet current astrophysical and nuclear physics constraints, suggesting a softer equation of state. This framework accommodates both the requirements of large stellar masses and small radii with realistic, physically motivated equations of state. It also allows for a radius of a 1.4 M⊙ star to be 11 km or less, unachievable with a singular family of compact stars.

My talk will explore one potential source of ultra-high-energy cosmic particles. I propose that the dense quark-gluon plasma, with a density significantly greater than that of normal nuclear matter and formed in QS, could generate these ultra-high-energy particles. Results from the RHIC and LHC experiments on ultrarelativistic heavy ion collisions suggest that the matter produced in such collisions expands rapidly, displaying collective behavior indicative of an early parton stage in the space-time evolution of the hot, dense matter. This behavior could lead to the formation of a coherent group of partons. A collision between a parton and a coherent parton group, similar to a photon colliding with a high-energy electron, could result in the parton gaining energy through the inverse Compton effect, thereby accelerating without an external field. This mechanism, potentially occurring in QS, might be a novel source of ultra-high-energy particles.

π MESON-Σ BARYON COUPLING CONSTANT IN THE HARD-WALL AdS/QCD MODEL

[1,2*]Taghiyeva Sh.I., [1,3]Mamedov Sh.A.

[1]Baku State University, Azerbaijan
[2]Shamakhy Astrophysical Observatory named after N. Tusi, Azerbaijan
[3]Institute of Physics, Ministry of Science and Education, Azerbaijan
shahnazilgarzade@gmail.com, sh.mamedov62@gmail.com

We define coupling constant between π meson Σ baryon using hard wall in AdS/QCD model which based on AdS/CFT correspondence.

The action for the bulk interaction is defined as:

$$S = \int d^5x \sqrt{g}\, \mathcal{L}_{int}, \tag{1}$$

where $\mathcal{L}_{int}$ is the Lagrangian of the interaction and is defined as below:

$$\mathcal{L}_{int} = -g_Y[\bar{B}_1 X B_2 + \bar{B}_2 X^+ B_1]. \tag{2}$$

We can determine the generating function in the bulk theory in the AdS space using (1) action expression. It is known from the holographic principle that this generating function is identified with the generating function of the boundary theory. Then we can find the vacuum value of the baryon current in the QCD by taking the variation from that generating function. We find the coupling constant between the π meson- Σ baryon comparing obtained current with the current in four-dimensional space as follows:

$$g_{\pi-\Sigma.} = \int_0^{z_m} \frac{dz}{z^5} v(z) P_\pi(z) g_Y \left(f_{1R}(z) f_{2L}(z) - f_{1L}(z) f_{2R}(z)\right). \qquad (3)$$

Here $P_\pi(z)$ and $f_{1,2R,L}(z)$ are profile functions correspondingly for pion and octet baryon fields, and $v(z)$ is expressed for Σ octet baryon as below:

$$v_{\Sigma s}(z) = 2c_2 v_u(z) + (c_2 - c_1) v_s(z). \qquad (4)$$

The numerical value of the π meson- Σ baryon was obtained by calculating the (3) integral expression using the "MATHEMATICA 9" package. The obtained result was compared by light cone QCD sum rule and chiral soliton model.

SINGULARITY ATTENUATION IN GENERAL RELATIVITY WITH QUANTIZED FUNDAMENTAL METRIC

[1*]Tawfik A., [2]Dabash T., [3]Alshehri A.

[1]Future University in Egypt, Egypt
[2]Tanta University, Egypt
[3]Hafr Elbaten University, KSA
a.tawfik@fue.edu.eg

In the most reliable solutions to Einstein's field equations (EFE), the Einstein–Gilbert–Straus (EGS) metric, the space and initial singularities are reexamined. In discretized Finsler geometry, additional curvatures and thereby geometric structures emerge. The resulting generalized fundamental tensor applies quantum-mechanically revisions to the Landau--Raychaudhuri evolution equations. The timelike geodesic congruence in EGS metric is then analyzed. The evolution of a family of trajectories whose congruence is defined by flow lines generated by velocity fields is determined, analytically and numerically. We conclude that both types of singularities seem to be attenuated or even regulate.

APPLICATION OF THE DISTORED-WAVE APPROXIMATION TO THE ELECTRON'S SCATTERING ON THE ATOMS

Mirabutalibov M.M., *Aliyeva M.B.
Azerbaijan State University Oil and Industry, Azerbaijan
mina.aliyeva.b@asoiu.edu.az

Differential section of elastic scattering of electrons, obtained in the distorted-wave approximation, is calculated on the basis of the proposed mathematical method. The electron density distribution in the atom is chosen as a function calculated in the Dirac-Hartree-Fock-Slater approximation, which is superposition of the spherically symmetric Yukawa potential. The differential cross section of scattering of the electrons with the energies 25 eV were calculated for 79Au atom. The obtained theoretical calculations of the cross sections were compared with the experimental data. Besides, the proposed mathematical method simplifies the calculation of integral expressions and makes it possible to obtain a convenient and simple expression for the atomic form factor. Data on the scattering cross sections of electrons on atoms are of considerable interest both in the field of fundamental science for in-depth study of interaction processes and in practical applications, and are necessary in many areas of research, such as modeling low-temperature plasma, astrophysics phenomena, laser physics, and atmospheric effects. etc. In addition to natural phenomena, the processes of collision of electrons with matter play an essential role in plasma technologies, such as, for example, microelectronics and biomedicine. Atomic physics, plasma physics and optics – fields directly related to electron-atom make a significant contribution to the fundamental understanding of the world. Despite the long study of the effects of electron scattering on atoms, and the results obtained in the physics of atomic collisions, this area still requires theoretical and experimental research, there is a significant lack of data on collision cross sections for their subsequent use in modeling and calculations. In particular, there are no systematized data on the cross sections for elastic scattering of high energy electrons by atom.

SYNTHESIS OF NICKEL NANOPARTICLES WITH MAGNETIC PROPERTIES USING THE CARBOTHERMY METHOD

[1*]Bohatyrenko V.A., [2]Kamenskyh D.S., [2]Tkachenko T.V., [2]Khimach N.Y.
[1]Dragomanov Ukrainian State University, Ukraine
[2]V.P.Kukhar Institute Bioorganic Chemistry and Petrochemistry, NAS of Ukraine, Ukraine
vitabog@gmail.com

Recently, there has been a significant increase in interest in the creation of simple methods for obtaining nanoparticles of Ni and some other transition metals that are stable in an oxidizing atmosphere, which is due to the possibility of using them in modern composite materials and, first of all, as carriers of catalytic activity. The complexity of this task is due to the fact, that highly dispersed metallic Ni is easily oxidized and it is necessary to take additional measures to prevent the oxidation of Ni-nanomaterials. Solving the problems of the synthesis of composite materials based on nickel, as well as its compounds (hydroxides and oxohydroxides), may allow replacing metals of the platinum group, which are used in various energy electrochemical processes, which, in turn, will contribute to the viability of the corresponding technologies.

Currently, many methods of obtaining Ni-nanomaterials are known, for example, well-known methods based on chemical and electrochemical deposition, sol-gel synthesis, new methods of hydrothermal, microwave, and sonochemical synthesis. The work used a combined method, where at the first stage the β-modification of nickel hydroxide was precipitated from aqueous solutions of nickel salts under the influence of magnesium. The β-phase is structurally similar to brucite and consists of ordered columns of oriented octahedral layers of $Ni(OH)_2$ (Fig. 1 B), which do not contain additional particles. At the next stage, restorative thermal firing was carried out

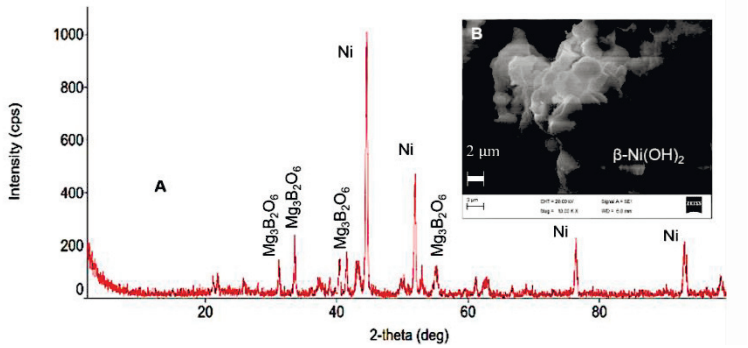

Fig. 1. Diffractogram of the magnetic powder of nickel nanoparticles stabilized by the cotoite phase (A); SEM image of β-$Ni(OH)_2$ – a precursor of soft magnetic powder synthesis Ni (B)

using the carbothermic method under conditions of lack of oxygen and at a temperature of 900 ^{0}C made it possible to obtain a non-pyrophoric highly dispersed nickel powder with the properties of a soft magnetic material, stabilized by the kotoite phase, Fig. 1 A.

The studied method of synthesis combines simplicity of execution with the possibility of obtaining a target product with properties that allow it to be used as a component of various functional composite materials.

SYNTHESIS AND CHARACTERIZATION OF VSi_2-SiC NANOCOMPOSITE POWDERS

Dondash D.O.
Osmaniye Korkut Ata University, Türkiye
didemovali@osmaniye.edu.tr

Ultra-high temperature ceramics (UHTCs) are being studied to find new materials that could be used in high-speed transportation vehicles and power plants. This is necessary since there is a demand for materials that can function in an environment with high levels of oxidation at temperatures as extreme as 2000°C. Today, notable high-temperature structural materials include composites based on SiC and Si_3N_4, oxide ceramics, and SiC-coated carbon/carbon composites. Moreover, recent research has focused on investigating transition metal silicides as structural ceramic materials, primarily because of their exceptional resistance to oxidation and corrosion, as well as their impressive mechanical abilities under high temperatures.

The present investigation employed a hybrid approach of mechanochemical and purifying techniques to obtain VSi_2-SiC nanoparticles. The experiment uses V_2O_5, Si, Mg, and C powders exhibiting a high level of purity as initial materials. An investigation was conducted to grasp the reaction process by varying the milling duration and starting initial powder quantities. The X-ray diffraction technique was utilized to identify the phases that formed during the reaction and those that were subsequently purified. The morphological characteristics of the produced powders were examined using scanning and transmission electron microscopy techniques. The findings indicate that VSi_2-SiC particles were produced along with another stoichiometry of vanadium silicides (V_3Si_5). The intended reaction instantly occurred within a milling period of 10 minutes. The average particle size of the resulting powders was less than 200 nm.

PREPARATION OF GO/AGNWS NANOCOMPOSITE AND INVESTIGATION OF THE EFFECT OF SULFIDATION AND ITS STRUCTURE AND OPTICAL CHARACTERISTICS

*Baghirov M.A., Muradov M.B., Eyvazova G.M., Mammadyarova S.J., Ahmadov X.I.
Baku State University, Azerbaijan
bmbaghir@gmail.com

The composite material consisting of Graphene Oxide (GO) and Silver Nanowires (AgNWs) has garnered significant attention in recent research. These composites exhibit noteworthy characteristics including photonic stability, plasmonic resonance, high surface energy, and biocompatibility. A key feature is the utilization of AgNWs, which possess a one-dimensional structure and are enveloped by GO sheets. This arrangement acts as a scaffold, enhancing the material's electrical conductivity and mechanical flexibility. Additionally, the positioning of AgNWs amidst the GO sheets prevents aggregation, and their separation eliminates issues associated with wire contact. Consequently, these composites find application in generating thin layers with exceptional electrical conductivity, addressing challenges encountered in solar cells and sensors.

In the conducted study, GO synthesized modified Hummer's method and AgNWs synthesized via the polyol approach were combined and treated with ultrasound for 20 minutes. The resulting mixture (GO/AgNWs) was filtered, dried at 60°C, and exposed to H_2S gas.

Structural analysis was performed using an X-ray diffractometer, revealing distinctive peaks at 2Θ=11.09° and 42.06° corresponding to GO, and peaks at 2Θ=38.33°, 44.51°, 64.63°, and 77.58° representing AgNWs in the composite. Following sulfidation, the peaks related to AgNWs vanished, and new peaks corresponding to Ag_2S (2Θ=28.92°, 32.34°, 57.59°) emerged. Additionally, the distance between GO sheets increased from d=80 nm to d=84 nm after sulfidation. This augmentation is attributed to the expanded surface area of AgNWs situated between the GO sheets due to sulfidation, leading to an increased gap between the GO sheets.

Furthermore, UV-Vis spectra of both the initial and sulfidized samples were acquired to assess changes in the band gap. The band gap of the GO/AgNWs composite was determined to be Eg=2.25 eV, whereas after sulfidation, this value decreased to Eg=2.00 eV. This reduction in the band gap is indicative of altered electronic properties in the composite material following the sulfidation process.

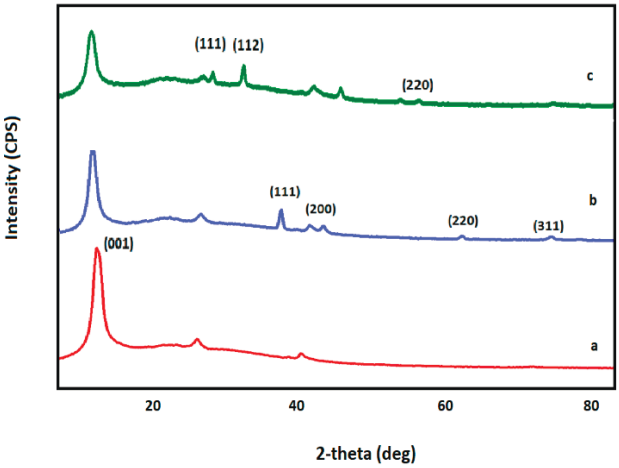

Fig. 1. XRD diffractogram for a) GO, b) GO/AgNWs, c) GO/AgNWs+H_2S

NANOPARTICLE FABRICATION OF $GeBi_2Te_4$ VAN DER WAALS COMPOUND VIA THE BALL-MILLING METHOD

[1*]Mehtiyeva Kh. Z., [1,2] Amiraslanov I. R., [1,2]Aliev Z. S.

[1]Baku State University, Azerbaijan

[2]Institute of Physics, Ministry of Science and Education, Azerbaijan

xatira.mehtiyeva@bsu.edu.az

Layered van der Waals compounds containing group 14 *p*-metals (Ge, Sn, Pb) in combination with pnictogens (Sb, Bi) have attracted considerable attention as quantum materials for their topological quantum states and excellent thermoelectric properties in recent years. Topological Insulators (TI) are a newly discovered topological state of quantum matter and their surface features an odd number of relativistic Dirac fermions. There are insulators in the bulk but show metallic conduction at the surface due to well-defined topological surface states. Their unique spin-oriented properties open up new opportunities for the realization of exotic devices having potential applications in quantum computing, spintronics, topotronics, etc. Manipulating TIs at the nanoscale enhances their quantum effects, making them promising candidates for spintronics, where they can facilitate efficient charge and spin transport, enabling advancements in low-power consumption devices and quantum information processing.

Herein, we report the nanoparticle fabrication of $GeSb_2Te_4$ compound via ball-milling technology based on “top-down” principle. The $GeSb_2Te_4$

single crystal used for raw materials was grown by the Bridgman method. Prior to nanofabrication, the single crystal was checked by XRD technique to test its quality. The typical and high-intensity diffraction peaks confirmed its high crystallinity and lack of any trace of the second phase. The nanofabrication was performed in an 80-mL WC bowl with 15 mm diameter balls, with milled time ranges from 1 hour up to 20h. The nanoparticle sizes were measured for each 5h. The ball-to-material ratio was 30:1 while the milling speed was kept at 450 rpm. In order to avoid particles overheating inside, the milling process was intermittently paused every 30 minutes for 10 minutes.

The crystallite size was determined by analyzing the powder XRD patterns displayed in Figure 1. The comparison of the diffraction lines for the ball-milled material with the single-crystalline one displays significant expansions. These expansions arise both from decreasing the crystalline size and the introduction of lattice strain induced by the ball-milling process. The average crystallite size in this study was calculated using the Scherrer equation.

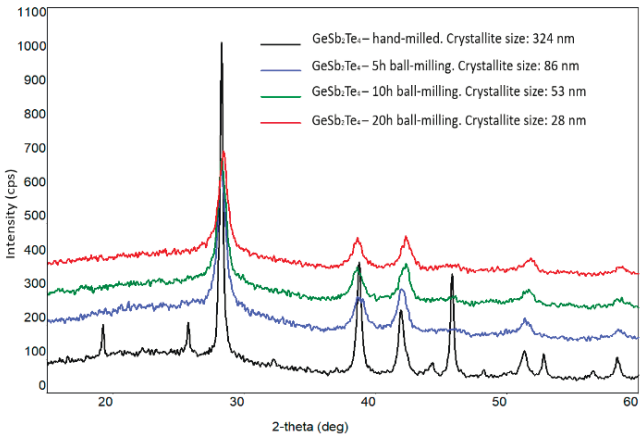

Fig. 1. XRD patterns for hand-milled and ball-milled $GeSb_2Te_4$

In conclusion, if we compare the crystallite size for the hand-milled powder and 20h-milled one (Fig. 1) we can say that the ball-milling technique for the nanoparticle fabrication of the layered $GeSb_2Te_4$ compound works well and this technique can be applied successfully for the other layered quantum materials.

GRAPHENE OXIDE-POLYVINYL ALCOHOL NANOFIBROUS COMPOSITES: ELECTRICAL PROPERTIES

[1]Khanmamadova E.A., [1]Abaszade R.G., [2]Jafarov M.A., [3*]Safarov R.Y.
[1]Azerbaijan State Oil and Industry University, Azerbaijan
[2]Baku State University, Azerbaijan
[3]French-Azerbaijani University, Azerbaijan
elmira.xanmammadova@asoiu.edu.az

Graphene oxide-polyvinyl alcohol (GO-PVS) nanofiber composites represent an attractive combination of materials science and physics. These advanced materials perfectly combine the remarkable properties of graphene oxide (GO) with the versatile and biophysical properties of polyvinyl alcohol (PVA). The synergistic interaction of these components has generated great interest in the fields of materials science and physics. This review highlights the complex manufacturing processes, unique properties, and rigorous electrical analyzes used to explore the fascinating world of GO-PVA nanofiber composites at the intersection of materials science and physics.

EFFECTS OF Se/(Sn+Zn+Sn) RATIO ON THE PROPERTIES OF SINGLE-STEP ELECTRODEPOSITED $Cu_2ZnSnSe_4$ THIN FILMS

[1,2*]El Otmani R., [4]El Khouja O., [1]El Manouni A., [4]GALCA A.C., [2,3]Almaggoussi A.
[1]Hassan II University, Faculty of Science and Technology, Morocco
[2]Cadi Ayyad University, Morocco
[3]Mohammed VI Polytechnic University, Morocco
[4]National Institute of Materials Physics, Romania
elotmani.rokaya@gmail.com

This study investigates the influence of the Se/(Sn+Zn+Sn) ratio on the properties of $Cu_2ZnSnSe_4$ (CZTSe) thin films synthesized via a simple and cost-effective electrodeposition technique. The Se/(Sn+Zn+Sn) ratios were systematically adjusted within the range of 0.01 to 0.09 without the need for selenization. The research explores how these ratios affect the structural, morphological, and optical characteristics of the films.

X-ray diffraction analysis revealed the formation of a kesterite crystal structure, with the degree of preferred orientation varying depending on the Se/(Sn+Zn+Sn) ratio. Raman spectroscopy analysis confirmed the

characteristic peaks of CZTSe films. Interestingly, films deposited with a Cu/(Zn+Sn) ratio of 0.09 exhibited the presence of ZnSe as a secondary phase. Scanning electron microscopy observations indicated changes in grain size, uniformity, and surface morphology as the Se/(Sn+Zn+Sn) ratio was adjusted. Furthermore, UV-visible spectroscopy measurements showed variations in the bandgap energy and absorption coefficient, signifying changes in the optical properties with different Se/(Sn+Zn+Sn) ratios. Notably, the bandgap decreased with an increase in the Se/(Sn+Zn+Sn) ratio.

These findings offer valuable insights into the significant role played by the Se/(Sn+Zn+Sn) ratio in shaping the properties of CZTSe thin films. The results underscore the potential to tailor the structural, morphological, and optical characteristics, with a ratio of 0.01 revealing well-structured morphology, nearly stoichiometric composition, and an optimal bandgap of 1.5 eV, making it an attractive option for efficient solar cell absorption.

INTERACTION OF α-In_2Se_3 CRYSTALS WITH 4-AMINOPYRIDINE

[1]Rahimli A.B., [1.2]Aliev Z.S., [1.2*]Amiraslanov I.R.

[1]Institute of Physics, Ministry of Science and Education, Azerbaijan
[2]Baku State University, Azerbaijan
iamiraslan@gmail.com

Indium selenide (α-In_2Se_3) is a compound semiconductor with a variety of applications, due to its unique electrical, optical, and structural properties. Since 1966, a number of papers have been dedicated to the synthesis and structural analysis of In_2Se_3 crystals.

This report is devoted to the synthesis of a new complex compound formed during the intercalation attempt of α-In_2Se_3 crystals with 4-aminopyridine (4AP) molecules. 4AP molecules cause the formation of new intercalation crystals as a result of their interaction with $InGaS_3$, $FePS_3$ and other layered crystals. Therefore, we thought that a new intercalation crystal would be formed from the interaction of 4AP with layered α-In_2Se_3 crystals. But the interaction of 4AP molecules with α-In_2Se_3 crystals causes more serious changes and leads to the formation of a new yellow complex compound (Fig. 1,a). Our research showed that this reaction occurs at a temperature of 200~250º C, as a result of solid-liquid interaction, that is, after the 4-AP crystals melt.

The diffraction spectrum was studied to obtain information about the structure of this new yellow compound (Fig. 2). It was found that YC is a homogeneous crystalline substance and is characterized by the following orthorhombic unit cell: s.g. $C222_1$, a=25.008(4), b=10.414(2), c=3.907(1). SEM EDS analysis and thermogravimetric analysis were performed to determine the composition. The latter confirm the composition of $In_2Se_3 \cdot 2C_5H_6N_2$ for YC (Fig. 1,b).

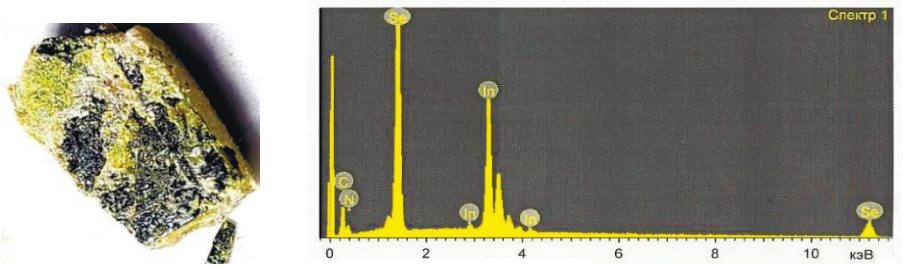

a) b)

Fig. 1. Original α-In_2Se_3 crystals (black regions) and the its interaction with 4-AP (yellow regions) (a); EDS analysis of the yellow substance (b).

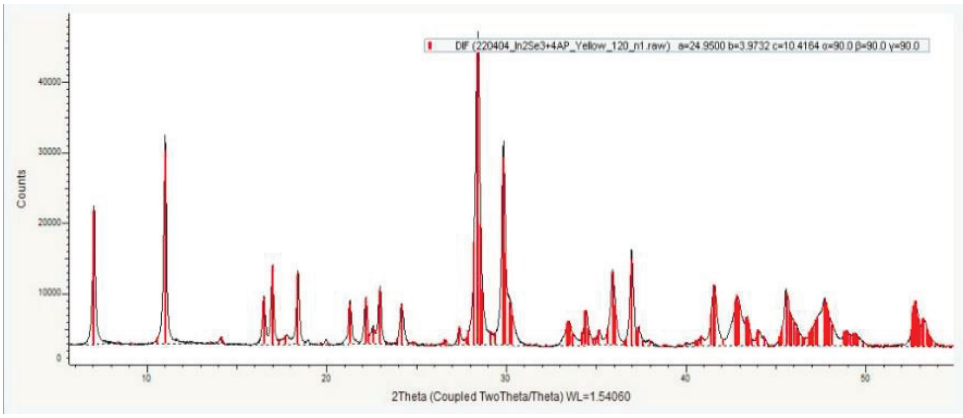

Fig. 2. The diffraction pattern of the yellow powder of interaction α-In_2Se_3 with 4AP.

MICRO-PIXEL HIGH Z SEMICONDUCTOR MATERIALS AS IMAGING DETECTORS

*Guliyev E., Hamzayeva R.
Redlen Technologies Inc., Canada
elmaddin.guliyev@redlen.com

High atomic number and wide band gap semiconductor materials have gained increasing popularity over the past decade. This surge in interest can be attributed to their remarkable performance at room temperature, their capacity to endure sustained exposure to high photon flux, and their ability to facilitate the fabrication of small pixel sizes while maintaining reasonable energy resolution and rapid response times.

In the realm of radiation detection, compounds utilizing Cadmium Zinc Telluride (CZT) have emerged as favored solutions. CZT-based detectors are gaining prominence due to their exceptional detection efficiency, their capability to operate at room temperature, and their proven reliability in compact detection systems utilized across various fields, including medical, astrophysical, and industrial applications. This versatile material is poised to play a pivotal role in advancing detection technology.

Synthesized adsorbents were characterized by the Scanning Electron Microscopy (SEM) with Energy Dispersive X-ray Spectroscopy (EDS) and Ultraviolet-visible Spectroscopy (Uv/Vis). Temperature stability of adsorbent has been investigated by thermal analysis methods (TG, DTA, DDTA).

Resulting products were applied for determination of Fe(III) ions in fruits.

COMPARATIVE ACOUSTIC ANALYSIS OF FIVE RENOWNED OPERATIC TENORS

Bruseldorff A.S.
Azerbaijan National Conservatory, Azerbaijan
alexandriasultan@outlook.com

The research task involves analyzing the unique acoustic characteristics of the voice of the People's Artist of Azerbaijan, professional classically trained opera tenor Samir Jafarov, singing the aria "*Una furtiva lagrima*" from the Italian opera *"L'elisir d'amore"* by Gaetano Donizetti. The comparative analysis also includes the voice characteristics of renowned opera

singers such as Luciano Pavarotti, Placido Domingo, Roberto Alagna, and Pene Pati singing the same aria. Samir Jafarov also has a background in singing mugham, a traditional Azerbaijani musical genre. To discern the unique qualities and nuances of Samir Jafarov's performance in the context of both musical genres, his rendition of the *Bayaty-Shiraz* mugham in a high-pitched *zil* range has also been included in the paper, serving as a point of comparison alongside the operatic compositions.

The same duration was ensured by selecting the same excerpt from the aria *"Una furtiva lagrima"* in each singer's rendition. The research uses the Long-Term Average Spectrum (LTAS) to investigate acoustic parameters, looking for common factors in energy distribution across frequency spectrums. This study focuses on identifying the presence or absence of the singer's formant and examining the spectral slope in the contour of the acoustic spectrum in all five opera singers.

Samir Jafarov's voice was recorded in a professional sound recording studio of the International Mugham Center of Azerbaijan in a soundproof environment. An audio mixing console, Behringer X32, and a NEWMANN U87 Ai professional microphone were used for the recordings at a 48000Hz sampling rate. The microphone was calibrated and positioned at a lip-to-mouth distance of 25 cm and 3 cm below the chin, with 0º angle of incidence.

The samples of the other four operatic tenors were taken from commercially available recordings. The first step involved isolating the instrumental tracks to analyze commercial recordings effectively. Then, all recorded sounds were resampled to 16000Hz using *Sopran* software (www.tolvan.com), a sound editor for processing and analysis of sound files.

The LTAS data showed prominent peaks and valleys in samples of all five singers. It was possible to identify a singer's formant for all samples. Although Azerbaijani vocal mugham singing is different from classical opera, the presence of the singer's formant was also evident in the voice of Samir Jafarov while performing mugham. The analysis of logarithmic trends also revealed that the average spectral slope in the 1000-2000 Hz range varied within 10-15 decibels per octave in four opera singers, while one singer exhibited a slope within the range of 16-17 decibels per octave.

INFLUENCE OF GAMMA RADIATION ON THE CRYSTALLISATION OF PVS/CdS NANOCOMPOSITES

Gasimova A.I., Nuriyev M.A.

Institute of Radiation Problems, Ministry of Sciences and Education, Azerbaijan
a.a7787@mail.ru

In recent years, obtaining new generation polymer-based nanocomposite materials that can be applied in various fields of industry and studying their structure and properties is one of the main priority issues of science and technology. The properties of nanocomposites are determined not only by the size of the filler particles, but also by the physicochemical properties of the polymer matrix.

The thermophysical properties of initial and gamma irradiated PVA/CdS nanocomposites obtained based on the formation of cadmium sulphide (CdS) semiconductor nanoparticles in polyvinyl alcohol (PVA) pores by layered chemical sorption method were studied by analytical methods such as differential scanning calorimetry (DSC). Structural changes induced by the amount of filler and the effect of gamma radiation are discussed.

Comparative analysis of DSC thermograms shows that the crystallization process in pure polyvinyl alcohol proceeds at a higher speed than in composites. Note that the crystallization time (t_c) during cooling after heating in composites was calculated with the help of the following equation:

$$t = (T_0 - T)/v$$

where T_o is the initial temperature of crystallization, and T – the final temperature, υ=10°C/min. - the cooling rate. During the calculations, it was found that as the amount of filler increases in the polymer matrix, the crystallization time also changes. As can be seen, while the crystallization time is low for PVA/3cyc.CdS nanocomposite, this time is increased for PVA/CdS composites formed at 5 and 10 cycles. We assume that the reason for this is that at low amounts of filler, the particles act as crystallization centers and accelerate crystallization. With the increase in the amount of CdS nanoparticles formed in the pores of the PVA matrix, they block the mobility of polymer macromolecules and cause an increase in the crystallization time, slowing down the crystallization process of the composite. The gamma radiation of the samples is higher at 200 and 500kGy doses for PVA and PVA/CdS composites formed at 3 cycles and 5 cycles of crystallization time. In the composites that received a dose of 300 kGy, the crystallization

time takes a smaller value. We believe that the reason for this is the cross-linking processes in amorphous phase of the polymer matrix in the samples that received a dose of 200 kGy, and in amorphous-crystalline phases of the matrix and the polymer-filler boundary in the samples treated with the absorption dose of 500 kGy. In the samples treated with a dose of 300kGy, the destruction begins in the amorphous phase, while the cross-linking process is not active enough in the interphase processes. This case is also evident from the change of melting time depending on the concentration of the nanoparticles and dose.

The sharp increase in the melting time with increasing filler amount in nanocomposites treated at a dose of 500kGy is associated with a decrease in the mobility of molecular chains as a result of crosslinking at the polymer-filler boundary. We can say that the reason for this is hydrogen bonds formed at the polymer-filler boundary and radiation crosslinking.

BAND GAP AND WAVE PROPAGATION ON PVDF BASED TOPOLOGICAL HAUSDORFF AND SERPINSKI DIMENSION OF QUASI-FRACTAL PHONONIC CRYSTALS: FINITE ELEMENTS ANALYSIS

[1]Palaz S., [2]Ozer Z., [3,4]Mamedov A.M., [3]Ozbay E.

[1]Harran University, Türkiye
[2]Mersin University, Türkiye
[3]Bilkent University, Türkiye
[4]Baku State University, Azerbaijan
mamedov46@gmail.com

In this study, the band structures and transmission losses of solid/solid and fluid/solid phononic crystals with Sierpinski Carpet fractal and the digit set of L2 Hausdorff fractal shapes have been investigated. The solid/solid phononic crystals consist of topological insulator (TI) pillars within the organic ferroelectric (PVDF-polyvinylıdene fluoride) matrix, while the fluid /solid phononic crystal consist of a liquid crystal (ZhK440) within the PVDF matrix. The pillars within the Sierpinski Carpet fractal have square and circular cross-sections. Sierpinski Carpet fractal unit cells and Hausdorff fractal unit cells were used to obtain fractal band structures, and these finite structure was used to obtain conduction losses of fractal phononic crystals. Solid Mechanics module in Comsol Multiphysics software was used for solid/solid phononic crystals and Pressure Acoustics modules were used for liquid/solid (ZhK440/PVDF) phononic crystal band structure.

Phononic band diagram ω = ω(k) for a 2- and 3D PC, in which non-dimensional frequencies ωa/2πc (c-velocity of wave) were plotted vs. the wavevector k along the Γ–X–M–Γ path in the square Brillouin zone shows many stop bands in the wide frequency range. The ferroelectric properties of PVDF and the unusual properties of a TI give us the ability to control the wave propagation through the PC over a wide frequency range. TI is a discrete component that allows conducting electricity on its surface but shows insulator properties through its bulk volume. TI is considered as an acoustic topological insulator as the extension of topological insulators into the field of "topological phononics".

COMPARISON OF THE PHYSICAL PROPERTIES OF CDXZN1-XS-BASED NANOCOMPOSITE MATERIALS PRODUCED VIA SONOCHEMICAL AND SILAR APPROACHES

[1]*Gahramanli L.R., [1]Muradov M.B., [1]Eyvazova G.M., [2]Ákos Kukovecz

[1]Baku State University, Azerbaijan
[2]University of Szeged, Hungary
qahramanli.lala@mail.ru

In the presented work, nanocomposite materials based on $Cd_xZn_{1-x}S$ were obtained in the form of thin film and nanoparticle (powder) by two different approaches – sonochemical and SILAR synthesis methods. Structures of thin films and nanoparticles are studied by X-ray Diffraction (XRD), Fourier-transform infrared spectroscopy (FTIR), and Raman microscopy to determine their chemical relationships, and the morphology of nanocomposite materials is determined by Scanning Electron Microscopy (SEM), depending on the synthesis method and the type of samples obtained. has been done. During the acquisition of samples by the sonochemical method, samples were used with 3 different stabilizers and different percentages of these stabilizers for comparison. During the production of thin layers by the SILAR method, these layers were obtained with different compositions (different values of x) and at different synthesis temperatures. The aim of the study is to study the effect of two ripening processes on the structure and physical properties of nanomaterials under the same technological conditions.

From the analysis of the samples by the XRD method, it was determined that the ternary $Cd_xZn_{1-x}S$ nanostructures obtained from the synthesis by the SILAR method and the sonochemical method have the same crystalline structure – hexagonal phase. However, the crystal structure

formed in binary-CdS nanostructures changed depending on the synthesis method. Thus, the CdS nanoparticles obtained by the SILAR method had a cubic structure, and the CdS thin film obtained by the SILAR method had a hexagonal structure.

In addition, depending on the synthesis method, these differences were also observed in the value of the forbidden zone width of the samples. The E_g value of $Cd_{0.2}Zn_{0.8}S$ obtained by the sonochemical method is 2.83 eV, and the E_g value of $Cd_{0.2}Zn_{0.8}S$ obtained by the SILAR method is 3.05 eV. By the same rule, this difference is clearly visible in the values of 2.25 eV (sonochemical) and 2.45 eV (SILAR) observed by CdS depending on these two synthesis methods. During the synthesis of CdS, as well as ternary $Cd_xZn_{1-x}S$ by sonochemical and SILAR methods, the observed differences in structure and E_g value vary depending on the synthesis method, growth mechanism, and reaction mechanism.

PROMISING CARBONS FROM LIGNOCELLULOSIC RAW MATERIALS AND THEIR PROCESSING WASTE

[1]Doroshenko S.O., [1*]Tkachenko T.V., [2]Tamarkina Y.V., [2]Kucherenko V.O., [3]Jafarov M.A., [1,4]Kamenskyh D.S., [1]Povazhny V.A., [1]Yevdokymenko V.O.

[1]V.P.Kukhar Institute of Bioorganic Chemistry and Petrochemistry, NAS of Ukraine, Ukraine

[2]L.M.Litvinenko Institute of Physical-Organic and Coal Chemistry, NAS of Ukraine, Ukraine

[3]Baku State University, Azerbaijan

[4]V. Bakul Institute for Superhard Materials, NAS of Ukraine, Ukraine

ttv13ttv@gmail.com

Lignocellulosic raw materials and their waste are the most promising renewable raw materials today. Even though the carbon materials majority are still obtained from traditional fossil fuels, the transition to lignocellulosic raw materials will reduce the emission of greenhouse gases. Therefore, the purpose of our work was to investigate the influence of different raw materials on the characteristics of the obtained carbon under the same conditions.

Both lignocellulosic raw materials (cotton and hemp) and waste from its processing (hydrolyzed lignin) were used to obtain carbon materials. Carbon materials were obtained by the method of alkaline activation at 700-800 ^oC. The contents of cellulose, hemicellulose, lignin and other chemical components in lignocellulosic raw materials were determined by

standard chemical analysis. All chemical analysis was carried out twice allowing calculating the mean values and standard deviations, which do not exceed 5 %. The obtained carbon materials were studied by using the following methods: low-temperature nitrogen sorption-desorption, XRD, XRF, FTIR-ATR, SEM, and adsorption capacity for iodine.

The SEM analysis showed that the carbon materials retained the shape of the original raw material. The carbon material produced from hydrolyzed lignin has the highest specific surface area of 991 m^2/g and the largest adsorption capacity for iodine at 941±11 mg/g. It has cylindrical pores ranging in size from 1.4 to 28 nm, which indicates the nanoporous structure of the obtained material. At the same time, carbon materials obtained from lignocellulosic raw materials have a specific surface area and adsorption capacity for iodine that is 2-4 times lower.

Thus, under the same production conditions, hydrolyzed lignin proved to be the best raw material for carbons obtaining.

We thank the Armed Forces of Ukraine for safety to carry out this work. This work was only possible thanks to the resilience and courage of the Ukrainian Army

LASER ABLATION ZnCdO THIN FILMS

Jafarov M.A., Mammadov H.M., *Mammadov V.U., Nasirov E.F.

Baku State University, Azerbaijan
mammadovv@gmail.com

Over the past decades, the advancement in the field of thin films technology paved the road for development of various semiconductor-based devices. In this context, zinc oxide (ZnCdO) thin films and nanostructures attracted a great interest, owing to their unique properties such as large exciton binding energy (60 meV), direct wide-bang gap of about 3.37 eV at room temperature, high optical transparency in the visible region, low electrical resistivity, as well as high electrochemical stability, high electron mobility, nontoxicity, and abundance in nature, therefore being used in a wide range of application in the UV region of optoelectronic devices.

Moreover, ZnCdO-based nanomaterials can be considered as promising candidates for solar cells, gas sensors, laser diodes, and so on. ZnCdO films can be grown by several physical and chemical methods such as sputtering, chemical vapor deposition, sol–gel method, molecular beam epitaxy, and pulsed laser deposition on a wide range of substrates. Laser ablation

has been a well-studied techniques since its early days and it has been showing the premises to be implemented to produce n-type ZnCdO thin films.

As an initial step towards our goal, in this study we focus on the preparation of highly oriented ZnCdO thin films by pulsed laser deposition at relatively low substrate temperatures. We take advantage of the PLD technique, namely, by the possibility of controlling the elemental composition of the deposited thin films much better than using other methods. The structure, morphology, composition, and optical properties of the obtained films are characterized by means of X-ray diffraction (XRD), scanning electron microscopy (SEM), and energy-dispersive X-ray spectroscopy (EDS) UV-VIS measurements.

The ZnCdO thin films were deposited on commercially available silicon wafers (cut 5 5 mm) using an ArF laser with a wavelength of 193 nm (Coherent COMPex Pro 205F) by ablating a sintered Zn,Cd target in high purity NaOH solution. The laser repetition rate can be varied from 1 to 50 Hz, and the energy per pulse can be set in the range of 10 to 400 mJ. For this study, the laser was operated at a frequency of 10 Hz with a constant power of 300 mJ.

The dependence of the thin films structure and properties was observed as a function of the substrate temperature. The crystallinity increased for the thin films with the increasing temperature from room temperature to 350◦C. The same behavior was observed for the band gap that changed from 3.12 eV at room temperature, close to the ideal value for the highest substrate temperature studied, with a value of 3.32 eV.

THE EFFECT OF CHARACTERISTIC LENGTHS ON THE NONSTATIONARY CONVERSION OF FREQUENCIES OF ULTRA SHORT LIGHT PULSES

Amirov Sh.Sh.

Baku State University, Azerbaijan
Azerbaijan Medical University, Azerbaijan
Khazar University, Azerbaijan
phys_med@mail.ru

Conversion of frequencies of ultra short light pulses is analyzed in the first and second order approximations of dispersion theory. Influence of group velocity mismatch and group velocity dispersion on the spectrum as well as energy of a light pulse is studied. Analytical expressions for both spectrum and energy of a signal wave in the second order dispersion theory are obtained. Narrowing of the spectrum of signal wave and shift of its

maxima toward smaller values of frequency with increase in the group velocity dispersion are observed.

To convert frequencies of coherent optical radiation along with frequency multiplication the processes of frequency mixing are also frequently used. The frequency mixing in the pump field often requires employment theory of nonstationary interaction of light waves. An interest to this problem is related with the realized of practical opportunity of obtaining of tunable ultraviolet radiation via frequency mixing.

Purpose of present paper is to study theoretically effect of group velocity mismatch and group velocity dispersion on the spectrum and energy of ultrashort light pulse. For this purpose, the theoretical dependences of spectral density as well as energy versus the characteric lengths: ratio of nonlinear length to the quasistatic length and the group velocity dispersion length. The influences of these characteristic lengths on the spectral density and energy of ultra shor pulse are revealed via the depicted dependences. Formula obtained for spectral density of a signal wave is

$$S_1(\omega, z) = D\frac{(sin\lambda' z - tg\lambda' l \cdot cos\lambda' z)^2}{\lambda'^2 + \frac{k^2}{4}tan^2\lambda' l} \cdot \exp\left(-\frac{\omega^2\tau^2}{1 + C^2\tau^4}\right)$$

where

$$D = cn_1\gamma_1^2 I_{30}\, I_{20}\tau^2/16\pi^2,$$

$$\lambda' = {l_{n/l}}^{-1}[\frac{1}{4}\left(\frac{1}{2}(\alpha - 1)\frac{l_{n/l}}{l_{dis.}}\omega^2\tau^2 + \frac{l_{n/l}}{l_v}\omega\nu - \frac{\Delta}{\Gamma_3}\right)^2 - 1]^{1/2},$$

$$k = {l_{n/l}}^{-1}[i(\frac{1}{4}(\alpha - 1)\frac{l_{n/l}}{l_{d.}}\omega^2\tau^2 + \frac{l_{n/l}}{l_v}\omega\nu - \frac{\Delta}{\Gamma_3})\,], \alpha = \frac{g_2}{g_1}$$

It was found that energy of a signal pulse has maxima as a function of ratio of nonlinear length to the quasistatic length at various values of phase modulation parameter.

SOLUTION OF REDUCED EQUATIONS FOR THE PROPAGATION OF AN ULTRASHORT LASER PULSE IN A METAMATERIAL

*Ahmadova A.R., Kasumova R.J., Safarova G.A.
Baku State University, Azerbaijan
asmar.ahmadova.r@bsu.edu.az

The electromagnetic properties of metamaterials are explained by the properties of the microstructures included in the composition of the composite material. The current level of technological development has

already made it possible to develop materials with a negative refractive index in the visible range.

The purpose of this work is to study the non-stationary interaction of waves when mixing three waves in a medium with negative refraction. The results of calculating the shape of the signal spectrum under low-frequency pumping are presented as a first approximation of the dispersion theory. We can analyze the non-stationary process of three-frequency nonlinear parametric interacting waves. For consideration, we assume that the medium is "left" only at the frequency of the signal wave ω_1. We hypothesize that the pump wave is a long pump pulse at a frequency ω_2, as opposed to a short wave pulse in the difference frequency $\omega_3 = \omega_1 + \omega_2$ ($u_{1,2,3}$ are group velocities of the corresponding waves).

We consider that the energy flows of the pump wave and the waves at the sum frequency $S_{2,3}$ normally fall on the left side surface of the metamaterial of length *l* and propagate along the positive direction of the axis. That's, in a medium with a negative refractive index, the energy transfer of the signal wave occurs in the opposite direction. In the first approximation of the dispersion theory, we ignore the effect of dispersive propagation. Let us solve the problem in the case when a pump wave and a wave at the frequency ω_3 are present at the entrance to the "left" medium, $A_1(z = l) = 0;\ A_2(z = l) = A_{20};\ A_3(z = l) = A_{30}$.

As a result, we get the next differential equation of the second order :

$$\frac{d^2A_1}{dz^2} - i(\omega\nu + \Delta)\frac{dA_1}{dz} - \Gamma_2^2 A_1 = 0,$$

where

$$\lambda = \sqrt{\frac{(\omega\nu + \Delta)^2}{4} - \Gamma_2^2}, \nu = \frac{1}{|u_1|} + \frac{1}{u_3}, \Gamma_2^2 = \gamma_1\gamma_3 I_{20}$$

and $I_{20} = A_{20} \cdot A_{20}^*$.

The analysis of the spectrum of the signal wave, which only takes into account the divergence of the group velocities, showed that the spectral dependence is symmetric. In the Gaussian form of the input excitation pulse, the energy of the side components is moved to the central maximum. Furthermore, as the group velocity mismatch increases, the spectrum of the excited pulse becomes narrower.

INFLUENCE OF RARE EARTH METALS ON ELECTROPHYSICAL PROPERTIES OF GES LAYERED MONOCRYSTALLINE

Dashdemirov A.O., *Alekperov A.S.
Azerbaijan State Pedagogical University, Azerbaijan
arzu.dashdemirov@adpu.edu.az

The photoconductivity of the GeS: Er layered monocrystalline in a wide range of temperatures has been studied. In the temperature domain 125÷250K, the activation energy was ΔE=0.20 eV, and in the temperature domain 250 ÷ 320K, it was E=0.4 eV. And when T > 300K, the crystal loses photosensitivity, the electrical conductivity is metallic. Complex complexes formed by ER atoms on the surface and volume of the crystal create deep centers of seizure and recombination. With an increase in temperature, there is a discharge of these centers, a jump of load carriers into the conductive zone. Because of this, the photosensitivity of the crystals decreases, the electrical conductivity is metallic. The restoration of its former photosensitivity by recooling of the crystal makes it possible to make thermoachar from GeS:Er layered monocrystals.

MODIFICATION OF SLC-0111 AS NOVEL CARBONIC ANHYDRASE INHIBITORS

*Guliyeva L., Trawally M., Demir-Yazıcı K., Guzel-Akdemir O.
Istanbul University, Türkiye
lalagulieva.lq@gmail.com

Carbonic anhydrases, which facilitate the interconversion of CO_2 and HCO_3^-, are metalloenzymes that are present in numerous organisms. As of now, a total of 16 α-CA isoenzymes have been identified, of which 13 are catalytic and 3 are acatalytic. Human CAs (hCAs) that are catalytically active are involved in a variety of vital physiological processes, including respiration, gluconeogenesis, lipogenesis, and ureagenesis. On the contrary, an uncontrolled activity and aberrant (over)expression have been linked to a variety of diseases, including oncogenesis (hCA IX and XII), retinal edema, glaucoma (hCA I), Alzheimer's disease, and epilepsy (hCA II). As a result, therapeutic interventions involving the development of potent molecules capable of selectively targeting these disease-associated isoenzymes appear extremely promising.

SLC-0111, a ureido substituted benzenesulfonamide compound that is presently undergoing Phase Ib/II clinical trials against solid tumours as a leading selective hCA IX inhibitor. SLC-0111 has K_i values of 5080, 9640, 4.5 and 45.1 nM for hCA I, II, IX, and XII, respectively. In this study, structural modification of SLC-0111 has been herein exploited as a lead molecule for development of novel series of thiosemicarbazone incorporating benzenesulfonamide. The designed compounds were synthesized, characterized and tested for their carbonic anhydrase inbitory activity against hCA I, II, IX and XII. Compounds 1, 2, 3 and 4 showed K_i values of 3.7, 0.4, 16.8 and 2.8 nM against hCA I, II, IX and XII, respectively.

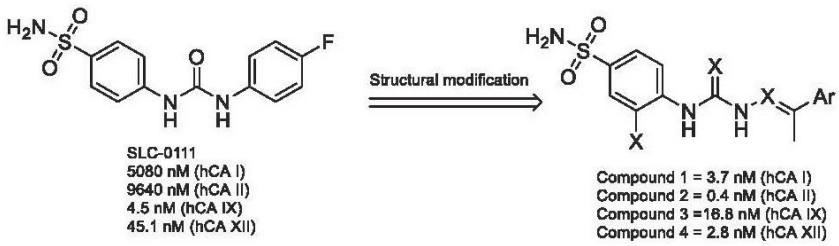

Fig. 1. Structural modification of SLC-0111

RADIOBIOLOGICAL RESEARCH AT JINR ACCELERATORS

Bugay A.N.
Joint Institute for Nuclear Research, Russia
bugay@jinr.r

Research infrastructure of JINR provides unique opportunities for conducting interdisciplinary basic and applied research in life sciences. JINR's radiobiological research program is aimed at studying the action of ionizing radiations, especially high energy heavy ion beams, at the molecular, cellular, tissue, and organismal levels of biological organization. Special attention is paid to the development of new approaches to increasing the effectiveness of radiation therapy of cancer and research on radiation-induced functional disorders of the brain.

INTERACTION MECHANISM OF GLYCYRRHIZIN FOR THE COVID-19 TREATMENT

*Galandarli L.E., Akverdieva G.A.
Baku State University, Azerbaijan
leyla_aktau@mail.ru

Identifying biological targets and studying the molecular mechanisms of action of drug compounds is a critical task from the point of view of not only fundamental science but is also necessary for the creation of new effective and safe drug compounds. Glycyrrhizin, a glycoside contained in extracts of licorice roots (Radices glycyrrhiza), is the calcium and potassium salt of tribasic glycyrrhizic acid, the aglycone of which is glycyrrhizic acid. Licorice root and its extracts have been used in traditional medicine to alleviate bronchitis, gastritis, and jaundice since ancient times. Anti-inflammatory, antiallergic, antiviral, mineralocorticoid, antitumor, immunomodulatory, antiulcer, hepatotropic, and other positive effects of glycyrrhizin on the human body have been shown. Recently, more and more publications have appeared on the effectiveness of glycyrrhizin against infection caused by SARS-CoV-2. The direct antiviral effect of glycyrrhizic acid on the SARS-CoV-2 coronavirus was proven by scientists from the University of Duisburg-Essen and the Ruhr University in Bochum (Germany). It turned out that glycyrrhizic acid caused the death of viruses by inhibiting the synthesis of protease, an enzyme vital for the SARS-CoV-2 virus.

In this work, molecular docking was used to examine the interactions between the glycyrrhizin molecule and SARS-CoV-2 main protease by AutoDock Vina software. The 3D crystal structure of the SARS-CoV-2 M^{pro} protease was retrieved from the protein data bank at http: //www.rcsb.org (PDB ID: 7ZQV). Water and ligand molecules in the receptor were removed, and the receptor was made ready for docking by adding only polar hydrogens. The structure of the glycyrrhizin compound was obtained with ChemSpider (ID: 14263). Kollman charges of the receptor were also calculated. Partial charges of ligand were calculated using the Geistenger method. PyMol and Discovery Studio 3.0 programs were used for 2D diagrams and 3D molecular visualization and analysis of receptor-ligand interactions. It was shown that the title molecule binds at the active site of the receptor and forms key interactions by nonpolar, polar, and ionic contacts. The calculated binding energy and *rmsd* can conclude that glycyrrhizin can be a potential inhibitor for the SARS-CoV-2 M^{pro} protease and

may be used for COVID-19 treatment. Based on the received results the model of pharmacophore of glycyrrhizin for its interaction with SARS-CoV-2 proteases was proposed.

DARK-INDUCED CHLOROFILL DEGRADATION IN COTTON PLANTS SEEDLINGS

***Ahmadov I.S., Eyvazova G.M., Hasanova F.V., Babanlı S.T.**

Baku State University, Azerbaijan

ismetahmadov@mail.ru

Leaf senescence is an active process due to degradation of chlorophyll pigment in photosynthetic cells and is a key aspect of plant life for remobilization of resources. Regulation of this process is an important condition for the normal development and productivity of plants. As a result of various studies, it has become clear that the degradation of chlorophyll pigment in the leaves of birches deprived of light is a complex process. Light in photosynthesizing leaves, in order of importance plays an important role in the regulation of leaf senescence. For many plant species, lack of light, that is, strong shading of the leaves, leads to their rapid yellowing. Until now, the mechanism of chlorophyll degradation and the factors influencing this process have not been fully studied. Degradation of chlorophylls in leaves occurs mainly through pheophorbide oxygenase (PAO). Recently, 6 types of enzymes responsible for chlorophyll catabolism have been identified and their functions have been clarified.

The aim of this study was to determine the effect of nanoparticles on the senescence of cotton leaves by measuring the content of chlorophyll. In the presented research, the effect of nanoparticles on the degradation of chlorophyll and carotenoids, photosynthetic rate, Fv/Fm ratio and production of oxidants, ie. H_2O_2 and superoxide radical (O_2^-), lipoxygenase enzyme activity (LOX), and antioxidant enzymes SOD and CAT activity in 14-day-old cotton seedlings under dark conditions was investigated. Metal-based nanoparticles (ZnO, CuO, Fe_2O_3,TiO_2) were used in the experiments. Cotton was grown in a controlled environment plant growth chamber. First, the compounds of chlorophyll and carotenoids were measured in the leaves of the third tiers of 14-day-old cotton seedlings, and then the seedlings were kept in the dark. The kinetics of the process depends on the composition and size of the nanoparticles. Nanoparticles do not signi-

ficantly affect the increase of H_2O_2, superoxide anion during chlorophyll degradation, but ZnO nanoparticles do. Lipoxygenase, SOD and CAT enzymes activity in this process of nanoparticles is not seriously affected. Thus, it can be concluded that nanoparticles can play an important role in the regulation of chlorophyll degradation.

STRUCTURAL ORGANIZATION OF LACTOFERROXINE C

*Agayeva L.N., Abdinova A.A., Akhmedova S.R., Akhmedov N.F.
Baku State University, Azerbaijan
leylanamig@mail.ru

A number of exogenous peptides derived from nutrients have opioid-like properties. Lactoferroxine is a glycoprotein present in milk and small amounts in exocrine fluids such as bile and tears. It consists of a single-chain polypeptide and is relatively resistant to proteolysis. Complete DNAs for lactoferroxine from human milk, neutrophils, and cow's milk have been reported, and recombinant proteins have been produced. It has been hypothesized that, due to its iron-binding properties, lactoferroxine plays a role in the absorption of iron by the intestinal mucosa and acts as a bacteriostatic agent by retaining iron in iron-requiring bacteria. In addition, lactoferroxine may act in non-iron-mediated pathways as a growth factor and bactericidal agent.

The three-dimensional structure of the lactoferroxin C molecule (H-Lys1-Tyr2-Leu3-Gly4-Pro5-Gly6-Tyr7-OH) was studied in fragments. First, based on the low-energy conformations of the corresponding amino acid residues, the conformational capabilities of the N-terminal tetrapeptide fragment Lys1-Tyr2-Leu3-Gly4 and the C-terminal tetrapeptide region Gly4-Pro5-Gly6-Tyr7 were studied. The calculation results showed that energy differentiation occurs between the main chain forms and conformations. The N-terminal tetrapeptide fragment is represented by eight forms of the main chain, the energy of which varies in the range of 0 – 8.0 kcal/mol. The C-terminal tetrapeptide region is also represented by eight forms of the main chain, the energy of which varies in the range of 0 – 4.0 kcal/mol. These forms of the main chain were chosen as initial approximations when calculating the spatial structure of the lactoferroxin C molecule.

As can be seen, these two fragments are connected by a common amino acid residue Gly4, which has four forms of the main chain R, B, L

and P. Therefore, when compiling the initial approximations, all these forms were taken into account and several hundred conformations of the heptapeptide molecule were calculated. The calculation results showed that a sharp energy differentiation occurs between shapes, main chain forms and conformations. It has been shown that the spatial structure of the lactoferroxin C molecule can be represented by eight forms of the main chain, the relative energy of which varies in the energy range 0 - 8.0 kcal/mol. In low-energy conformations, the energy of nonvalent interactions changes in the energy range (-31.4) – (-19.5) kcal/mol, the energy of electrostatic interactions in the range (5.3) – (9.3) kcal/mol and torsion interactions in the range (3.3) – (8.2) kcal/mol. The most stable conformation for the lactoferroxin C molecule is $B_{1222}R_1R_{21}BBB_{311}B_3$. It turns out to be advantageous in terms of non-valence and electrostatic interactions. In this structure, the Tyr2-Leu3 residues form an unfolded form of the main chain, which allocates the first amino acid residue Lys1 and the C-terminal tetrapeptide region -Gly4-Pro5-Gly6-Tyr7.

ULTRASTRUCTURAL CHARACTERISTICS OF THE ACCUMULATION OF IRON NANOPARTICLES IN INTESTINE AND LIVER OF COMMON CARP (*CYPRINUS CARPIO* LINNAEUS, 1758)

*Mammadov Ch.A., Hajiyeva A.D., Khalilov R.I.
Baku State University, Azerbaijan
m_chingiz@yahoo.com

The penetration, bioaccumulation of Fe_3O_4 nanoparticles, which widely used in the industry, having magnetic features, in the intestine and liver, its structural elements of common carp (*Cyprinus carpio* Linnaeus, 1758) breed in aquaculture conditions, and the ultrastructural characteristics of possible pathomorphological changes occurring there were studied using light and electron microscopic methods.

Two different doses (10 and 100 mg per 10 g of food) of Fe_3O_4 nanoparticles with size 20 nm were fed to fingerlings for 7 days, then intestinal and liver samples were taken and studied. In addition studying to the normal ultrastructure of the small intestine of the fish, on the 7th day of the use of nanoparticles (at a dose of 10 mg), the disintegration of the villi of the enterocytes of the mucosa layer and the pathology of the cytoplasmic structures of the cells was observed. Also, ultrastructure of the fish's liver in

norm, liver studied after the administration of a small dose (10 mg) of nanoparticles and changes were observed in erythrocytes located in the lumen of blood vessels, hepatocytes, intracellular canaliculi and bile ducts. On the 7th day of administration of a 100 mg dose of nanoparticles, it was determined at the ultrastructural level that destructive changes occurred in all layers of the small intestine (serosa, muscularis, sub-mucosa and mucosa) and its structural elements. At a high dose (100 mg) the capsule of the liver was damaged, some of the hepatocytes were completely destroyed, the wall of the blood vessels was damaged, and the structure of the wall of the biliary ductule was disturbed. The sequential entry and bioaccumulation of Fe_3O_4 nanoparticles consumed with food into the host organism have been confirmed by electron microscopy, starting from microvilli located on the apical surface of enterocytes in the intestinal villi. From there, they enter the cytoplasm of epithelial cells, including cytoplasmic organelles such as the nucleus, mitochondria, lysosomes, and microvilli. Subsequently, they pass through the specialized lining of the small intestine and interact with the endothelium of blood vessels and erythrocytes in the mesentery. Finally, they reach hepatocytes, cytoplasmic organelles within them, and are further distributed into lymphatic capillaries and lymphatic vessels.

TEMPERATURE-INDUCED PHASE TRANSITIONS OF LIPIDS EXTRACTED FROM HUMAN LUNG CARCINOMA AND NORMAL CELLS

[1*]Aydemirova A.H., [1]Bakhishova M.J., [1]Aslanov R.B., [1,2]Melikova L.A., [1]Gasymov O.K.

[1]Institute of Biophysics, Ministry of Science and Education, Azerbaijan
[2]National Center of Oncology, Ministry of Health, Azerbaijan
arzuaydemirova491@gmail.com

Cancer is one of the deadliest diseases and is a central healthcare problem in the world. Lung cancer, also known as lung carcinoma, is the most common and serious type of cancer. Cancer cells of various organs, such as the lung, breast, colon, etc, experience multistep metabolic changes in their development. The lipid re-programming of cancer cells is a critical metabolic event. As a result, lipid compositions of the cancer cell membranes are significantly altered. The desaturation process observed in cancer cells significantly modifies the physicochemical properties of cell membranes. Particularly, cis-conformation in monounsaturated fatty acids bends acyl chains and decreases packing density that, in turn, increases the dynamics of the cell membranes.

FTIR spectroscopy was applied to the lipids extracted from human lung carcinoma and normal cells for structural characterizations of the lipids. Temperature-induced phase transitions of the lipids were evaluated using the CH_2 symmetric stretching (around 2850 cm^{-1}) and CH_2 asymmetric stretching (around 2923 cm^{-1}) frequencies. The positions of both bands are sensitive to the order parameters of the lipid chains. The CH_2 symmetric stretching for ordered and disordered systems shows frequencies at 2849 cm^{-1} and 2854.5 cm^{-1}, respectively. The CH_2 asymmetric stretching for ordered and disordered acyl chains display frequencies of 2917 cm^{-1} and 2927.0 cm^{-1}, respectively. Temperature-induced phase transitions were evaluated in temperature interval of 20°C- 44°C. All lipid samples show ordered to disordered transitions upon increased temperatures. However, there are significant differences in the phase transitions of lipids of cancer cells compared to those of healthy cells. The CH_2 symmetric stretching frequencies show a midpoint of transition for healthy and cancer cells 312.4 ± 2.5°C and 307.7± 2.6°C, respectively. Very similar data were obtained for the CH_2 asymmetric stretching mode. The cooperativity of temperature-induced transitions of lipid fractions of normal and cancer cells are also significantly different. The lipids from normal cells show a more cooperative transition compared to that of the carcinoma cells. Cooperativity values for the lipids extracted from healthy and cancer cells were determined to be 0.14± 0.09 and 0.08±0.03 (p-value= 0.022).

Thus, the temperature-induced phase transition of lipid fractions of healthy and cancer cells show considerably different characteristics that are consistent with our previous finding indicating more dynamic behavior for cancer cell membranes.

MOLECULAR MODELING APPLIED TO THE NEW CHEMICAL COMPOUNDS

*Akverdieva G.A, Demukhamedova S.D.
Baku State University, Azerbaijan
hagverdigulnara@gmail.com

Numerous chemical compounds are the most important objects that play a significant role in the targeted synthesis of new advanced materials including physiologically active drugs with improved properties. The study of various important reactions is carried out based on created models. Therefore, the search for new chemical substances with specific

activity is a problem that requires the use of modern molecular modeling techniques. In this work, the role and possibilities of molecular modeling methods in research on the two newly synthesized chemical compounds - N-substituted thiourea and its complex with $CuCl_2$, and also titanium complex ligand of the ionic-liquid type (ILT) are discussed. Thiourea and its complexes with various metals play an exceptional role in almost every field of chemistry and can be widely used in both medicine and industry. Phenolate complexes of transition metals with various bi- and polydentate heteroatomic ligands have attracted the attention of researchers as highly efficient precursors of catalysts for olefin oligomerization and polymerization. The DFT/B3LYP level of theory has been used to determine the geometric, energy, and electronic parameters, frontier molecular orbitals energies, atomic charges, HOMO-LUMO energy gap, and chemical reactivity descriptors for these compounds. MEP has been visualized to identify the sites of electrophilic and nucleophilic regions of these molecules. To elucidate the electron density transfer hyperconjugative interactions NBO analysis has been carried out for these compounds at the same level of DFT theory. The study results indicate the formation of stable states of the investigated new chemical compounds. The data obtained allowed us to predict the reactivity abovementioned substituents.

The nature of the substituent in thiourea favors the formation of a stable five-membered ring via coordinate bonding N_6-Cu_{25} and N_{17}-Cu_{25}. In addition, the thiocarbonyl and methyl groups form a pseudo-six-membered ring via the $C_{10}H_{13}\cdots S_5$ hydrogen bond in this complex. The possible canonical structures due to typical resonance interactions of the functional groups were revealed for this compound and its complex. NBO analysis demonstrates that the strongest delocalizations arise at the transfer from n_1(N1) and n_1(N6) hydrogen-bonded N atoms into the σ*(C4-S5) anti-bonding orbital in thiourea with the stabilization energy of 64.54 and 74.67 kcal/mol, respectively, and into the π*(C4-S5) anti-bonding orbital in complex with the stabilization energy of 34.24 and 17.49 kcal/mol, respectively.

The proposed model of the titanium complex forms a stable structure that is stabilized by forming coordinate interactions Ti_1-O_2 and Ti_1-O_3. It was found the distances H_{35}-Cl_{73} and H_{37}-Cl_{72} distances underwent significant changes, leading the values of the distances N - H to 1.62Å, and H - Cl to 1.37Å. According to the NBO analysis, we obtained rather strong

interactions, which are typical for the determination of the intermolecular hydrogen bonds nN···σ* between lone pair of nitrogen atoms N_{34} and N_{36} and antibonding orbitals Cl_{73}-H_{35} and Cl_{72}-H_{37} with stabilization energy of 46.80 and 48.86 kcal/mol, respectively.

It was found the optimized structures of the investigated chemical compounds agree with the experimental data.

REFRACTOMETRIC INVESTIGATION OF THE HYDRATION PROCESS IN ELECTROLYTES

Masimov E.A., Pashayev B.G., Shahbazova G.M., *Teymurova J.Z.
Baku State University, Azerbaijan
jalateymurova98@gmail.com

It is known that the solvation process (hydration process when the solvent is water) in electrolyte solutions characterizes the interactions of all components of the solution with the solvent and with each other. The hydration process is the basis of all energetic and structural changes that occur in such systems.

The experiences show that the translational movements (displacement mobilities) of water molecules that are very close to the ion change due to the influence of dissociated ions in the aqueous solutions of electrolytes. In some cases, the mobility increases depending on the nature of the ions, while in other cases, it decreases. It should be noted that these changes in mobility bring about different values compared to the values in pure water for transport phenomena such as viscosity, diffusion, heat conduction, and so on. Certainly, in both cases, the structure and thermodynamic state of water change.

The direction and degree of changes in translational movements are related to the ion's polarization ability, radius and surface charge density. Ions with a small radius and a high surface charge density accelerate the movement of water molecules around ions. Conversely, ions with a large radius and a low surface charge density weaken them. These processes also alter the equilibrium lifetime of water molecules around ions (in a certain dance), the activation energy required for their exchange with water molecules, the exchange probability, and the exchange rates.

Taking into account what has been said, it should be noted that the hydration process is not limited by this. The electric field of the ion affects the distribution of charges to some extent within water molecules that are bonded to each other via hydrogen bonds, and it also changes the conditions for the formation of hydrogen bonds. This leads to a change in the overall structure of the system. However it can be challenging to determine the range over which the ion's field affects water molecules. Therefore, we believe that evaluating these effects may be more appropriate by investigating the structure or thermodynamic state of the solution, rather than solely by determining the properties of hydration numbers. In the presented work, it has been taken into consideration that determining the sum of hydration numbers ($h_1 + h_2$) of dissociated ions in electrolytes is more useful in studying their influence on the structure of aqueous solutions. This approach has been experimentally investigated for several ions. For this purpose, a simple refractometric method has been used.

It has been found that the values of the parameter $h_1 + h_2$ differ directly among ions with different characteristics. At the same time, the addition of certain polymers to aqueous solutions of electrolytes also alters the $h_1 + h_2$ parameter. The obtained results indicate that the changes are related to the interactions of polymer molecules with water molecules, depending on the nature of the hydrophobic and hydrogen groups present in their composition.

NON-LETHAL TESTING OF THE ACUTE TOXICITY OF NEWLY DEVELOPED COMBINED CANCER TREATMENT MODALITIES AGAINST CHICK EMBRYOS AND WARM BLOODED MAMMALS

[1]*Mitagvaria N., [1]Chirakadze A., [1]Chubinidze G., [1]Dvali N., [1]Khuskivadze N., [2]Shanidze R., [2]Abuladze M., [3]Khomeriki I., [3]Tserodze K.

[1]Caucasus International University, Georgia
[2]Kutaisi International University, Georgia
[3]Georgian Technical University, Georgia
nodmit@gmail.com

One of the most important characteristics of medical and veterinary drugs is their acute toxicity to the warm-blooded mammals, birds and other animals. Modern standards of humane treatment of test animals exclude the death of animals, causing them severe pain, significant deterio-

ration of health, prolonged forced immobility, whole body anesthesia, etc.) are becoming increasingly stringent, and the modern methods of animal testing must be fitted to all modern 4 R (replace, refine, reduce, responsibility) principles of the humane treatment of laboratory animals. Our team for several years successfully develops and applies various original methods of the non-lethal and sub-lethal testing of acute toxicity of the developed drugs, insecticides and other modalities against chick embryos, using the so called visible (red and green) light and infrared ovoscopy methods in combination with plethysmography, as well against the white rats passing through the branched maze, using the so called combined toxicity index (CTI) method, which accounts for eight dimensionless values characterizing the total number of decisions, total number of mistakes, total time of passing through the maze, the total time spent in the lighted areas, and the relative change of blood systolic pressure, body temperature, concentratio of reactive oxygen species in blood and the absolute averaged value of the blood oxygen saturation during passing through the branched maze. Acute toxicity of gemcitabine, of mixture of gemcitabine and DMSO, and of the four newly developed anticancer combinations (containing cesium chloride, rubidium chloride, cesium carbonate, rubidium carbonate, DMSO and saline solutions) against chick embryos and white Wistar rats was tested using the both above non-lethal methods. Images derived using visible light ovoscopy of chick eggs with normally developing Golden Wyandotte embryos provide sufficent resolution during the first 8 days of incubation. After the 8th day of incubation it is rather difficult to get high resolution red light images, and the green light ovoscopy becomes highly preferable. After day 14 plethysmography becomes the best one and allows to monitor the development of embryos until they hatch. It is highly important, that the viability of embryos is more than 90% and that all exposed rats fully restore their behavioral and physiological status in 14-15 days after the exposure. The results obtained are in good coincidence testifying in favor of the confidence and reliability of the obtained data. Acute toxicity of gemcitabine was found to be significantly higher, than the toxicity of newly developed anticancer drugs.

ALKALI METAL SALT SOLUTION BASED COMBINED CANCER THERAPY AND THE "HIGH PH THERAPY" CONCEPT

[1*]Khuskivadze N., [1]Chubinidze G., [1]Mitagvaria N., [1]Chirakadze A., [1]Dvali N., [1]Chichua T., [2]Abuladze M., [3]Khomeriki I., [3]Buachidze Z.

[1]Caucasus International University, Georgia
[2]Kutaisi International University, Georgia
[3]Georgian Technical University, Georgia
nanakhuskivadze53@gmail.com

The concept of multicomponent strongly localized combined therapy of malignant tumors including various widely used and novel anticancer treatments was first proposed at the end of the last decade. This concept has acquired a particular importance due to Georgia and whole South Caucasus after founding of a modern proton therapy center in Kutaisi. One of the modern approaches is the implementation of the so-called "high pH hypothesis" suggesting that alkali metal salts create a highly alkaline intracellular environment and can cause death of cancer cells, whereas heavier elements can have a more pronounced effect. According to this concept, dysregulation of cellular pH is very frequent in solid tumours and provides potential opportunities for therapeutic intervention. This can promote migration, invasion and metastasis of cancer cells through a variety of mechanisms. Thus, the increase of intracellular alkalinity could be an effective tool against the tumour proliferation In order to assess the ability of RbCl, CsCl, Rb_2Co_3, Cs_2Co_3 to inhibit the proliferation of A549 (lung cancer cells) and NHDF cells (normal human dermal fibroblast cell) MTT assay was performed using Gemcetabine standard saline solution and Gemcitabine DMSO solutions as as standard control samples due to their very high apoptotic activity. The cytotoxicity (anti-proliferative efficacy) of all above formulas in terms of LC_{50} and cell viability was determined, which showed it to be quite high, although significantly lower than the efficacy of gemcitabine solution. All of the tested compounds possess differential yet significant cytotoxicity to A549 cancer cell lines several times lower cytotoxicity to the towards the normal NHDF cell line in comparison to both Gemcetabine solutions. Despite of our expectations, based on the so called "high pH Therapy" concept, RbCl efficacy in inhibiting proliferation of A549 (LC_{50}: 56.82 ± 3.51 μM) was significantly higher as compared to CsCl, Rb_2Co3 and Cs_2Co_3. The most important finding of the research (approved by the Annexin V-FITC/PI staining tests showing the high apoptotic potency

of RbCl and other Cs and Rb based solutions mixed with DMSO), is that due to the considerably higher toxicity to cancer cells compared with healthy cells they can provide the increased effectiveness and safety in comparison to the widely ised chemotherapeutic drugs (gemcitabine, cisplatin, etc.).

ISOTOPIC ENRICHED BORON AND BORON NITRIDE NANOMATERIALS FOR PROTON-BORON CAPTURE AND BORON NEUTRON CAPTURE THERAPY OF CANCER

[1*]Dvali N., [1]Khuskivadze N., [1]Chubinidze G., [1]Mitagvaria N., [1]Chirakadze A., [1]Chichua T., [2]Chikadze N., [3]Khomeriki I., [3]Buachidze Z.

[1]Caucasus International University, Georgia
[2]Tbilisi State University, Georgia
[3]Georgian Technical University, Georgia
ndvdvali@gmail.com

The first experimental proof of the capacity of $^{11}B + p$ reaction to enhance the proton therapy effectiveness was reported by G. Cirrone et al in 2018. Along with the advantage of using a neutron-free nuclear fusion reaction, $p+^{11}B \rightarrow 3\alpha$ cross section becomes signifcantly high at relatively low incident proton energy, i.e. around the Bragg peak area. Numerical simulation carried out in the Institute of Physics of the National Academy of Science of Ukraine according our request showed that an optimized distribution of the highly enriched isotopic ^{10}B, ^{11}B nanoparticles and Li atoms, generated as a yield of nuclear reactions $p+^{11}B \rightarrow 3\alpha$ and $^{10}B + n \rightarrow \alpha + ^{7}Li$, can also improve the spatial distribution of the proton beam and reduce the spread of secondary neutrons in the healthy tissues. Even if a non-negligible concentration of ^{11}B nuclei is present in the healthy tissues surrounding the tumor, the number of fusion events would be relatively low, or completely absent, due to the non-favourable incident proton energy spectrum away from the tumor region. Cirrone et al showed that the isotopically enriched boron enhanced Proton therapy could acquire the benefts of an enhanced efciency in cancer cell killing, moving close to ^{12}C ion hadrontherapy, but without complications of the latter. Taking into account that lithium induces autophagy by inhibiting inositol monophosphatase, the potenty of lithium for increasing the biological effectiveness of proton therapy utilizing the nuclear reactions is also of great interest. The bioavalibility and manufacturability of boron nitride nanosheets with encapsulated nanoparticles are significantly higher than that of pure boron,

that is why we started the development of an enhanced low-temperature gaseous synthesis of boron nitride nanosheets with encapsulated silver doped lanthanum manganite and nickel-copper alloy superparamagnetic nanoparticles and the study of their morphology, crystallinity, magnetic properties and acute toxicity of the synthesized nanomaterials. The proposed paper reports the main results on the synthesis methods and properties of the nanosheets and thehighly promizing possibility of combining boron-neutron/therapy, boron-proton capture therapy with Curie temperature controlled magnetic hyperthermia based on the boron nitride nanosheets decoreted with various superparamagnetic particles.

VISIBLE LIGHT AND INFRARED OVOSCOPIC STUDY, PLETHYSMOGRAPHY AND SONOGRAPHY OF BIRD EMBRYOS AND LONG TERM MONITORING OF BEHAVIORAL AND PHYSIOLOGICAL PARAMETER OF WHITE RATS IN TESTING OF ACUTE TOXICITY OF DRUGS

[1*]Chichua,T., [1]Dvali N., [1]Khuskivadze N., [1]Chubinidze G., [1]Mitagvaria N., [1]Chirakadze A., [2]Chikadze N., [3]Khomeriki I., [3]Buachidze Z.

[1]Caucasus International University, Georgia
[2]Tbilisi State University, Georgia
[3]Georgian Technical University, Georgia
temchi@gmail.com

Researchers are using animals to learn about the most widespread diseases of the age, including heart disease and cancer, as well as to gain basic knowledge in genetics, physiology, and other life sciences. Animals are also needed to combat new diseases, of which the SARS-2 syndrome is currently the most prominent example. According to the Nuremberg Code adopted in 1947, any experiments carried out on human beings should be “designed and based on the results of animal research”. The Helsinki Declaration, adopted in 1964 also notes that medical research on human subjects “should be based on laboratory and animal experiments or other scientifically established facts”. In our opinion, many currently used mandatory near-lethal methods of animal laboratory testing, apart from ethical and humane concerns, do not meet the requirements of adequacy and reliability, as they are obtained on healthy animals, but are usually applied to seriously or even critically ill patients. That is why we propose a novel approach that aims to achieve as much balance as

possible between patient interests, reliable and adequate testing using laboratory animals, and maximal consideration of ethical values and the requirements of the humane treatment of animals. The most important component of our conceptual approach is the ovoscopic and sonographic testing of acute toxicity of drugs on chicken embryos and testing of the behavioral and physiological para meters of warm-blooded white rat mammals using long-term (14-21 days) monitoring under conditions of exposure and keeping that exclude death, infliction of severe pain, prolonged immobilization or severe restriction of mobility, prolonged anesthesia, prolonged forced separation or prolonged isolation of animals or other forms of inhumane treatment. Presented paper reports all the three newly developed methodologies for the non-lethal testing of the acute toxicity of a wide range of the widely used chemotherapeutic drugs in comparison withg gemcitabine and a number of their combinations. The paper clearly shows the advantages of combining the all above methods of the non-lethal testing.

THE PRODUCTION OF AAA-BOSONS IN e^-e^+-ANNIHILATION

Abdullayev S.K., *Gojayev M.Sh.
Baku State University, Azerbaijan
macidqojayev@gmail.com

The process of the generation of CP-odd AAA-bosons in electron-positron annihilation $e^-e^+ \to AAA$ is investigated within the framework of the Minimal Supersymmetric Standard Model (MSSM) and taking into account arbitrary polarization states of the e^-e^+-pair. As is known, the vertices ZHH, Zhh, ZhH and ZAA are forbidden by CP-invariance in the MSSM, where $H(h)$ and A – CP-even and CP-odd Higgs bosons. In the model under consideration, the allowed vertices are ZHA and ZhA. In this case, the process $e^-e^+ \to AAA$ occurs according to the following scheme: e^-e^+-pair annihilates into a vector Z^*-boson, which decays into CP-odd A-boson and CP-even Φ^*-boson ($\Phi^* = H^*$ or h^*), and then the virtual Φ^*-boson decays into two A-bosons.

With the longitudinal polarization of the e^-e^+-pair, the expression for the differential cross section of the reaction $e^-e^+ \to AAA$ is obtained as

$$\frac{d\sigma(\lambda_1,\lambda_2)}{dx_1 dx_2 d\Omega} = \frac{G_F^3 M_Z^6}{248\sqrt{2}\pi^4} \cdot \frac{r_Z}{s(1-r_Z)^2} \times$$

$$\times [g_L^2(1-\lambda_1)(1+\lambda_2) + g_R^2(1+\lambda_1)(1-\lambda_2)F_1, \quad (1)$$

where s is the square of the total energy e^-e^+-pairs in the center of mass system, λ_1 and λ_2 are the helicity of the electron and positron, $r_Z = M_Z^2/s\,, x_i = 2E_i/\sqrt{s}\ (i = 1,2,3)$ is the scaling energy of the Higgs bosons, g_L and g_R are the left and right coupling constants of the electron with the Z-boson, F_1 is some function of the energies x_1, x_2, x_3 and the departure angles of the Higgs bosons θ_1, θ_2 and θ_3, $d\Omega$ is the solid departure angle of the A-boson with 4-momentum k_1. It follows from formula (1) that an electron and a positron must have opposite helicities $e_L^- e_R^+$ or $e_R^+ e_L^-$. Therefore, the process $e^-e^+ \to AAA$ must have a right-left spin asymmetry

$$A_{LR} = \frac{g_L^2 - g_R^2}{g_L^2 + g_R^2} = \frac{1-4x_W}{1-4x_W+8x_W^2}, \quad (2)$$

depending only on the Weinberg parameter $x_W = sin^2\theta_W$. With the value of this parameter $x_W = 0.2315$, the left-right spin asymmetry is A_{LR} =14%.

In the case of transverse polarization of the e^-e^+-pair, the differential cross-section of the process under consideration is expressed by the formula

$$\frac{d\sigma(\vec{\eta}_1, \vec{\eta}_2)}{dx_1 dx_2 d\Omega} = \frac{G_F^3 M_Z^6}{248\sqrt{2}\pi^4} \cdot \frac{r_Z}{s(1-r_Z)^2} [(g_L^2 + g_R^2)F_1 + 2g_L g_R \eta_1 \eta_2 F_2], \quad (3)$$

where F_2 is a function depending on the variables $x_1, x_2, x_3, \theta_1, \theta_2$ and θ_3. From formula (3) it can be seen that the process $e^-e^+ \to AAA$ must have a transverse spin asymmetry

$$A_\varphi = \frac{2g_L g_R}{g_L^2 + g_R^2} \cdot \frac{F_2}{F_1}. \quad (4)$$

Calculations show that the value A_φ is negative and decreases with an increase in the departure angle θ_1. The experimental study of the $e^-e^+ \to AAA$ process is it allows us to determine the constants of the three Higgs boson interactions λ_{hAA} and λ_{HAA}.

CURRENT OSCILLATIONS IN SEMICONDUCTORS

*Rzayeva U., Hasanov E.
Baku State University, Azerbaijan
Ulviyyerzayeva58@gmail.com

At availability of an electric field electronic and holes receive from electric field energy can overcome Coulomb barrier of unitary infected center and to be grasped. Due to thermal junction, electrons can be generated from impurity centers from deep traps in the conduction band. The capture process decreases, and the transfer process increases the number of electrons in the conduction band.

$$n_0 = n_+ n_-.$$

The continuity equation for electrons and holes in a semiconductor will be:

$$\frac{\partial n_-}{\partial t} + divj_- = Y_-(0)n_{1-}n_- - Y_-(E)n_-n,$$

$$\frac{\partial n_+}{\partial t} + divj_+ = Y_+(E)n_{1+}n_+ - Y_+(0)n_+n,$$

$$\omega_1^4 = \omega^4 + \omega^2(v_-^2 + v_+^2) + v_-^2 v_+^2,$$

$$E_0(\omega) = E_1 = \frac{|R_1|\mu}{R|\theta_-^\mu|} \cdot \frac{1}{e\eta\delta}, E_2 = \frac{4|R_1|}{R|\theta_-^\mu|}\frac{\mu}{\mu_-} \cdot \frac{1}{e\eta\delta}\frac{v_-}{v_+} = E_2$$

$$E_0 = E_3 = \frac{6|R_1|\mu}{R|\theta_-^\mu|\mu_+} \cdot \frac{1}{e\eta\delta}\frac{\eta_-}{v_+}$$

Waves with frequencies $\omega_1 < \omega_2 < \omega_3$ are excited at electric fields $E_1 < E_2 < E_3$. expressions for the oscillation frequency of the current and for the electric field show that the carrier scattering constants $\theta_\pm^\mu$ have a negative sign. With current oscillations in the circuit, resistance of a negative nature occurs.

If

$$R = |R_1|, \frac{\mu}{\mu_+} \approx 10, \frac{v_-}{v_+} \sim 10, ev\delta \sim 10^{-1}$$

$$E_1 \sim 10^3\ V/sm,\ E_2 \sim 4 \cdot 10^3\ V/sm;\ E_3 \sim 6 \cdot 10^3\ V/sm$$

With these estimates, the frequency of oscillation

$$\omega_1 \sim 3 \cdot 10^7, \omega_2 \sim \frac{\sqrt{5}-1}{2} \cdot 10^9 \frac{1}{sec}, \omega_3 \sim \frac{\sqrt{5}+1}{2} \cdot 10^9 \frac{1}{sec}$$

It means that microwave current oscillations occur i.e. microwave radiation energy from the above semiconductor. The magnetic field is determined from the inequality $\mu_{\pm} H \gg C$. To determine the range of variation of the electric field, and the frequency of oscillation with a further increase in the electric field, we must construct a nonlinear theory.

ANALYTICAL SOLUTION OF THE DIRAC EQUATION FOR THE LINEAR COMBINATION OF THE MANNING-ROSEN AND YUKAWA POTENTIAL IN THE CASE OF EXACT SPIN SYMMETRY

*Ahmadov A.I., Aslanova S.M.
Baku State University, Azerbaijan
sariyaaslanova@bsu.edu.az

The Dirac equation, which is the relativistic wave equation of fermions, can be written in the atomic unit system ($\hbar = c = 1$) for a particle of mass M, influenced by a repulsive vector potential $V(r)$ and an attractive scalar potential $S(r)$ fields:

$$[\vec{\alpha}\vec{p} + \beta(M + S(r))]\psi(r) = [E - V(r)]\psi(r) \qquad (1)$$

The main goal of this work is to analytically solve the Dirac equation for the sum of the Manning–Rosen and Yukawa potentials in the case of exact spin symmetry. In the case of exact spin symmetry, accepting condition $d\Delta/dr = 0$ gives $\Delta = const$. Consider the case where $\Sigma(r)$ is equal to the sum of the Manning-Rosen and Yukawa potentials $\Sigma(r) = V_{MR}(r) + V_y(r)$, then we get:

$$V_{MRY}(r) = \frac{2\delta^2\alpha(\alpha-1)e^{-4\delta r}}{M(1-e^{-2\delta r})^2} - \frac{2\delta^2}{M} \cdot \frac{Ae^{-2\delta r}}{1-e^{-2\delta r}} - \frac{2\delta V_0 e^{-2\delta r}}{1-e^{-2\delta r}}. \qquad (2)$$

We consider the potential (2) in the Dirac equation.

$$\left\{\frac{d^2}{dr^2}-\frac{k(k+1)}{r^2}-[M+E_{nk}-C]\sum(r)+\right.$$

$$+[E_{nk}^2-M^2+C(M-E_{nk})]\}F_{nk}(r)=0. \quad (3)$$

Here we apply a new approximation to the centrifugal limit in equation (3) $1/r^2=(4\delta^2e^{-2\delta r})/(1-e^{-2\delta r})^2$:

$$\frac{d^2F_{nk}}{ds^2}+\frac{1-s}{s(1-s)}\frac{dF_{nk}}{ds}+\frac{1}{s^2(1-s)^2}\times$$

$$[\alpha^2s^2-\beta^2s(1-s)-\gamma^2(1-s)^2-k(k+1)s]F_{nk}=0 \quad (4)$$

By applying the Nikiforov-Uvarov method and solving equation (4), we can write the energy spectrum in the following form for the general case where the vector potential is different from the scalar potential:

$$M^2-E_{nk}^2=C(M-E_{nk})\times$$

$$\left[\frac{\beta^2-k(k+1)-\frac{1}{2}-n(n+1)-(2n+1)\sqrt{\left(k+\frac{1}{2}\right)^2+\alpha^2}}{n+\frac{1}{2}+\sqrt{\left(k+\frac{1}{2}\right)^2+\alpha^2}}\cdot\delta\right]^2 \quad (5)$$

Using the relationship between the Jacobian polynomial and the hypergeometric function, we can write the function $F_{nk}(s)$ as follows:

$$F_{nk}(s)=C_ns^\gamma(1-s)^{\frac{1}{2}-\sqrt{\left(k+\frac{1}{2}\right)^2+\alpha^2}}\cdot P_n^{(2\gamma,2\sqrt{\left(k+\frac{1}{2}\right)^2+\alpha^2})}(1-2s), \quad (6)$$

here, the normalization constant C_n is found from the normalization condition and is as follows:

$$C_n=\sqrt{\frac{2\delta\cdot n!\,(n+k+1+\gamma)\Gamma(2\gamma+1)\Gamma(n+2\gamma+k}{(n+k+1)\Gamma(2\gamma)\Gamma(n+2\gamma+1)\Gamma(n+2k+2)}}. \quad (7)$$

As a result of the research, the Dirac equation was solved analytically in the case of exact spin symmetry for the linear sum of the Manning-Rosen and Yukawa potentials. Analytical expressions dependent on quantum numbers n and k were obtained here for the specific value and specific function of energy.

PAIRED SPIN CORRELATIONS OF ELECTRONS, POSITRONS AND γ - QUANTA IN THE PROCESS OF PHOTOLOGY OF e^+e^--PAIRS ON NUCLEI WITH ACCOUNT OF RECOIL EFFECTS AND NUCLEI STRUCTURE

Rajabov M.R.

Baku State University, Azerbaijan
m_rajabov@mail.ru

The process of photoproduction of e^+e^--pairs on nuclei is not only a source of electron and positron beams, but also a reliable tool for studying the electromagnetic structure of nuclei.

In this work, the differential cross section of the process is integrated over the emission angles of electrons and positrons and an analytical expression is obtained taking into account nuclear recoil and pair electron-positron, photon-lepton and photon-antilepton spin correlations.

From the integral cross section it follows that a pair can be produced in spin states where the electron and positron have both the same and opposite helicity. Taking into account pair spin correlations of particles, the energy distribution of both the relative probabilities of pair formation and the degrees of pair polarization for the same and opposite orientations of the electron and positron spins was studied. Calculations show that the energy distribution of the degrees of polarization of the pair and the relative probabilities of production strongly depend on the structure and recoil energy of the nuclei.

OPTICAL PROPERTIES OF $PBMOO_4$ CRYSTALS DETERMINED BY SPECTROSCOPIC ELLIPSOMETRY

[1*]Darvishov N.H., [1]Rustamov F.A., [1]Mamedov M.Z., [1,2]Gasanly N.M.

[1]Baku State University, Azerbaijan
[2]Middle East Technical University, Türkiye
n_darvishov@mail.ru

We investigated the optical properties of $PbMoO_4$ single crystals grown by Czochralski method. PbMoO4 belongs to space group of ($I4_1/a$) and possesses C_{4h}^6 symmetry group and four molecular formula unit cell (Z = 4). Tetragonal lattice structure forms for $PbMoO_4$ with lattice constants a = b = 5.4360 Å and c = 12.1106 Å. The melts prepared by heating of PbO and MoO_3 oxides were placed in a Pt crucible for crystal growth

process. The pulling, rotation and cooling rates were adjusted to 2 mm/h, 20 rpm and 30 ◦C/h, respectively, in the growth period. The produced long crystal was cut and both faces of the resulting piece of the crystal was polished to obtain high quality $PbMoO_4$ material. The dimensions of the studied sample were around 15 × 12 × 1.5 mm^3. The structural properties of the grown crystals were explored by XRD measurement carried out by Rigaku Miniflex diffractometer having Cu-Kα (λ = 1.54 Å) radiation source. Room temperature spectroscopic ellipsometry measurements were achieved by a SOPRA GES-5E rotating-polarizer ellipsometer operated in the spectral region between 1.0 and 5.5 eV with steps of 0.01 eV. Incident beam was dispatched to prepared sample at an angle of 70º.

Optical band gap of $PbMoO_4$ crystals was found to be 3.09 eV by the help of Tauc plot revealing an existence of indirect band gap in the crystal band structure. Real part of the complex dielectric function and refractive index exhibited increasing behavior up to around 4.0 eV in which they had immediate decrease above this value. Zero frequency refractive index and dielectric constant were found to be 2.04 and 4.15, respectively, using Wemple and DiDomenico model. High frequency dielectric constant was predicted as 4.36 by Spitzer-Fan model. Presence of two critical point energies was revealed with energies of 3.57 and 4.34 eV by achieving the second-energy derivative analysis of dielectric function. It was determined that $[MoO_4]^{2-}$ complexes and charge transfer from Pb^{2+} ions into the neighboring Mo groups were responsible for these interband transitions. Dissipation function increased with increasing photon energy.

THE TEMPERATURE DEPENDENT DIELECTRICAL PROPERTIES OF PtSi/nSi SCHOTTKY DIODES

[1*]Afandiyeva I.M., [1]Lebedeva N.N., [1]Akhundov Ch.G., [1]Bagirova S.E., [2]Babayeva R.F.

[1]Baku State University, Azerbaijan

[2]Azerbaijan State University of Economics, Azerbaijan

afandiyeva@mail.ru

Contact structures based on the Schottky barrier play an important role in modern electronics. These structures have some advantages over p-n-junctions: simple technology, a wide selection of contact materials, high conversion speed, small geometric areas.

In the presented work, a diode structure with small geometric area ($8x10^{-6}$ cm^2) was fabrication by the using magnetron sputtering method.

n-Si (111) with a resistance of 0.7 Ω·sm and a thickness of 3.5 μm was used as a semiconductor wafer.

Al was used as an ohmic contact. However, it is known that Al has great diffusion ability. To prevent the penetration of Al through the silicide film, a diffusion barrier of an amorphous $Ti_{10}W_{90}$ alloy was placed between PtSi and Al.

To study the dielectric parameters of the diode, the dependences of capacitance and conductance on voltage were measured in the temperature range of 79K-360K. Based on the obtained data, the real and imaginary parts of the dielectric constant and the loss tangent were calculated. The dependences of the parameters on voltage and temperature were analyzed.

It was revealed that with an increase in the applied voltage, ε' and ε'' increase. With increasing temperature, an increase in these parameters is also observed. However, the dependence on temperature is irregular. In the dependence of $tan\delta$ on voltage, a peak is observed at 0.74-0.82V. At voltages greater than 1 V, $tan\delta$ values do not depend on voltage. At the same time, $tan\delta$ values increase with increasing temperature.

The obtained result correlates with those previously presented in our article. It was revealed that in the border region there are patches in which the concentration of carriers is different and a tunneling process is observed at low temperatures.

ACTIVATION ENERGY OF GAMMA-IRRADIATED HDPE+ %A-AL_2O_3 NANOCOMPOSITES

Nabieva A.N.

Institute of Radiation Problems, Ministry of Sciences and Education, Azerbaijan
aysel.nabiyeva21@gmail.com

In the power industry, inorganic filler (particularly aluminum nitride (AlN), boron nitride (BN), silicon dioxide or silica (SiO_2), aluminum oxide or alumina (Al_2O_3), titanium oxide or titania (TiO_2), silicon carbide (SiC) and zinc oxide (ZnO), etc.) are usually incorporated into electrical insulating polymers to achieve specific electrical, mechanical, and thermal properties. In this work, the activation energy of composite system based on high-density polyethylene (HDPE) with filler of alumina oxide (α-Al_2O_3) was studied using the method of Thermally Stimulated Depolarization

Current (TSDC) spectroscopy. HDPE+α-Al_2O_3 nanocomposite system (the volume of Al_2O_3 was 0-10%) obtained by hot pressing method in powder technology.

Firstly, the samples are converted into electrets by keeping them in the corona discharge zone at 6kV voltage for 300 seconds. TSDC spectra are recorded in the temperature range of 0-170°C by placing between two planar electrodes. Irradiation of polymer and composite samples with gamma quanta was carried out in the MRX-γ-25 device, which works on the basis of the ^{60}Co isotope.

Before and after irradiation (D=0,50kGy,100kGy), the conductivity activation energies were calculated according to the main maximum in the TSDC spectrum of the samples by the initial growth method.

As a result of the research, it was determined that for corona electrets obtained at a voltage of 6kV, in the case of D=0Gy, the activation energy in HDPE+10% α-Al_2O_3 samples before irradiation is the highest (E_a=0.43eV), and in HDPE+5% α-Al_2O_3 samples, the activation energy is the lowest (E_a=0.189eV).

After D=50 kGy γ-irradiation, the value of activation energy for pure HDPE practically does not change (from 0.94eV to 0.92 eV). The value of activation energy of HDPE+1% α-Al_2O_3 composite samples increases from 0.49 eV to 0.69 eV. After irradiation, the smallest E_a was observed in the HDPE+10%α-Al_2O_3 composite sample (Ea=0.34eV).

After D=100 kGy γ-irradiation, the value of activation energy for pure HDPE is decreases from 0,92eV to 0,35 eV. As the volume fraction of the filler increases up to 10%, the value of activation energy increases, as can be seen from table1.

Table 1

D, kGy	0	1%	5%	10%
0	0,94	0,49	0,189	0,43
50	0,92	0,69	0,7	0,34
100	0,35	1,16	1,44	1,63

Consequently, the influnce of the volume fraction of the filler and γ-irradiation to the composite system are individual.

DIELECTRIC PROPERTIES OF POLYPROPYLENE/ZnO BASED NANOCOMPOSITES

*Nuriyeva S.G., Gasimova J.N., Shirinova H.A., Karimova A.H., Gahramanli L.R.
Baku State University, Azerbaijan
aliyeva-s@list.ru

It was discovered that the dielectric properties of polymer nanocomposite materials containing ZnO nanoparticles were different. This provides the way for their use in a wide range of electrical applications. The dielectric properties of these nanocomposites are determined by the matrix-particle adhesion, numerous interactions between the semiconductor and dielectric phases, the composite's supermolecular structure, and the manner of nanocomposite material creation.

Using solution mixing and hot pressing techniques, nanocomposite materials are created by incorporating ZnO nanoparticles (NPs) into a polypropylene (PP) matrix. Thin films of PP/ZnO polymer nanocomposites with various weight compositions were prepared: 1%, 3%, 5%, 7%, and 10%.The dielectric permitivity of PP/ZnO nanocomposites at room temperature has been examined in dependence on logarithmic frequency and temperature.It has been demonstrated that the dielectric permitivity increases as the number of ZnO nanoparticles in the PP matrix increases.The dielectric permivity of the nanocomposites decreases as the frequency of the applied field increases. This is due to the material's dipoles being unable to follow the high frequency of the applied field, resulting in a decrease in dielectric permivity at high frequencies.

ELECTRICAL CONDUCTIVITY OF $FEGA_{0.4}IN_{1.6}SE_4$ CRYSTAL IN ALTERNATING ELECTRIC FIELD

[1*]Niftiyev N.N., [1,2]Mammadov F.M., [1]Aghayeva R.M., [3]Muradov M.B.
[1]Azerbaijan State Pedagogical University, Azerbaijan
[2]Institute of Catalysis and Inorganic Chemistry, Ministry of Sciences and Education, Azerbaijan
[3]Baku State University, Azerbaijan
namiq7@bk.ru

In this work, the electrical conductivity of $FeGa_{0.4}In_{1.6}Se_4$ compound at different frequencies and temperatures was studied. $FeGa_{0.4}In_{1.6}Se_4$ crystallizes into trigonal syngonium with lattice parameters $a = 3.983$ Å and $c = 38.811$ Å.

Figure 1 shows the dependence graph of electrical conductivity on the frequency of the electric field in the temperature range of $294{,}5 \div 343K$ for the $FeGa_{0.4}In_{1.6}Se_4$ crystal. It can be seen from the figure that with the increase in frequency, the electrical conductivity increases according to the law $\sigma \sim f^S$. It is known that in crystalline and amorphous semiconductors, if the change of electrical conductivity depending on the frequency occurs according to the law $\sigma(\omega) \sim \omega^S$, $0.01 \leq S \leq 1.0$, then it is assumed that there is a jump mechanism in the conductivity [1].

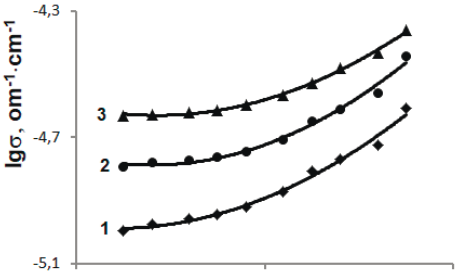

Fig. 1

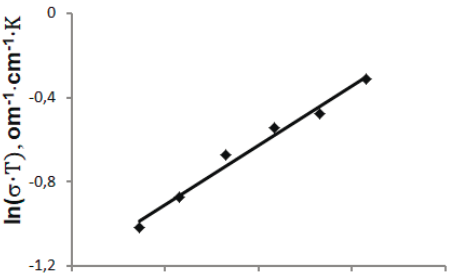

Fig. 2

So, this time, the frequency dependence of the conductivity is expressed as follows:

$$\sigma(\omega)T \sim \omega \left\{ ln\left(\frac{\nu_f}{\omega}\right)\right\}^4 \sim \omega^S \qquad (1)$$

The temperature dependence of σ is expressed as follows:

$$\sigma(T)_\omega \sim \frac{1}{T} exp\left(\frac{T}{T_o}\right) \qquad (2)$$

Here – ν_f is the phonon frequency, T_0 is the characteristic temperature. According to expression (2), the dependence of electrical conductivity on temperature at temperatures $T > T_0$ should give a straight line in the coordinate $ln(\sigma \cdot T) \sim f(T)$. The experimental dependence of $ln(\sigma \cdot T) \sim f(T)$ at the frequency $\nu = 10^6\ Hz$ in the $FeGa_{0.4}In_{1.6}Se_4$ crystal is shown in Fig. 2. It can be seen from the figure that the dependence is in the form of a straight line. This corresponds to the conductivity jump mechanism. On the other hand, the temperature dependence of electrical conductivity in the $FeGa_{0.4}In_{1.6}Se_4$ crystal has the character of activation. Therefore, the conductivity in the $FeGa_{0.4}In_{1.6}Se_4$ compound is characterized by the mixed zone – jump mechanism.

NICKEL-CONTAINING THERMOPLASTIC ELASTOMER NANOCOMPOSITES BASED ON POLYPROPYLENE

*Guliyeva T.M., Kurbanova N.I.
Institute of Polymer Materials, Ministry of Science and Education, Azerbaijan
turkanquliyeva30@gmail.com

Thermoplastic elastomers (TPE) are one of the major constructional materials in modern mechanical engineering. Its products are widely applied as sealing elements in various cars and mechanisms. Despite the obvious advantages of thermoplastic elastomers in their manufacture, there are problems associated with the compatibility of the blended components of the mixture. This problem becomes even more urgent when polar polymers are used as blended polymers. In particular, we are talking about non-polar polyolefins and polar synthetic elastomers. In this regard, various methods are being adopted to improve the technological compatibility of polymer mixtures by introducing into their composition various modifiers, compatibilizers, structurants, plasticizers, etc.

In the presented work, we studied the effect of small additives of nanofillers (NF) containing nickel oxide (NiO) nanoparticles stabilized by a polymer matrix of high-density polyethylene, the properties of mixed TPE based on isotactic PP and NBR with 18% acrylonitrile. Ratio of composition components (wt. %): PP/NBR/NF=50/50/ (0.5; 1.0; 2.0). The phase composition of the obtained nanocomposite was studied by X-ray diffraction analysis. It is shown that in the studied nanocomposites reflections from the planes of the crystal lattice of metals were observed, corresponding to the d_{hkl} series of nickel oxide (NiO), according to the ASTM file.

The physic-mechanical and thermophysical properties of the resulting nanocomposites were studied. Introduction to the composition of 1.0 wt. % NF leads to an increase in the strength index from 9.77 to 13.38 MPa, and strain at break of the composite by 1.2 times. A study of the Vicat softening point of the obtained compositions showed that the introduction of PP/BNR (1.0 wt. %) of the nanofiller leads to an increase in the heat resistance index from 110 to 145°C.

SEM analysis of the resulting nanocomposites showed that when nickel oxide nanoparticles are added to PP/NBR, a relatively compatible consistency is formed in the interphase regions of the composite and a smooth surface with a fine spherulite structure is formed.

OBTAINING AND STUDYING THE PROPERTIES OF NANOCOMPOSITES BASED ON A MIXTURE OF POLYETHYLENES OF HIGH AND LOW PRESSURE WITH METAL-CONTAINING NANO FILLERS

[1*]Mamedova G.H., [2]Kurbanova N.I

[1]Azerbaijan State Oil and Industry University, Azerbaijan

[2]Institute Polymer Materials, Ministry of Science and Education, Azerbaijan

gunay1991@bk.ru

It is known that the use of d-valence metal nanoparticles (copper, zinc, cobalt, nickel, etc.) in polymers makes it possible to obtain fundamentally new materials that are widely used in radio and optoelectronics as magnetic, electrically conductive and optical media.

The purpose of this work was to obtain and study the structure and properties of composites based on HDPE and LDPE with copper-containing nanofillers (NF) stabilized by a polymer matrix. In the work used: - High-pressure polyethylene brand 15803-020, ρ = 0.917 - 0.921, MFI 1.5 - 2.5 $g \cdot 10^{-1}$min (T=190ºC, load 2.16 kg); - Low pressure polyethylene brand HM0349PE, ρ = 0.949, MFI 8.3 $g \cdot 10^{-1}$min (T=190ºC, load 21.6 kg). Nickel-containing nanoparticles stabilized by a polymer matrix were used as a nanofiller. The ratio of the components of the composition (wt %): LDPE/HDPE/NF=50/50/(0;0.3; 0.5; 1.0). Nanocomposite polymeric materials are obtained by mixing sequentially HDPE and LDPE and then with a copper-containing nanofiller on laboratory rollers at a temperature of 150ºC for 15 minutes. To carry out mechanical tests, the obtained mixtures were pressed in the form of plates 1 mm thick at 190ºC and a pressure of 10 MPa for 10 minutes.

Nanocomposite polymer materials based on LDPE and HDPE with copper-containing nanofillers were obtained. The physical-mechanical, thermophysical and thermal properties of the obtained nanocomposites are studied. It has been shown that the introduction of 0.3 – 0.5 mass% of ND into the composition leads to an increase in the strength index from 16.69 to 19.97 MPa and the deformation values at break of the composite in 1.7 times, the Vicat softening temperature leads from 155°C to 175°C, the activation energy (E_a) of the decay of the thermal-oxidative destruction of the obtained nanocomposite is increased from 232.96 to 261.76 kJ/mol.

The obtained results indicate that small quantities of nanofiller introduced into the polymer, evidently, play the role of structure-forming agents – artificial crystallization nuclei, which favors the appearance of fine spherulite structure in the polymer, characterized by improved physical-mechanical and thermal properties of the obtained nanocomposite.

PHOTOLUMINESCENCE SPECTRA OF POLYCRYSTALLINE CVD ZnSe WHEN CHANGING THE WAVELENGTH OF EXCITATION LIGHT

[1*]Musayev M.A., [2]Huseynov J.I., [1]Askerov D.J., [1]Abbasov I.I., [1]Hadiyeva A.A., [3]Mammadova A.J., [1]Hasimova N.N.

[1]Azerbaijan State Oil and Industry University, Azerbaijan
[2]Azerbaijan State Pedagogical University, Azerbaijan
[3]Institute of Biophysics, Ministry of Science and Education, Azerbaijan
ibrahimabbasov179 @gmail.com

Samples of polycrystalline ZnSe 3 mm thick were obtained by chemical vapor deposition (CVD) at the Institute of Chemistry of High-Purity Substances, Russian Academy of Sciences (Nizhny Novgorod. Growth samples specially not doped. The concentration of background impurities for the studied sample of polycrystalline CVD ZnSe was determined by two methods: atomic emission spectroscopy and laser mass spectrometry. Total impurity content $<10^{16}$–10^{17} см$^{-3}$ (Cu~10^{16} см$^{-3}$). The oxygen concentration is controlled by chemical gas chromatographic analysis: O~ 10^{18}-10^{20} см$^{-3}$.

The homogeneity region of CVD-zinc selenide has a two-sided character and, unlike other zinc chalcogenides, it is characterized by a wide range of compositions with an excess of oxygen and selenium – ZnSe(O)Se. Photoluminescence spectra were obtained using a universal fluorescence spectrometer – Fluo Time 300 Easy Tau. A xenon lamp with a power of 300 W was used as an excitation source in the spectrometer. All measurements were carried out at T=300K.

When the excitation energy was changed stepwise with an interval of 5 nm close to the LO-phonon energy (~37-31 meV) in ZnSe, the PL spectra were observed in wavelength range 451–497 nm, i.e. multi-band exciton spectra were observed, and when excitation was from 455 nm to 515 nm with an interval of 10 nm and 20 nm, mainly green and yellow-green spectra were observed in the wavelength range 507-547 nm (Fig.). Wavelength range 451–497 nm, i.e. multiband exciton spectra were considered and analyzed in. Green and yellow-green spectra in the wavelength range 507-547 nm can be attributed to impurity-defect luminescence of polycrystalline CVD ZnSe, which is due to oxygen centers on structural defects of the lattice, including background copper impurities. We believe that the green luminescence with maxima in the wavelength range 507-547 nm is due to electron transfer from a small donor (E_D ~ 10 - 20 meV) to an associative acceptor center including oxygen and copper – {Cu_i Ose}.

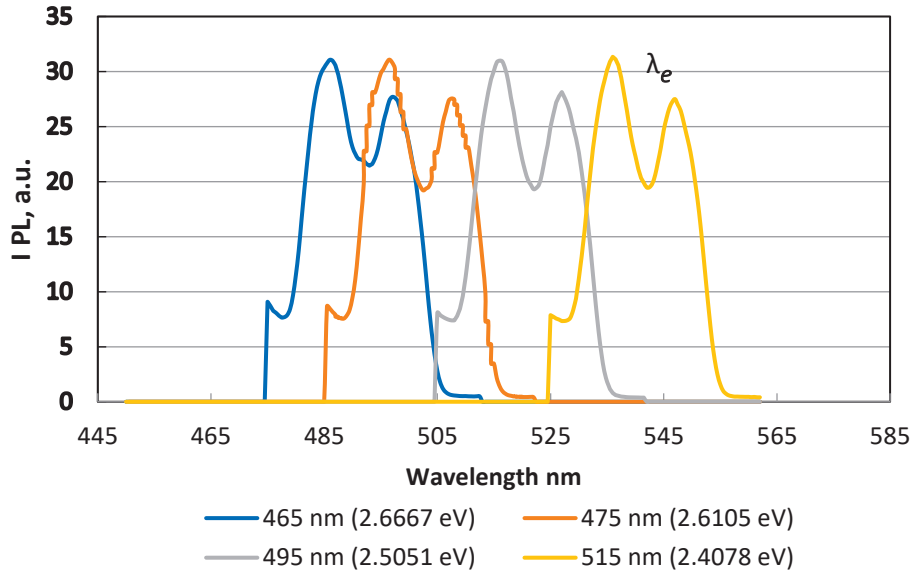

Fiq. 1. PL spectra of CVD ZnSe upon excitation with lengths waves: 465-515 nm.

ELECTRONIC RAMAN SCATTERING IN $Hg_{1-x}Cd_xTe$

[1*]Ismayilov T., [1,2]Zeynalova S.

[1]Baku State University, Azerbaijan

[2]Institute of Physics, Ministry of Science and Education, Azerbaijan

tariyel.i@gmail.com[1]

Solid solutions $Hg_{1-x}Cd_xTe$ have proven their advantages in practice and there are now quite a lot of areas where they are used. Thermal imaging equipment based on the use of photodetectors in the infrared range for wavelengths of 1–30 μm is used in various areas. HgCdTe is the only common material that can detect infrared radiation in both of the accessible atmospheric windows. These are from 3 to 5 μm (the mid-wave infrared window, MWIR) and from 10 to 12 μm (the long-wave window, LWIR). HgCdTe can also detect in the shortwave infrared (SWIR) atmospheric windows of 2.2 to 2.4 μm and 1.5 to 1.8 μm. It has many more competitors today than ever before. However, none of them can compete with HgCdTe in fundamental properties. The main advantages of HgCdTe are a direct band gap, the ability to obtain both low and high concentrations of charge carriers, high electron mobility and low dielectric constant. An extremely small change in the crystal lattice period with a change in

composition makes it possible to grow high-quality multilayer structures and structures with a stepped bandgap.

In this paper the theory of the interband electronic Raman scattering (IERS), for $Hg_{1-x}Cd_xTe$ with the inverted band structure within the framework of the two-band Kane model is developed. The calculations of the differential effective cross section (DECS) are made. The analytical expression for DECS in the case of XX polarizations of incident and scattered radiation in dependence on the frequency shift and "band-gap" ε_g is obtained. A number of general features of the scattering process and the resulting Raman spectrum are examined. The non-resonant and resonant cases are considered. In both cases, the dependences of DECS on the frequency shift are plotted for various values of the band gap.

THERMOELECTRIC EFFECTS IN SUPERLATTICES DUE TO ELECTRON SCATTERING BY SHORT-RANGE POTENTIAL

[1*]Figarova S.R., [2]Huseynov H.I.

[1]Baku State University, Azerbaijan

[2]Azerbaijan University of Architecture and Construction, Azerbaijan

sofyafiqarova@bsu.edu.az

In this work, the anisotropy of electrical conductivity and thermopower of superlattices during the scattering of current carriers by a short-range potential are studied. It has been revealed that changing the parameters of superlattices, namely, the period and width of the miniband and the concentration of impurities leads to a significant increase in the Seebeck coefficient, which can be used to create thermoelectric converters. The superlattices with a cosine dispersion law are considered.

The electrical conductivity and thermopower components of quasi-two-dimensional electronic systems were calculated based on the expression for current density. In the case of a degenerate electron gas for the transverse and longitudinal components of the electrical conductivity and thermopower are obtained.

As seen from obtained expressions the electrical conductivity depends on the position of the Fermi level relative to the superlattice miniband, the impurity concentration and also on the degree of filling of the superlattice miniband. The longitudinal component of electrical conductivity, in addition, is depended on the effective mass anisotropy. It is shown that the anisotropy of electrical conductivity increases with increasing degree of filling

of the miniband and is determined by the anisotropy of the effective mass. With an increase in the effective mass along the axis of the superlattice, the anisotropy of electrical conductivity increases several times.

For thermopower in the plane of the layers and in the direction perpendicular to the layers the analytic expressions are found. From this expressions is follow that in the case of scattering of current carriers by strongly screened impurity ions, thermopower across the layers is zero. It is pointed that thermopower has a peculiarity associated with the Coulomb divergence of the relaxation time. It is shown that thermopower is proportional to the density of states.

It is noted that the significant increase in thermopower compared to a bulk sample is observed for a quasi-three-dimensional electron gas, when the Fermi surface is an ellipsoid. The work indicates the possibility of changing the sign of the thermopower.

Based on the obtained formulas it is shown that in a superlattice with a high electron gas density and a small miniband width, it is achieved the essentially higher thermoelectric figure of merit, as compared with a bulk sample, which results in an increase in the thermoelectric converter efficiency. This increase in thermoelectric efficiency is associated with the strong scattering of conduction electrons in superlattices and the dimensionality of the electron gas.

TO THE TEMPERATURE DEPENDENCE OF PHOTOCONDUCTIVITY IN GeS LAYERED MONOCRYSTALLINE OF ER ADDITIVE ATOMS EFFECT

[1*]Alekperov A.S., [2]Ilyasova T.I., [3]Ismailov M.I.

[1]Azerbaijan State Pedagogical University, Azerbaijan
[2]Azerbaijan University of Construction and Architecture, Azerbaijan
[3]Nahchivan State University, Azerbaijan
[1]aydin60@inbox.ru, [2]azmiu_telli@mail.ru

The photoconductivity of the GeS: Er layered monocrystalline in a wide range of temperatures has been studied. In the temperature domain 125÷250K, the activation energy was ΔE=0.20 eV, and in the temperature domain 250 ÷ 320K, it was. e=0.4 eV. And when T > 300K, the crystal loses photosensitivity, the electrical conductivity is metallic. Complex formed by ER atoms on the surface and volume of the crystal create deep centers of seizure and recombination. With an increase in temperature, there is a discharge of these centers, a jump of load carriers into the conductive

zone. Because of this, the photosensitivity of the crystals decreases, the electrical conductivity is metallic. The restoration of its former photosensitivity by recooling of the crystal makes it possible to make thermokey from GeS:Er layered monocrystals.

TEMPERATURE DEPENDENCE of the KINETIC COEFFICIENTS of $Bi_{0.97}$ $Sb_{0.03}$ ALLOY

[1*]Musayev A.A., [2]Yuzbashov E.R.

[1]National Aviation Academy, Azerbaijan
[2]Institute of Physics, Ministry of Science and Education, Azerbaijan
eltaj.yuzbashov@physics.science.az

Investigation of solid solutions of $Bi_{1-x}Sb_x$ displays that those solutions are perspective materials for fundamental materials science, condensed matter physics, low temperature thermoelectrics, infrared applications, and beyond. Moreover, those materials are of broad interest from the theoretical aspect. Due to the smallness of the characteristic energetic parameters of solid solutions of Bi-Sb, those materials are very sensitive to the external impacts (temperature, pressure, presence of electroactive impurities, defects, etc.). By varying external influence in comparatively small range, it is possible to investigate topology of Fermi surface, various phase transitions, alter the statistics of charge carriers in rather broad range etc. That is why these materials are still being investigated as bulk materials, thin films and nanoscale structures. Also, it was predicted that different kinds of Dirac cone systems can be synthesized based on the single crystal $Bi_{1-x}Sb_x$ thin films materials, including single-Dirac cone, bi-Dirac cone, tri-Dirac cone, exact-Dirac cone, semi-Dirac cone, and quasi-Dirac cone, and also including Dirac cones with different anisotropic degrees. Fu and Kane predicted the topological insulator phase in $Bi_{1-x}Sb_x$ surface states, which is experimentally proved by Hsieh et al. These discovers in $Bi_{1-x}Sb_x$ surface states directly lead to the intensively focused area of topological insulator, which promises potential applications in spintronics, superconductivity, quantum computing, etc.

The temperature dependence (in the 80 K – 300 K range) of the following components of the tensor of electric resistance in low magnetic fields – two components of specific resistance (ρ_{11} and ρ_{33}), two components of Hall effect (ρ_{231} and ρ_{123}) and, five components of magnetoresistance ($\rho_{11,11}$, $\rho_{11,22}$, $\rho_{11,33}$, $\rho_{33,11}$, $\rho_{33,33}$) – for the alloy of $Bi_{0.97}Sb_{0.03}$ were measured.

Due to the calculations the following kinetic parameters were determined: carrier densities of electrons N and holes P; their mobilities μ_1, μ_2, μ_3 and ν_1, ν_2, ν_3, correspondingly; and the tilt angle of electronic isoenergetic ellipsoids to the bisectrix axis (ϕ_e). Calculations were carried out for two-band (L electrons and T holes) and three-band (L electrons, L and T holes) models. When looking for suitable materials for thermoelectric converters, it is often enough to know the average kinetic parameters for single crystals or parameters for polycrystalline samples of the same composition. So, to estimate the values of some kinetic coefficients we used the averaged values of the measured galvanomagnetic coefficients too.

COMPARATIVE ADSORPTION STUDY OF Fe(III) IONS ONTO ODIFIED ADSORBENTS

*Eyyubova E.E.., Nagiyev Kh.J., Chyragov F.M.
Baku State University, Azerbaijan
esmira024@yahoo.com

This work includes synthesis of a new adsorbent based on maleic anhydride styrene copolymer (MAST) and amines (S) and further modification of them with 4,4'-(ethane-1,2-diylbis(azanylylidene))bis(pentane-2-one). Synthesis of adsorbent was carried by the known method. Further we modified resulting products with R. Afterwards results of modified with reagent products were compared with basic products before modification.

During research we studied influence of various parameters on adsorption process, especially effect of pH, contact time, ionic strength, initial metal ions concentration and etc. Thesis also involves studying of desorption process and influence of various organic and Inorganic acids on desorption process. Results have shown that HNO_3 is the best eluent.

Adsorption process was characterized by several adsorption isotherms and kinetic models. Results agreed best with Langmuir model. It was found that equilibrium data can best be explained the pseudo-second-order model. Investigation have shown that compared to initial products, for which adsorption capacities were equal to 404.88 and 348 mg/g, modified adsorbents show higher adsorption capacity over Fe(III) ions and are equal to 890.68 and 479.2 mg/g correspondingly.

Synthesized adsorbents were characterized by the Scanning Electron Microscopy (SEM) with Energy Dispersive X-ray Spectroscopy (EDS) and

Ultraviolet-visible Spectroscopy (Uv/Vis). Temperature stability of adsorbent has been investigated by thermal analysis methods (TG, DTA, DDTA).

Resulting products were applied for determination of Fe(III) ions in fruits.

SPATIAL STRUCTURE OF THE HUMEN β-CASOMORPHIN-7 MOLECULE

*Akhmedov N.A., Agayeva L.N., Ismailova L.I.
Baku State University, Azerbaijan
Namiq.49@bk.ru

The first known exorphins were obtained by in vitro pepsin hydrolysis of α-casein and wheat gluten. The resistance of exorphins to the action of pancreatic enzymes has been proven, and the opioid activity of these peptides in vivo has been confirmed. It turned out that opioid-like derivatives of casein and gluten inhibit the activity of adenylate cyclase in cell culture, inhibit contractions of the mouse vas deferens, and also displace radiolabeled opioid receptor agonists from the binding sites on rat brain slices. Among the exorphins of animal origin, the derivatives of milk proteins are best studied. The most famous are milk exorphins (β-casomorphins-4, -5, -6, -7) - products of enzymatic hydrolysis of β-casein in cow's milk.

The spatial structure of the human β-casomorphin–7 molecule H-Tyr1-Pro2-Phe3-Val4-Glu5-Pro6-Ile7-OH has been studied in fragments. At the first stage, based on the low-energy structures of the corresponding amino acid residues, the conformational capabilities of the N-terminal Tyr1-Val4 and C-terminal Val4-Ile7 tetrapeptide fragments were studied. At the second stage, based on the optimal conformations of these tetrapeptide regions, the spatial structure of the human β-casomorphin-7 molecule was studied. The calculation showed that there is a sharp differentiation between the energies of shapes, main chain forms and conformations. The conformations of eight shapes and eight forms of the main chain fall into the energy range of 0-7 kcal/mol.

It was shown that the N-terminal tetrapeptide fragment is conformationally rigid, and the C-terminal tetrapeptide region is conformationally labile. For the N-terminal tetrapeptide fragment, 3 structures are possible. In stable conformations, the contribution of nonvalent interactions varies in the energy range (-30.2) – (-24.4) kcal/mol, electrostatic - (0.5-8.3) kcal/mol, torsion - (3.9) - (6.1) kcal/mol. The global conformation of the molecule is $B_1BR_1R_2B_{22}BB_{21}$ of the eeffee shape. This conformation is profitable for

nonvalent and electrostatic interactions. In it, the N- and C-terminal dipeptide regions are in the unfolded form of the main chain, and the central tripeptide fragment is in the folded form. This brings the N- and C-termini of the molecule closer together, which leads to their effective interactions and the formation of a hydrogen bond between them. In other low-energy conformations, effective electrostatic interactions do not occur.

Thus, the spatial structure of the β-casomorphin-7 molecule can be represented by nine structural types. It can be suggested that the molecule performs its physiological functions in these structures. Based on these structures, synthetic analogs of the molecule can be proposed. The theoretical conformational analysis of the β-casomorphin-7 heptapeptide has led to such a structural organization of the molecule that does not exclude the implementation by the molecule of a number of functions that require strictly specific interactions with various receptors.

STRUCTURE OF THE IRON OXIDE Fe_xO_y COMPLEXES WITH GLUCOSE AND DI-GLUCOSE

Abbasova G.C., *Hajiyeva L.S.
Baku State University, Azerbaijan
abbasova1962@mail.ru

The most promising directions in the research of the structure and properties of biological systems at the molecular and cellular level are related to nanobiotechnology, the purpose of which is to control the transport of medicines and diagnostic tools. The prospects of modern diagnostic and clinical medicine are based on the use of nanoparticles, that seek out tumors and bind to their blood vessels, and then attract more nanoparticles to the tumor target. The prospects for nanomedicine are since a particle can perform more functions than a drug. Nanoparticles from superparamagnetic from superparamagnetic amino dextran-coated iron oxide (SPIO) are widely used in the clinic to enhance MRI imaging.

In this report the spatial and electronic structure of the glucose and di-glucose, the dextran monomer units, and their complexes with iron oxide Fe_xO_y was investigated by molecular mechanics and quantum chemistry methods. Calculation models were constructed on the base of atoms coordinates in accordance with results of molecular mechanics calculations by the MM+ method. The main electronic parameters such as electron and nuclear energy, electron density distribution, electron and

nuclear forces, total dipole moments and dipole moments of individual bonds in dependence of low-energy conformational state were analyzed according to result of PM3 semiempirical calculation method.

The geometrical parameters of the di-glucose complex with iron oxide are characterized by the following values: (i) Fe=O and Fe-O bond lengths are 1.73 Å and 1.85 Å (instead of 1.49 Å and 1.77 Å for the free iron oxide); (ii) Fe-O-Fe valence angle is 119.360; (iii) O=Fe-O is 119.00.

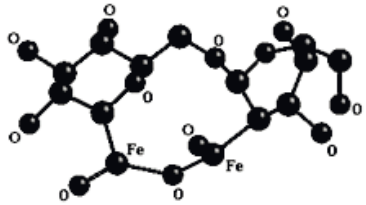

Fig. 1. Spatial model of a complex of di-glucose with iron oxide

The calculation results will be used for describing the attachment of tumor seeking peptide molecules to the dextran-coated iron oxide nanoparticles. SPIO's labeled with a set of different peptides with individual targeting might be of interest in the future.

EPR AND TEM STUDIES OF BIOLOGICAL SYSTEMS

*Nasibova A.N., Khalilov R.I.
Baku State University, Azerbaijan
Institute of Radiation Problems, Ministry of Science and Education, Azerbaijan
aygunnasibova21@gmail.com

In our research conducted by the EPR method, new paramagnetic centers formed under the influence of the stress factor in natural systems characteristic of the Absheron Peninsula were studied. For the first time, when studying the effect of different stress factors on different natural systems, it was found that a broad EPR signal (g=2.32; ΔH=320 G) characterizing iron oxide magnetic nanoparticles is recorded in living systems as a result of the biomineralization during the influence of stress factors. The obtained EPR spectra suggest that stress induces new magnetic properties in natural systems.

In order to clarify the events, further studies were devoted to in vitro studies with chloroplasts isolated from higher plants (spinach (*Spinacia*)) to clarify the mechanism of the formation of magnetic nanoparticles in biological systems. It has been studied by the EPR method that iron ions affect the photosynthetic activity of chloroplasts and iron-based magnetic

nanoparticles are formed in the initial stages of photosynthesis in chloroplasts during stress.

Experiments conducted with some animal organisms (laboratory rats (*Wistar albino*), grape snails (*Helix pomatia*)) showed that nanophase crystalline magnetic particles are generated in their various organs during the influence of stress factors.

Our results were confirmed by microscopic studies, Transmission Electron Microscopy (TEM) method and Messbauer spectroscopy method. Microscopic images of the distribution of nanoparticles in chloroplasts and liver organs of laboratory rats were obtained.

UREA-ETHANOL-WATER SYSTEMS RESEARCH BY VISCOSIMETRY METHOD

[1*]Hajiyeva Sh.N., [1*]Ahmedova A.B., [2]Orucova N.F., [1]Babayeva F.Kh.

[1]Baku State University, Azerbaijan

[2]Azerbaijan Technology University, Azerbaijan

m-shahla@yandex.ru;, orucovan432@gmail.com

Water is the most common substance in nature. This seemingly simple substance is a very mysterious liquid from a scientific point of view. Although water is a model of all substances in our consciousness, we call it extraordinary. It may be asked what is the unusualness of water. The point is that one cannot show a property of water that is not anomalous, that is, the change of state of water due to changes in pressure, temperature and other factors, unlike other liquids, does not deviate from the general principles of physics. The unusual properties of water help it perform a number of functions in living organisms. Water transports substances through osmosis and diffusion in the body, protects cells and organs, etc. performs very important functions. The study of changes in the structure of water under the influence of various substances is one of the most urgent problems facing modern science.

In order to characterize the structural features that arise in solution, it is very useful to analyze the changes of the viscous flow activation parameters due to change of temperature and concentration. In this work, the density and dynamic viscosity of urea-ethanol-water systems in different concentration and temperature ranges were measured and the activation parameters of viscous flow were calculated, as well as the concentration dependences of various isotherms of the activation parameters of viscous flow were studied. Note that the activation Gibbs energy of viscous

flow was calculated based on Eyring's theory, and the activation enthalpy of viscous flow and the activation entropy of viscous flow were calculated based on thermodynamic relations.

It was determined that urea has a destructive effect on the structure of both water and the ethanol-water system in the entire concentration range. Ethanol has a structuring effect on the structure of both water and the urea-water system in small concentrations, and has a destructive effect starting from a certain concentration value. The destructive effect of urea on the structure of water has been confirmed by many methods. This is proven again if we look at the changes in the viscous flow activation parameters. We can describe the interaction of water with ethyl alcohol as follows: in small concentrations of ethyl alcohol, its molecules enter the cage without destroying the water cage. OH groups of alcohol are connected to water molecules in the cage due to hydrogen bonding, and as a result, water becomes more structured. It is clear that the penetration of alcohol molecules into the cage without destroying the structure of water can last only up to a certain concentration. It can be assumed that in a certain concentration range, two structures or "microphases" exist in the solution, one of which is inside the other. In one "microphase", water molecules participate in the formation of a single network of hydrogen bonds, and in the other phase, there are ethyl alcohol molecules, which destroy the structure by combining water molecules with itself. Thus, an increase in the concentration of ethyl alcohol in the solution leads to the disintegration of the created structure.

STRUCTURAL CHARACTERISTICS OF KI IN AQUEOUS SOLUTION

Pashayev B.G.
Baku State University, Azerbaijan
p.g.bakhtiyar@gmail.com

Potassium and iodine ions (K^+ and I^-) play an important role in most biological processes in the living organism: Potassium ion regulates the amount of water in seeds, improves heart function, plays an important role in the functioning of the nervous system, and iodine ion regulates the activity of the nervous and cardiovascular systems, it is also necessary to increase immunity and synthesize thyroxine, the hormone of the thyroid gland, etc. In this regard, it is necessary and very interesting to study the structural characteristics of KI salt in aqueous solutions.

In this work, the structural characteristics of the water-KI system were studied based on the study of viscous flow, volume, electrical conductivity and spectroscopic properties of the solutions in the infrared region. For this purpose, the dynamic viscosity, density and specific electrical conductivity of aqueous solutions of KI salt at different temperatures and concentrations were measured, also, absorption spectra of solutions in different concentrations at room temperature in the infrared range were recorded and the frequency of OH valence oscillations of water molecules was determined. Using results from experience of aqueous solutions of the KI salt at the considered temperatures and concentrations activation Gibbs energy of viscous flow, activation enthalpy of viscous flow, activation entropy of viscous flow, partial molar volume of KI in solution, thermal volume expansion coefficient of solution, activation Gibbs energy of ionic conductivity, activation enthalpy of ionic conductivity, activation entropy of ionic conductivity, effective radii and hydration numbers of potassium and iodine ions, hydrogen bond energy and length were calculated.

The analysis of viscous flow properties of an aqueous solution of KI salt shows that the activation Gibbs energy of viscous flow first decreases with increasing concentration at low temperatures, passes through the minimum (minimum observed concentration $x_{min}\approx0.04$ at 10°C, $x_{min}\approx0.03$ at 20°C, $x_{min}\approx0.02$ at 30°C, $x_{min}\approx0.01$ at 50°C corresponds to the molar part), then it increases, and at high temperatures (55°C, 60°C) it only increases. The activation enthalpy and entropy of viscous flow only decrease with increasing concentration. The analysis of the volume properties of the aqueous solution of KI salt shows that the thermal expansion coefficient and the partial molar volume of KI in solution increase depending on the concentration. The analysis of electrical conductivity properties of the aqueous solution of KI salt shows that the effective radii and hydration numbers of potassium and iodine ions are $r_{ef}(K^+)\approx3.18$Å, $r_{ef}(I^-)\approx3.13$Å and $N_h(K^+)\approx11.4$, $N_h(I^-)\approx7.6$ becomes, also in the temperature range considered values of effective radius and hydration number for both ions are almost independent of temperature. The activation Gibbs energy, activation enthalpy and activation entropy of ionic conductivity decrease with increasing temperature. The analysis of spectroscopic properties of the aqueous solution of KI salt in the infrared range shows that with the increase in concentration, the frequency of OH valence oscillations and the length of the hydrogen bond increase, while the energy of the hydrogen bond decreases.

The obtained results can be explained on the basis of the hydration

process, which occurs due to the electrostatic connection effects between ions and water molecules. Since potassium and iodine ions are negatively hydrated ions, in the electric field of these ions, water molecules are weakly connected to each other than in pure water. This situation manifests itself in the concentration dependences of the activation entropy of the viscous flow, the partial molar volume of KI in the solution, the hydrogen bond energy, as well as the values of the effective radii and hydration numbers of potassium and iodine ions. Thus, the analysis of viscous flow, volume, electrical conductivity and spectroscopic properties of the water-KI system in the infrared region shows that KI salt has a destructive effect on the structure of water, and this effect becomes stronger with an increase in the concentration of KI in the solution.

STRUCTURE AND CONFORMATION OF MACROMOLECULAR CHAIN IN WATER-PEG-KI SYSTEMS

Masimov E.A., Pashayev B.G., *Hajiyeva Sh.N.
Baku State University, Azerbaijan
pgbakhtiyar@gmail.com

The processes happened in water-polyethylene glycol-salt biological systems can be imagined as a simple model of the processes happened in the living world. Consequently, the study of such systems is interesting. Determining the conformation, sizes, and intensity of interactions between particles of polyethylene glycol (PEG) macromolecule in water-polyethylene glycol-salt systems and studying the effect of various salts on these conditions are urgent issues.

In this study, the kinematic viscosity of water-PEG-KI systems was studied, the concentration range of KI was 0-0.05 molar parts and polyethylene glycol was 0-5 g/dl, and fractions of PEG with molecular masses of 1000, 1500, 3000, 4000 and 6000 were taken. The characteristic viscosity ([η]) of the studied aqueous solutions, the Huggins constant (K_H), the α parameter included in the Mark-Kun-Hauvink formula, the characteristic viscosity in θ-solvent ($[\eta]_\theta$), the swelling coefficient of the PEG macromolecule (β), in the solution ($\langle h \rangle$) and in the θ-solvent ($\langle h_\theta \rangle$) the mean square distance between the ends of the PEG macromolecule chain, the length of the Kuhn segment in the solution (A) and the θ-solvent (A_θ), and these parameters are determined from the concentration of KI (*x*) dependent changes were analyzed.

Researchers show that for fractionated PEG taken in water-PEG-KI systems, with increasing concentration of KI, the value of characteristic viscosity decreases, while the value of Huggins constant increases. The decrease in the characteristic viscosity of the solution depending on the concentration of KI is due to the decrease in the volume of the PEG macromolecule and the decrease in the viscosity of the solution. As the concentration of KI increases, the value of the Huggins constant increases, indicating that the solubility of PEG in water-KI systems deteriorates depending on the concentration. This is probably due to the hydration of KI ions (K^+ and I^-) in the solution. For water-PEG-KI system, the value of parameter α included in the Mark-Kun-Hauvink formula was determined. The α parameter takes values in the range (0.71-0.78) at a temperature of 20^0C and in the concentration range of KI, we are looking at. This indicates that the PEG macromolecule is in the form of a wash in the water-KI environment, which the surrounding liquid can penetrate. The α parameter increases somewhat with the increase in the concentration of KI. This indicates the opening of the PEG macromolecular mesh with increasing concentration.

It was determined that the characteristic viscosity of the θ-solvent chosen for the water-PEG-KI systems decreases with the increase in the concentration of KI. This is probably due to a partial decrease in the volume of the molecular shell and the viscosity of the θ-solvent medium. One of the parameters that determine the characteristics of a macromolecule in solution is the swelling coefficient. It was determined that $\beta > 1$ for all considered cases and the swelling coefficient of PEG macromolecule in water-KI systems increases with increasing concentration of KI. It can be assumed that as the concentration of KI in the solution increases, β increases, K^+ and I^- ions in the solution have negative hydration, the viscosity of the medium decreases, and the conformational transformation of the macromolecule is related. The obtained results show that the mean square distance between the ends of the PEG macromolecule chain, both excited in the water-PEG-KI system and unexcited in the θ-solvent, decreases with the increase in the concentration of KI. Probably, as the concentration of KI increases, the parameters $\langle h \rangle$ and $\langle h_\theta \rangle$ decrease due to the decrease in the hydration number of PEG and the decrease in the volume of the macromolecular wash. It was determined that the length of the Kuhn segment of PEG macromolecule excited in water-PEG-KI systems and unexcited in θ-solvent decreases as the concentration of KI in the solution increases. When adding KI to the water-PEG system, since K^+ and I^- ions are also hydrated, the hydration number of the PEG macromolecule

decreases, its size decreases, and its polarity decreases, as a result, the interactions between water and PEG molecules are weakened. We believe that for these reasons, as the concentration of KI in the water-PEG-KI system and θ-solvent increases, the mobility of the PEG macromolecule increases.

SYNTHESIS AND STRUCTURAL PROPERTIES OF CHITOSAN AND CROSS-LINKED CHITOSAN COATED MAGNETITE NANOPARTICLES FOR ANTICANCER APPLICATIONS

[1*]Karimova A.H., [1]Mehdiyeva A.R., [2]Yagublu V., [1]Nuriyeva S.G., [2]Shirinova H.A., [1]Gahramanli L.R.

[1]Baku State University, Azerbaijan
[2]University of Heidelberg, Germany
aynurakarimova16@gmail.com

In the last decades, the development of innovative methods for cancer therapy has drawn intense attention due to the increasing of patients' amount and the inefficiency of the present conventional treatments. In this study, superparamagnetic iron oxide nanoparticles (SPIONs) were synthesized by the co-precipitation method. Then the nanoparticles were modified by coating them with chitosan and crosslinked chitosan to improve their biocompatibility and increase drug loading efficiency. The structure of the coated and drug-loaded SPIONs was learned by X-ray diffraction. It was found that depending on the type of coating agent, the size of the crystallites was changed. Thus, the crystallite sizes in chitosan and crosslinked chitosan-coated samples were approximately 13 nm and 17 nm, respectively. Furthermore, UV-Vis analysis showed that the drug loading efficiency in crosslinked chitosan-coated samples increased by ~26%, while no significant changes in the size of the crystallites were observed according to the results of the X-ray structure analysis. This study emphasizes the significance of optimizing the surface properties of magnetic nanoparticles when using them in biomedical applications.

The potential of magnetic nanoparticles (MNPs) in drug delivery systems (DDSs) is mainly related to its magnetic core and surface coating. These coatings can eliminate or minimize their aggregation under physiological conditions. Also, they can provide functional groups for bioconjugation to anticancer drugs and/or targeted ligands.

THE ROLE OF SPECTRAL TRAJECTORY CORRESPONDING TO VOICE ENERGY MAXIMA IN PERSON IDENTIFICATION

[1]Aliyev L.P., [2]Gaziyeva N.G., [1*]Guliyeva S.K.

[1]Forensic Expertise Center of the Ministry of Justice, Azerbaijan
[2]Institute of Linguistics n.a. Nasimi of ANAS, Azerbaijan
n.qazi@inbox.ru, Seva.quliyeva1993@mail.ru

Formant frequencies are frequencies corresponding to the main acoustic resonances - energy maxima, which depend on the dimensions of the vocal tract in the spectrum of the speech signal. The flow of air from the human lungs makes the source of sound - the vocal cords - vibrate. The vibration of the vocal cords creates the main tone and many harmonics. The oral cavity, nasal cavity and pharynx cavity together are a system of resonators, which can change their configuration (and therefore also change their specific frequency) in relation to each other. The sound source creates its own oscillations in the system of resonators. The human voice we hear is a complex sound obtained as a result of the transformation of the sounds generated in the sound source, the resonator system. The specific frequencies of the resonator, which are relatively strong in the spectral composition of the sound, are formant frequencies.

Formants are created during the propagation of sound waves from the sound source in the vocal tract. The sound wave from the vocal fold reaches the lip and is partly radiated from the lip and partly reflected back from the lip. The sound wave traveling from the vocal folds to the speaker's lips and returning from the lips creates resonance. If the sound wave reflected from the open end of the tract – the lip – returns to its source, then the returning wave is in the same phase or the opposite phase with the original wave radiated from the sound source. When the meeting waves are in the same phase (when the path difference is equal to an integer multiple of the wavelength), energy maxima occur, which makes it possible to equalize the dimensions of the vocal tract.

The frequency of the formant is determined by the configuration of the speech source and is not affected by the sound source property. The fact that the resonance property of the system of resonators consisting of the nose, throat and oral cavity does not depend on the sound source allows to associate the formant frequency only with the property of the pronunciation organs. That is, it is possible to make a judgment about the state of the organs of pronunciation according to the formant frequency.

In the acoustic classification of vowels, the characteristics of the

division of formant trajectories according to phases act as an important identification indicator. Conducted studies show that the division of formant trajectories of vowel sounds by phases does not only depend on the consonant sounds surrounded by the vowel sound, but also characterizes the geometric dimensions of the speaker's speech apparatus, which is considered an important criterion for speaker identification.

LASER ABLATION Si THIN FILMS

Mammadov V.U.
Baku State University, Azerbaijan
mammadovv@gmail.com

The rapid development of lasers with ultrashort pulses opens new possibilities for precision processing of materials, in particular silicon. Due to its thermodynamic, physicochemical and semiconductor properties, silicon is widely used in micro- and nanoelectronics, sensor technology, biomedicine, etc. In this regard, at present, interest in the effect of laser radiation on silicon and the SiO_2/Si system (a layer of silicon dioxide on the surface of a single-crystal silicon wafer) is continuously growing. It is known that when laser pulses impact the surface of crystalline solids and a single crystal of silicon, the generation of structural defects in the surface layer is possible - vacancies and interstitial silicon atoms, the concentration of which during laser exposure can change compared to the original by several orders of magnitude and reach values of 1019–1021 cm^{-3}. The combination of extended defects into larger defects (in networks of dislocations or accumulation of pores) can initiate the formation of microcracks and destruction of the surface even before the start of melting. In, solid-phase destruction of the silicon surface under the influence of laser pulses in air and vacuum was studied.

The studies were carried out on industrial silicon wafers KDB-10 (111), KEF-4.5 (100) with a layer of native silicon oxide several tens of nanometers thick and a SiO_2 layer thickness from 120 to 300 nm, grown by thermal oxidation. Irradiation was carried out using the Mini Marker 2 laser system. This system includes a pulsed laser with a wavelength λ = 1062 nm. Nominal laser output power 20 W, pulse duration 100 ns. The pulse repetition rate can be adjusted from 20 kHz to 100 kHz. Control of experimental samples was carried out using an optical microscope of the Axio Imager A1m type from Carl Zeiss, equipped with a high-resolution digital video camera.

All experiments were carried out in the focused laser beam mode when the diameter of the irradiation spot on the substrate was 50 μm. The substrate surface temperature and its area distribution were assessed in real time using a FLIR SC7000 series thermal imager.

The results of micro structuring of the SiO_2/Si system are influenced by factors such as radiation power, radiation energy density, pulse repetition frequency and duration, beam scanning speed, and the amount of overlap of the irradiation area by scanning lines. Based on this, at the initial stage, studies were carried out related to the choice of modes for scanning a laser spot on the irradiated area of the substrate (irradiation area 5 × 5 mm2, spot diameter 50 μm), since such data were absent in the literature. As a result of this stage of work, the laser beam scanning modes were selected: scanning speed – 100 mm/s, amount of scanning line overlap – 1000 lines/mm.

The paper presents the results of a study of the process of laser ablation of silicon when irradiated by a scanning laser beam with a wavelength λ = 1062 nm. It has been shown that the process of silicon ablation under these conditions occurs without silicon melting. The determining factor in this process is the total number of laser pulses incident on the irradiation area. Irradiation modes that affect the composition of the resulting ablation products have been determined. The process of silicon ablation with the subsequent formation of silicon dioxide in the above modes is not affected by either the silicon parameters (conductivity type, orientation, and resistivity) or the presence or absence of a silicon dioxide layer on the surface of the silicon substrate.

SYNTHESIS OF NEW COMPLEXES OF 1 PHENYL-2,3-DIMETHYLPYROZALON-5-AZO-4 PYROGALLOL REAGENT AND CETYLTRIMETHYLAMMONIUM BROMIDE WITH SILVER NANOPARTICLES

[1]*Imamaliyeva A., [2]Hajiyeva F., [3]Ciraqov F.
Baku State University, Azerbaijan
aytenimamaliyeva@hotmail.com

Silver (Ag) nanoparticles have been intensively studied in recent years due to their potential application in bio diagnostics, visualization, sensing, analytical determination, and other fields. Ag nanoparticles have unusual physicochemical properties, including size, shape, distance, optical properties, and high molar extinction coefficient.

In this study, new complexes of silver nanoparticles were synthesized based on 1 phenyl-2,3-dimethylpyrazolone-5-azo-4-pyrogallol reagent (R) and cetyltrimethylammonium bromide. First, a 10^{-3} M solution of the reagent is prepared in a water-alcohol mixture. 10 ml of pre-prepared 0.01 M Ag nanoparticle solution was added to 50 ml of 10-3 M reagent and stirred in a magnetic stirrer for 2 hours. The color of the obtained solution changes from dark red to red and a binary complex is formed. Then, to synthesize the ternary complex, 10 ml of 0.01 M Ag nanoparticle solution was added to 50 ml of 10^{-3} M reagent and mixed again for 2 hours. After 2 hours, 5 ml of 0.5% CTAB solution was added to it and continued to be mixed. The color of the solution changes from red to light red and a ternary complex is obtained. CTAB plays the role of an additional stabilizer for the stability of the complex when silver nanoparticles form a complex with a given reactant.

UV spectra of binary and ternary complexes formed by silver nanoparticles with 1 phenyl-2,3-dimethylpyrazolon-5-azo-4 pyrogallol reagent and CTAB were studied. As is known from the literature, depending on the size of silver nanoparticles, the maximum intensity of their absorption bands varies between 400-450 nm. The maximum peak in the absorption band of silver nanoparticles is located at a wavelength of 416 nm. In the UV absorption band of 1 phenyl-2,3-dimethylpyrazolone-5-azo-4 pyrogallol reagent, maxima are observed at wavelengths of 234 nm, 271 nm, 354 nm, 386 nm, 422 nm. In the UV spectrum of the Ag-R binary complex, maxima are observed at 211 nm, 261 nm, 365 nm, 401 nm, and 429 nm wavelengths. During the formation of the binary complex, a bathochromic shift occurs due to the reagent. The peaks in the absorption band of the ternary complex formed upon the addition of CTAB shift to 207 nm, 237 nm, 276 nm due to the reagent and at this time hypochromic shift is observed. Ag nanoparticles coated with surfactant and forming a complex with 1 phenyl-2,3dimethylpyrazolone-5-azo-4 pyrogallol reagent is explained by the formation of new peaks in the absorption band and color change due to surface plasmon resonance.

SPECTRAL TRAJECTORY REFLECTION OF THE INFLUENCE OF NEIGHBORING SOUNDS ON THE ENERGY MAXIMUM F2 OF A VOWEL SOUND

[1]Aliyev L.P., [2*]Gaziyeva N.G., [1]Guliyeva I. I., [1]Aghamaliyeva A.V.
[1]Forensic Expertise Center of the Ministry of Justice, Azerbaijan
[2]Institute of Linguistics named after Nasimi of ANAS, Azerbaijan
latif_aliyev@mail.ru

In the spectral representation of sound, the stronger specific frequency of the resonator system consisting of the mouth, nose and pharyngeal cavities - formants is considered an important identifying feature in the identification of a person according to his oral speech. The absolute values of formant frequencies depend on the size of the vocal tract, and each formant is determined by all parts of the speech tract. Therefore, when talking about the F-landscape of vowels, it is necessary to take into account not the absolute values of the formants, but their location relative to the boundaries of the formant space.

The distribution of the formant trajectory according to the transition phases is closely related to the sounds the vowel is surrounded by, and co-articular effects have a greater effect on the F2 formant, which is closely related to the constriction of the vocal tract. Sometimes, the II phase of the F2 formant-the stationary phase disappears altogether (Fig. 2).

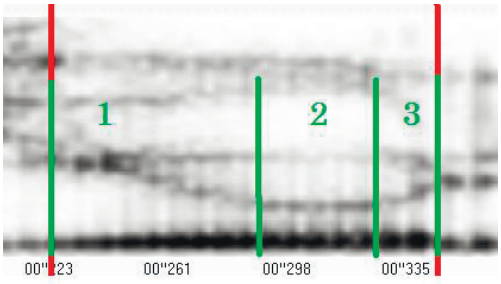

Fig. 1. Division of accented vowel (i) according to transition phases of formant trajectories. 1 – excursion, 2 – stationary, 3 – recursion.

The characteristics of the coarticulation part are characterized by different points depending on the acoustic quality of the sounds used together, and this area reflects the characteristics of both the vowel and the consonant that precedes it. So, the F1 of the vowel used after the morphing consonant is always reduced. F2 either decreases or increases depending on the value of the stationary part of the vowel and the value of F2 of the

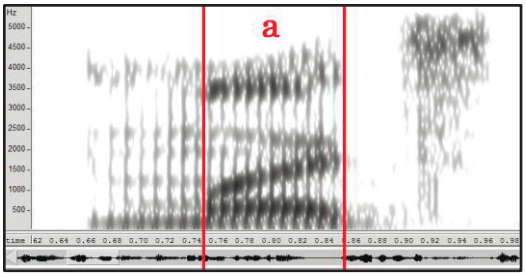

Fig. 2. In sound (a), the stationary part of the F2 formant is lost.

consonant. It depends on the place of formation of consonants. Since nasal consonants, unlike other sonorants, have not two, but three resonators, the open transition to the nasal cavity creates a very large resonator and, accordingly, a strong resonance in the region of 200-300 Hs. For /n/, which is a small oral resonator, this resonance is slightly higher. In addition, a case of weakening (anti-resonance) is observed in the F2 region of the neighboring vowel for nasal consonants. In Figure 2, the loss of the stationary part of the F2 formant in the /a/ sound is related to the acoustic quality of the /n/ sound processed before it and the effect of these features.

MoS_2 THIN FILM: PREPARATION TECHNOLOGY AND CHARACTERIZATION

Bagiyev E.A.

Institute of Physics, Ministry of Science and Education, Azerbaijan
elnurbagiyev@gmail.com

Molybdenum disulfide (MoS_2), consisting of weakly interacting layers have attracted a lot of attention in recent years because of its fascinating electrical and optical properties and the tunable band gap depending on the number of atomic layers. Bulk MoS_2 has an indirect band gap of ~1.2 eV, whereas a single layer has a direct band gap of ~1.8 eV. Moreover, a monolayer of MoS_2 is working as a highly efficient photoresponsive semiconducting material in the visible range, making the material interesting for optoelectronic applications, such as LEDs, photovoltaic and solar energy harvesting. Not long ago, a single-layer MoS_2 films were used to construct a high-gain transistors and phototransistors.

The MoO_3 films of 3, 5 and 30 nm nominal thicknesses were deposited onto SiO_2/Si substrates (SiO_2 thickness was about 100 nm) in a Plasma Enhanced-Atomic Layer Deposition (PE-ALD) system (SI ALD LL, SENTECH Instruments).

For the sulfurization procedure, MoO_3 films were placed at the center of a 1-inch diameter single zone tube furnace. The furnace and samples were pumped/purged multiple times from low vacuum to atmospheric pressure under Ar flow (250 sccm 99.999% Ar). The temperature of the furnace was increased from room temperature to 700°C over 10-20 minutes and kept at temperature for 60 minutes at atmospheric pressure. During heating, H_2S (10 sccm 99.6% H_2S) was introduced at 300 °C and removed at the end of the 60 min anneal. The furnace was then purged with Ar (250 sccm) during cooldown. After cooling to ∼400 °C the furnace was opened for rapid cooling to ∼120 °C over ∼10 minutes.

The MoS_2 films obtained on the top of SiO_2/Si were characterized using SEM, XRD, CRS and SE. The results show good quality of the fabricated films, which can be used for optoelectronic applications.

THE EFFECT OF NICKEL OXIDE NANOPARTICLES ON THE STRUCTURE AND PROPERTIES OF NANOCOMPOSITES BASED ON HIGH-PRESSURE POLYETHYLENE CONTAINING MULTIWALLED CARBON NANOTUBES

[1]*Kurbanova N.I., [1]Mirzoev N.A., [2]Zeynalov E.B., [3]Gadzhieva F.V., [3]Gahramanli L.R.

[1]Institute of Polymer Materials, Ministry of Science and Education, Azerbaijan
[2]Institute Catalysis and Inorganic Chemistry, Ministry Science and Education, Azerbaijan
[3]Baku Science University, Azerbaijan
kurbanova.nushaba@mail.ru

Due to the unique properties of modern nanomaterials, many companies design complex electronic devices that are used in the aviation and space spheres to assemble powerful computers, video equipment, help diagnose various diseases, as well as quickly transmit information. Such nanostructured materials are obtained by embedding nanoparticles into various polymer matrices.

The effect of nickel oxide nanoparticles (NiONPs) stabilized by a matrix of high-pressure polyethylene (PE) obtained by the mechanochemical method on the structure and properties of nanocomposites based on high-pressure polyethylene (PE) containing multiwalled carbon nanotubes (CNT) has been studied. The physical-mechanical, thermophysical and thermal properties of the obtained composites were studied using DTA and AFM analysis methods. The optimal composition of components for obtaining nanocomposites with improved properties has been determined.

It is shown that the introduction of nickel oxide nanoparticles into the furmulation of a polyethylene composition with CNT leads to a high degree of dispersion of fillers with the formation of a globular structure, the physical-mechanical and thermal properties of the composite are quite high: an increase in the strength index from 11.39 to 12.15 MPa, composite rupture strain values from 400 to 740%, the heat resistance index from 130 to 145°C., half-life temperatures of samples (T_{50}) from 350 to 420 °C activation energy (E_a) of thermo-oxidative degradation from 129.45 to 267.91 kJ/mol.

The morphology of the nanocompositions was studied using Integra-Prima atomic force microscopy (NT-MDT, Zelenograd). To carry out scanning, special silicon cantilevers were used, manufactured by plasma-chemical etching, with a needle curvature radius of 20 nm and a resonant frequency of 1-5 Hz. The measurements were carried out in the semi-contact microscopy mode in air; changes in the vibration amplitude of the cantilever needle were recorded, which determines the surface topography. For each sample, images of the surface topography, histograms of the size distribution of the surface topography features of the samples were obtained.

AFM micrographs show the complex interweaving of nanoparticles with each other and the polymer matrix and the formation of a new fine-crystalline supramolecular structure related to the interfacial interaction of nickel-containing nanoparticles with multilayer carbon nanotubes, which contributes to the maximum increase in the physical-mechanical and thermal properties of the resulting nanocomposite.

p-n JUNCTIONS BASED ON PbTe FILMS DOPED WITH OXYGEN

*Sarmasov S.N., Rahimov R.Sh.
Baku State University, Azerbaijan
ssarmasov@rambler.ru

Fabrication of active elements of electronic circuits in a single technological act is one of the main tasks of microelectronics. In our work we attempted to obtain p-n junctions in epitaxial films of lead telluride when growing them by condensation of molecular flow in a vacuum of ~10^{-6} mm Hg without disturbing the growth process and forced introduction of alloying impurities.

Evaporation was carried out from a graphite Knudsen cell. A crushed n-type lead telluride crystal was used as a source, and mica chips served as

substrates. The source temperature was varied from 900 to 1000 K, and the substrate temperature was remained constant Tn=598 K. The condensation rate ϑ_k was set by the source temperature. Cultivation was carried out through a movable slide mask with slits, which provided the film in the form of intersecting systems of strips with a width of 0.3 to 0.5 mm. After deposition of one system of strips at the evaporator temperature T_1, the flap was closed and for 1-2 min. And a new temperature value T_2 was set, and then another system of strips was deposited at the same substrate temperature.

The volt-ampere characteristic was taken at T=77 K using a two-channel recorder and oscilloscope. In-Au alloy was used as ohmic contacts to the p-layer.

The grown films are oriented with edge (111) parallel to the substrate. At condensation rate ϑ_k= 0.035 nm/s, the films possess hole conductivity with charge carrier concentration $n=5\cdot10^{17}cm^{-3}$ and mobility μ_p=400 $cm^2/V\cdot s$. Increase of ϑ_k up to 0.12 nm/s and more leads to growth of films with electronic conductivity with carriers' concentration $n=10^{16}cm^{-3}$ and mobility μ_p=1000 $cm^2/V\cdot s$ (at T=300K). The area of the p-n junctions was of the magnitude of (1-3) 10^{-3} cm^2 and the differential resistance at zero bias was $R_0=10_5$ Ohms. All p-n junctions were photosensitive in the IR region of the spectrum. The photosensitivity maximum falls at a wavelength of ~ 4.5 λ_{max} μm with a gentle decline to λ ~ 6 μm.

The study of the direct branches of the volt-ampere characteristic in the temperature range 77-120 K has shown that the current flowing through the p-n junction consists of two parts: at small offsets the dependence of the current on U is exponential with the index β=2, at large offsets the slope of the VAC does not change with temperature. This is due to the tunneling mechanism of current flow through the p-n junction.

COSMOLOGICAL MODELS

[1]*Jafarzade A.F., [2]Rajabov B.A.

[1]Baku State University, Azerbaijan

[2]Shamakhy Astrophysical Observatory named after N. Tusi, Azerbaijan

aytacmrceferzade@gmail.com

The foundation of modern cosmology rests upon Einstein's General Theory of Relativity and the cosmological principle. According to Einstein's theory, space-time should be understood as a pseudo-Riemannian geometry, with its variables encompassing the movement and distribution of

matter. The cosmological principle, derived from various astronomical observations, posits that the Universe is largely homogeneous and isotropic. In establishing the cosmological principle, the crucial factors include the distribution of galaxies, the homogeneity in the arrangement of their clusters, and the discovery of relict photons with their isotropic properties.

Various cosmological models are employed to explore the laws governing the development and structure of the universe. These models are categorized into static and dynamic forms. Einstein was the first to employ General Relativity in proposing a static cosmological model of the Universe. To achieve this, he introduced the parameter Λ, known as the cosmological constant, into his equations. [2, 3] In 1917, Willem de Sitter discovered maximally symmetric cosmological solutions related to Einstein's cosmological constant, characterizing an empty Universe or vacuum. De Sitter's model, unlike Einstein's, could explain the redshift but depicted a Universe devoid of matter.

In 1922, Alexander Friedman demonstrated the possibility of non-static solutions to Einstein's field equations with the parameter Λ. Examination and exploration of these non-static solutions revealed their better alignment with astronomical observations. In 1927, George Lemaître concluded that a linear relationship exists between intergalactic distances and redshift, attributing the expansion of the Universe to changes in these distances. Hubble's own observations supported this linear dependence. Robertson and Walker contributed a mathematical classification of pseudo-Riemannian metrics describing non-static models, revealing that in all dynamical models, when traced backward in time, the universe originated from a singularity with infinite density and high temperature – the Big Bang. The universe's evolution subsequent to the Big Bang is expounded through inflationary scenarios. Notably, the early phases of the Universe's development are marked by a De Sitter model.

THE PRODUCTION OF ZAA-BOSONS IN e^-e^+-COLLISIONS

Abdullayev S.K., *Gojayev M.Sh.
Baku State University, Azerbaijan
macidqojayev@gmail.com

In this paper, the process of the production of a vector Z-boson and two CP-odd Higgs bosons in electron-positron collisions is investigated: $e^-e^+ \to ZAA$. The study was carried out within the framework of the

Minimal Supersymmetric Standard Model (MSSM) and taking into account arbitrary polarization states of the e^-e^+-pair. It is known that in the MSSM vertices ZHH, Zhh, ZhH and ZAA are forbidden by CP-invariance, possible vertices are $Z\Phi A$, where $\Phi = H$- or h-CP is an even Higgs boson. The process $e^-e^+ \to ZAA$ corresponds to four Feynman diagrams. In the first diagram a) the e^-e^+-pair is annihilated into a vector Z-boson, which emits a CP-even Φ^*-boson ($\Phi^* = H^*$ or h^*), which decays into two A-bosons. In the second diagram b) the e^-e^+-pair turns into a Z-boson, which emits two A-bosons at one point and passes into the final state. In diagram c) the e^-e^+-pair annihilates into a Z^*-boson, which decays into vector Z- and CP-odd $A(k_1)$-bosons. Diagram d) differs from diagram c) by swapping the CP-odd Higgs bosons $A(k_1)$ and $A(k_2)$.

The differential cross section of the reaction $e^-e^+ \to ZAA$ is generally expressed by the formula

$$\frac{d\sigma(\lambda_1,\lambda_2;\eta_1,\eta_2)}{dx_1dx_2d\Omega_Z} = \frac{\sqrt{2}G_F^3M_Z^6}{128\pi^4 s}\cdot\frac{1}{(1-r_Z)^2}\{[(g_L^2(1-\lambda_1)(1+\lambda_2) + g_R^2(1+\lambda_1)(1-\lambda_2)]\cdot\psi_1 + 2g_Lg_R\eta_1\eta_2\psi_2\}, \quad (1)$$

where $x_{1,2} = 2E_{1,2}/\sqrt{s}$ – scaling energy of Higgs bosons, $d\Omega_Z$ – angle of departure of the Z-boson, ψ_1 and ψ_2 – some functions depending on the energies and angles of the particles.

When the initial particles are longitudinally polarized, the electron and positron must have different helicities: $e_L^-e_R^+$ or $e_R^+e_L^-$. As a result, there is a left-right spin asymmetry

$$A_{LR} = \frac{1/4 - x_W}{1/4 - x_W + 2x_W^2}, \quad (2)$$

which depends only on the Weinberg parameter x_W. With the value of the Weinberg parameter x_W =0.2315, the left-right spin asymmetry is equal to: A_{LR} =14%.

In the case of transverse polarization of the e^-e^+-pair, the $e^-e^+ \to ZAA$ process must have transverse spin asymmetry

$$A_\varphi = \frac{2g_Lg_R}{g_L^2+g_R^2}\cdot\frac{\psi_2}{\psi_1}. \quad (3)$$

At the beginning of the angular spectrum, the transverse spin asymmetry is positive, with an increase in the angle θ_Z decreases and reaches a minimum at $\theta_Z = 90°$, and with a further increase in this angle, the transverse spin asymmetry begins to grow.

The experimental study of the $e^- e^+ \to ZAA$ reaction is of great interest, since it allows us to accurately determine the constants of the three-boson interactions λ_{HAA} and λ_{hAA}.

BOUND STATE SOLUTIONS OF THE KLEIN-FOCK-GORDON EQUATION FOR THE DENQ-FAN POTENTIAL

[1]Aliyeva T.H., [2*]Dadashov E.A.
[1]Baku State University, Azerbaijan
[2]Lankaran State University, Azerbaijan
aliyevataranah@gmail.com

For a long time, quantum mechanics has grown from the advanced theory to the separate branch of physics. A study of precisely solvable problems for physical potentials is still important for it. Will be helpful noted that central potential describes quantum system in the radial direction. We attempt the investigation Denq-Fan potential within KFG equation. The shifted Deng-Fan potential is of the following form:

$$V(r) = D\left(\frac{(e^{\alpha r_e}-1)^2}{(e^{\alpha r}-1)^2} - \frac{2(e^{\alpha r_e}-1)}{e^{\alpha r}-1}\right)^2, \qquad (1)$$

where D as the dissociation energy r_e for the equilibrium bond length and α for the potential range. We are well aware that in relativistic quantum mechanics, the dynamics of the spin of zero particles is described by the Klein-Fock-Gordon equation. For the scalar $S(\vec{r})$ and vector $V(\vec{r})$, potentials, the KFG equation in atomic units $(\hbar = c = 1)$ in the spherical system of coordinates has the form

$$[-\nabla^2 + (M + S(\vec{r}))^2]\psi(r,\theta,\varphi) = [E - V(\vec{r})]^2\psi(r,\theta,\varphi), \qquad (2)$$

where M —is the rest mass of a scalar particle, and E —is the energy of a relativistic particle. For simplicity, in Eq. (3) we consider that the scalar potential is equal to the vector potential $S(\vec{r}) = V(\vec{r})$. Then obtain:

$$\left[\nabla^2 + E^2 - M^2 - 2(E+M)V(r) - 2(E+M)\frac{f(\theta)}{r^2}\right]\psi(\vec{r}) = 0. \qquad (3)$$

This equation in the spherical system of coordinates admits separation of variables. Therefore, the wave function $\psi(\vec{r})$ can be written as

$$\psi(\vec{r}) = \frac{\chi(r)}{r}\Theta(\theta)\Phi(\varphi), \tag{4}$$

After substitution of function (4) into Eq. (3), we obtain radial KFG in this form:

$$\chi''(r) + \left[E^2 - M^2 - 2V(r)(E+M) - \frac{\lambda}{r^2}\right]\chi(r) = 0, \tag{5}$$

where λ is separation constant. To analytically solve Eq. (5) for the case $\lambda \neq 0$, we apply a special approximation to the centrifugal potential. Then we get

$$\chi''(r) + \left[\varepsilon^2 - \gamma D\left(1 - \frac{\sigma(1+e^{-2\alpha r})}{(1-e^{-2\alpha r})}\right)^2 - \frac{4\alpha^2\mu e^{-2\alpha r}}{(1-e^{-2\alpha r})^2}\right]\chi(r) = 0. \tag{6}$$

Thus, we find an analytical expression for the energy eigenvalues and for radial wave function $\chi_{nl}(r)$ in the form:

$$M^2 - E^2 = -\alpha^2 \times$$

$$\left[\frac{[\beta^2 - n^2 - l(l+1) - l(l+1) - (2n+1)\left(1 + 2\sqrt{\eta^2 + (l+1/2)^2}\right)}{(2n+1) + \sqrt{\eta^2 + (l+\frac{1}{2})^2}}\right]^2 -$$

$$-l(l+1)d_0\alpha^2. \tag{7}$$

$$\chi_{nl}(r) = C_{nl}e^{\sqrt{L}\alpha r}(1-s)^K P_n^{\left(2\sqrt{L},2K-1\right)}(1-2s). \tag{8}$$

CURRENT FLUCTUATIONS IN IMPURITY SEMICONDUCTORS

*Aliyev S.R., Hasanov E.R.
Baku State University, Azerbaijan
senanvselmir@gmail.com

In conducting media, under the influence of an external electric field, charge carriers receive additional energy from the electric field. In this case, redistribution of charge carriers occurs in the form of a wave. These waves may become unstable and begin to radiate energy. The mechanism and cause of the occurrence of unstable waves in different conducting

media are different. Therefore, theoretical studies of unstable states require different mathematical approaches. In impurity semiconductors, the conditions for excitation of unstable waves depend on a number of factors due to the presence of different impurity centers in the medium. Impurity levels are located at different distances from the conduction band of the semiconductor. Depending on the temperature of the semiconductor, these energy levels are more or less active levels. This theoretical work examines current oscillation (i.e., external instability) in semiconductors with singly and doubly negative impurity centers in an external and electric E_0 field in the presence of weak magnetic fields (i.e., $\mu_{\pm}H_0 << c$, $\mu_{\pm}$ – mobility of holes and electrons, c – speed of light).

Basic equations of the problem

In the presence of an external magnetic field and a temperature gradient, the current densities for electrons and holes have the form:

$$\vec{j}_- = -N_-\nu_-E^* - N_-\nu_{1-}[E^*H] - \alpha_-\vec{\nabla}T - \alpha'_-\left[\vec{\nabla}T\vec{H}\right],$$
$$\vec{j}_+ = N_+\nu_+E^* + N_+\nu_{1+}[E^*H] + \alpha_+\vec{\nabla}T + \alpha'_+[\vec{\nabla}T\vec{H}], \quad (1)$$

$$\vec{j} = e(\vec{j}_+ - \vec{j}_-). \quad (2)$$

Substituting (1) into (2)

$$E^* = \frac{\vec{j}}{\sigma} - \frac{\sigma_1}{\sigma}\left[\vec{E}^*\vec{H}\right] - \frac{\alpha}{\sigma}\vec{\nabla}T + \frac{\alpha_1}{\sigma}\left[\vec{\nabla}T\vec{H}\right], \quad (3)$$

$$\vec{E} = -\frac{\left[\vec{V}\vec{H}\right]}{c} - \frac{\Lambda'}{\sigma}\left[\vec{\nabla}T\vec{H}\right] + \frac{\vec{j}}{\sigma} - \frac{\sigma_1}{\sigma^2}\left[\vec{j}\vec{H}\right] + \Lambda\vec{\nabla}T + \frac{T}{e}\left(\frac{\nabla n'_-}{n^0_-} - \frac{\nabla n'_+}{n^0_+}\right). \quad (4)$$

$E'(x,t)$ is found from (5)

$$E'_x = \frac{J'_x}{\sigma_0\varphi} + \frac{iT}{e\varphi}(k_1 + k_2)\left(\frac{N'_-}{N^0_-} - \frac{N'_+}{N^0_+}\right),$$
$$E_0 = \frac{E_1}{1 \pm \frac{4T}{eZ_0r}\frac{\mu_-}{\mu_+}\left(\frac{\delta_-}{N^0_-} - \frac{\delta_+}{N^0_+}\right)}. \quad (5)$$

IKEDA WITH LINEAR AND NON-LINEAR RELATIONSHIP COMBINED SYNCHRONIZATION BETWEEN SYSTEMS

[1*]Nuriyev R.A., [2]Pashayev B.G.

[1]Institute of Physics, Ministry of Science and Education, Azerbaijan

[2]Baku State University, Azerbaijan

[1]rus.nuriyev.74@mail.ru, p.g.bakhtiyar@gmail.com

If complete (identical) synchronization occurs between controlled systems, generalized synchronization occurs between the controlling system and the controlled system. The concept of generalized synchronization was first used in the context of one-way communication between systems, and then it was extended to networked systems. Consider the synchronization of the two x and y Ikeda systems, which are linearly connected to one another:

$$\frac{dx}{dt} = -\alpha x + m_1 \sin x_{\tau_1}, \qquad \frac{dy}{dt} = -\alpha y + m_2 \sin y_{\tau_2} + K(x - y)$$

Note that there is x=y complete synchronization between the x and y Ikeda systems under the condition $m_1 = m_2$ and $\tau_1 = \tau_2$, and this synchronization mode is stable under the $\alpha + K > |m_1|$ condition. Let's assume that $\tau_1 \neq \tau_2$. At this time, it can be determined that, already, $x = y$ is not a synchronization mode. In this study, it is demonstrated that a synchronization mode may exist. For this purpose, the requirements of the full synchronization mode of the dynamic variables y and z controlled by the controlling dynamic variable x has to be defined. Remember that dynamical system z is a duplicate of system y:

$$\frac{dz}{dt} = -\alpha z + m_2 \sin z_{\tau_2} + K(x - z).$$

The condition of complete synchronization between the dynamic variables y and z, and thus the generalized synchronization between the dynamic variables x and y, can be found as a result of studying the $y - z$ dynamics of the error signal:

$$\alpha + K > |m_2|$$

If a parameter discrepancy occurs between m_1 and m_2, the preceding generalized synchronization condition can still be obtained. Let us now investigate generalized synchronization between nonlinearly connected Ikeda systems. Remember that this contact time is equal to τ_3.

$$\frac{dx}{dt} = -\alpha x + m_1 \sin x_{\tau_1}, \qquad \frac{dy}{dt} = -\alpha y + m_2 \sin y_{\tau_2} + K \sin x_{\tau_3}.$$

It was determined that the synchronization mode $y = x_{\tau_3 - \tau_1}$ is possible under the conditions $\tau_1 = \tau_2$ and $m_1 = m_2 + K$. It is clear that the dependence between the dynamic variables y and $x_{\tau_3 - \tau_1}$ is linear. Now let's look at the parameter discrepancy case. Suppose $\tau_1 \neq \tau_2$. Then it is clear that already, $y = x_{\tau_3 - \tau_1}$ is not a synchronization mode. Let's investigate the possibility of generalized synchronization. For this, it is sufficient to investigate the complete synchronization between the dynamic system y and its copy system z:

$$\frac{dz}{dt} = -\alpha z + m_2 \sin z_{\tau_2} + K \sin x_{\tau_3}.$$

The dynamics of the error signal $\Delta = y - z$ can be written in the following form:

$$\frac{d\Delta}{dt} = -\alpha \Delta + m_2 \Delta_{\tau_2} \cos y_{\tau_2}.$$

From here it can be concluded that the generalized synchronization between y and $x_{\tau_3 - \tau_1}$ is possible within the $\alpha + K > |m_1|$ condition. There is good agreement between computer modeling of Ikeda systems and theoretical results. Ikeda systems with non-linear connections were studied by computer modeling at values of parameters $\alpha = 1$, $\tau_1 = 7$, $\tau_2 = 13$,$\tau_3 = 5$, $m_1 = 9$, $m_2 = 0.9$, $K = 8.1$.

ELECTROMAGNETIC SHOWER IN CRYSTALS

Rajabov M.R.
Baku State University, Azerbaijan
m_rajabov@mail.ru

It is known that the interaction of electrons and γ-quanta with matter leads to the formation of electromagnetic showers. Showers in amorphous targets are described quite well by the well-known cascade theory. However, it should be noted that the formation of an electromagnetic shower in a crystal differs significantly from the formation of a shower in an amorphous substance. In this regard, a theoretical study was carried out on the formation of an electromagnetic shower in a crystal, taking into account the coherent nature of the processes of bremsstrahlung of

electrons and positrons, as well as the photoproduction of e+e pairs, which is due to the formation of shower particles. The dependence of the number of shower particles on energy, the angle of entry of the initial electrons into the crystal, and the penetration depth was obtained.

LITERATURE REVIEW ON INCLUSION OF SOLAR PANEL SYSTEMS, BENEFITS AND CHALLENGES IN ALBANIA

Zeneli M.
Aleksander Moisiu University, Albania
manjolazeneli2@yahoo.com

Albania, like many other countries, is currently exploring the integration of solar panel systems into its energy infrastructure to harness the benefits of renewable energy sources. This literature review examines the various aspects of incorporating solar panel systems in Albania, focusing on the benefits and challenges associated with this transition.

The review begins by providing an overview of Albania's energy landscape and its increasing dependence on fossil fuels. It then delves into the potential benefits of solar panel systems in the context of Albania, including reduced greenhouse gas emissions, energy independence, and job creation. The discussion also highlights the role of solar energy in mitigating climate change, addressing energy security concerns, and fostering economic growth.

On the flip side, this literature review comprehensively addresses the challenges associated with the integration of solar panel systems in Albania. These challenges encompass technical issues, such as grid integration and intermittent, as well as economic and policy-related barriers like financing, subsidies, and regulatory frameworks either they are on the right way since for families the government has structures and applied some procedure. The review also explores social and cultural factors that may influence the adoption of solar energy technologies in Albania.

Moreover, the literature review examines existing case studies and research findings from similar contexts to draw insights applicable to the Albanian context. It emphasizes the importance of a multidisciplinary approach, involving government policies, industry stakeholders, and public awareness campaigns in fostering a sustainable transition to solar energy.

This review aims to provide a holistic understanding of the prospects, hurdles, and potential strategies for the successful inclusion of solar panel

systems in Albania's energy portfolio. By synthesizing and analyzing existing literature, it offers valuable insights for policymakers, researchers, and practitioners involved in the development of sustainable energy strategies for Albania and other regions with similar challenges and opportunities.

DEFINITION OF ELECTRIC PARAMETERS OF Re/n-GaAs SCHOTTKY DIODE USING I–V MEASUREMENTS

[1*]Afandiyeva I.M., [1]Godjayev N.N., [3]Babayeva R.F.
[1]Baku State University, Azerbaijan
[2]Azerbaijan State University of Economics, Azerbaijan
afandiyeva@mail.ru

Contact phenomena are used in the vast majority of modern semiconductor devices. The advantages of metal-semiconductor contacts with a Schottky barrier are taken into account when solving a number of practical problems. The electrical properties and fabrication of Schottky barrier diodes (SBDs) very interesting both in electronic applications and in understanding other semiconductor devices. The main parameters, performance and reliability of these diodes depend on the choice of contacting materials, their crystal structure, the uniformity of the metal-semiconductor interface.

SBDs on the basis of GaAs are an important element of integrated circuits. On the other hand, rhenium is also an interesting material due to high melting point, chemical resistance, catalytic activity. Its advantages are stability at high temperatures, high stability of films, a low temperature coefficient of resistance, a slight change in resistance with increasing film thickness. However, there is practically no experimental information in the literature about Re/n-GaAs SBDs. The aim of this study is investigation of main parameters of Re/n-GaAs on the basis $I-V$ characteristic measured at room temperature.

The diodes were fabricated by using PLD technique. Characteristics parameters such as potential barrier height (Φ_{B0}), ideality factor (n) and series resistance (R_s) have been calculated by using different methods and compared. On the basis of the current-voltage-characteristics from Ohm's law the resistance of Re/n-GaAs SBDs (R_i) ($R_i = (dV_i)/(dI_i)$) and from the voltage-dependent profile of the resistance $R_i - V$ important parameters as series resistance R_s and shunt resistance (R_{sh}) characterizing the reliability of the diode were derived (R_s=3.92 Ω, R_{sh}=2.19E+1 Ω) at (+4V) and (-4V), respectively).Besides, $I-V$ characteristic has been analyzed by the

depending LnI vs LnV. Changing the slope of the characteristic does not allow to accurately determine the height of the potential barrier, ideality factor and series resistance. To determine Φ_B and R_s Norde's method has been used. For the definition of Potential barrier height and series resistance at room temperature for the Re/n-GaAs diode was used the minimum point of $F(V)$ vs V plot. The $\mathrm{V_{min}}$, $F(V_{min})$, Φ_{Bn} and R_s values were found to be 0.3 V, 5.88x10^{-1} V, 0.78 eV and 4.13 Ω, respectively. Another way to solve the identified problem is to use the method developed by Cheung. The method has been used in order to compute Re/n-GaAs SBD parameters like the Φ_B, n and R_s. Besides, another method for the obtaining of series resistance and ideality factor is Verner's method has been used. That is method based on differential conductance ($L = dI/dV$). The obtained results indicates the difference between the selected models and ideal model. To explain the obtained results, it should be taken into account that the ratio of the lattice parameters of the metal and semiconductor plays a significant role in the formation of a contact.

EFFECT OF THERMAL TREATMENT METHODS ON MAGNETIC HYSTERESIS PROPERTIES OF Fe-Ni-Si-B BASED AMORPHOUS MAGNETS

Abdullayev A.P., *Rafiyev N.M., Isayeva A.A., Asgarova G.Z.
Azerbaijan University of Architecture and Construction, Azerbaijan
adilabdullayev@rambler.ru, nrafiyev@mail.ru, isayeva_aida86@mail.ru, gunelesger85@gmail.com

Soft magnetic amorphous materials are considered a new type of magnets. Although amorphous materials have a wide scope in modern times, new areas of application can be obtained by improving their properties. In this study, as a result of heat treatment of the composition $Fe_{59}Ni_{19}Si_9B_{13}$ and $Fe_{39}Ni_{39}Si_9B_{13}$, materials with properties suitable for operation were obtained.

In this research work, improvement of magnetic hysteresis properties was carried out by thermal processing of 1-$Fe_{59}Ni_{19}Si_9B_{13}$ and 2-$Fe_{39}Ni_{39}Si_9B_{13}$ alloys in two compositions, obtained in amorphous state by cooling at high speed. For this, the samples were kept for 40 minutes in 3 different temperature conditions. The purpose of the heat treatment was to relieve the bending stresses generated during the casting process and to achieve bidirectional adjustment processes.

In sample 1, an increase in the rectangularity of the hysteresis loop and

the maximum magnetic induction B_m was determined as a result of processing at a temperature of 513K for 40 minutes. As a result of thermal treatment, a sharp increase in the coercive force is observed by holding at a temperature of 683K for 40 minutes, an increase in the value of saturation magnetic induction and residual magnetization was detected. In sample 2, it is observed that the rectangularity of the hysteresis loop changes less as a result of processing at 513K temperature for 40 minutes, the increase of the maximum magnetic induction B_m was determined. As a result of thermal treatment, no increase in the coercive force was observed, and a small increase in the value of saturation magnetic induction and residual magnetization was detected by keeping it at 683K temperature for 40 minutes (Fig. 1).

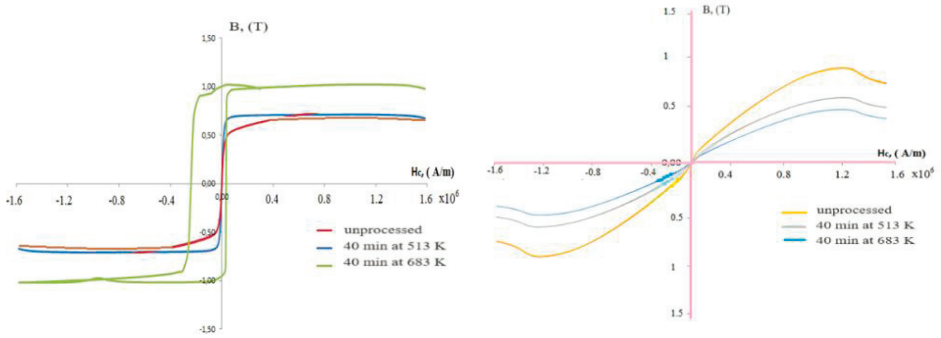

a) b)

Fig. 1. Changes of the hysteresis loop as a result of alloy processing.
a – 1 sample and b – 2 sample

The parameters of the hysteresis loop and the value of the specific electrical resistance of the two-component amorphous alloy indicate that these materials are suitable for use in the magnetic materials industry.

DIELECTRIC FUNCTION OF MoS_2 THIN FILMS

*Jalilli J.N., Alizade E.H., Hidiyev K.H., Mammadov D.A.
Institute of Physics, Ministry of Science and Education, Azerbaijan
Cavid199329@gmail.com

Spectroscopic ellipsometry was then applied to the obtained MoS_2/SiO_2/Si structures. The ellipsometric data collected at difference angles of incidence were analyzed within three phase (MoS_2/SiO_2/Si) optical model and the complex dielectric function of each MoS_2 film was retrieved in the

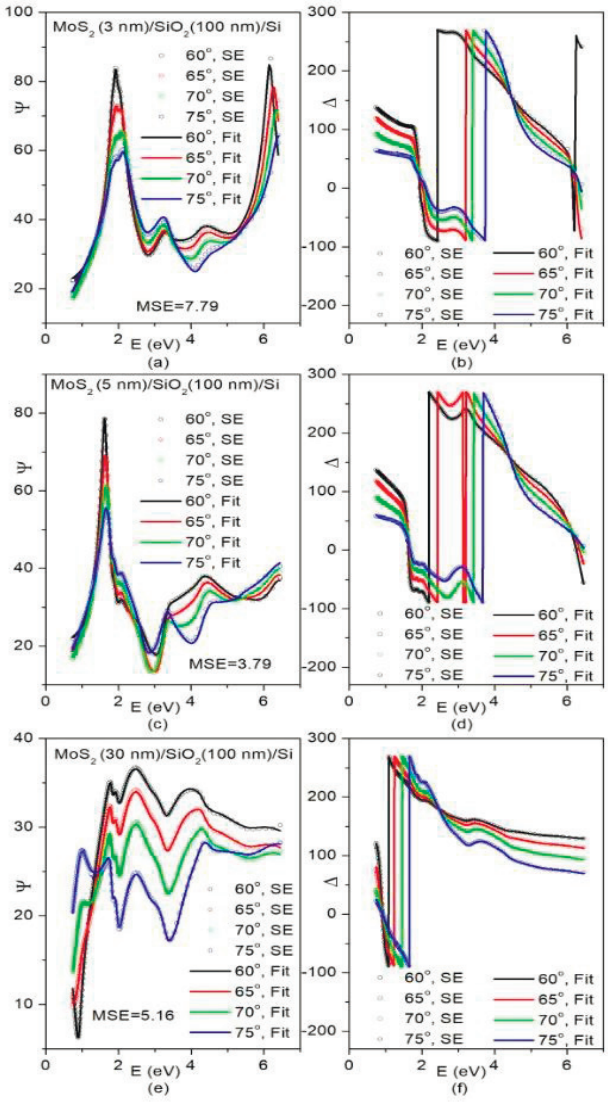

Fig. Ellipsometric parameters Psi and Delta with fit

photon energy range from 0.73 to 6.4 eV. Spectroscopic ellipsometry was used to trace down the evolution of the electronic energy spectrum in the photon energy range of 0.07-6.5 eV as the MoS_2 thickness was reduced from 30 to 5 and 3 nm. Experimental approaches verify preservation of the well-known, distinctive A, B, C, and E exciton structures at and above the direct energy gap down to 3 nm film.

DEVELOPMENT OF METHODS FOR CONCENTRATING PALLADIUM WITH SYNTHETIC SORBENTS BASED ON A COPOLYMER OF MALEIC ANHYDRIDE WITH STYRENE

*Abilova U.M., Hajiyeva S.R., Chiraqov F.M.
Baku State University, Azerbaijan
u.abilova@mail.ru

New chelating polymeric sorbent on the basis of maleic anhydride styrene copolymer by the chemically modification with streptocide has been synthesized. A new chelate polymer sorbent based on a copolymer of maleic anhydride and styrene was synthesized by chemical modification with amines.

This work includes the synthesis of a new adsorbent based on a copolymer of styrene maleic anhydride (MAST) and the amines diamino benzidine (M_1) and orthophenylenediamine (M_2). The synthesis of adsorbents was carried out in a known manner.

During the study, we studied the influence of various parameters on the adsorption process, especially the influence of pH, contact time, ionic strength, and initial concentration of palladium metal ions. The desorption process and the influence of various organic and inorganic acids on the desorption process were also studied. The results showed that $HClO_4$ is the best eluent.

The adsorption process was characterized by several adsorption isotherms and kinetic models. The results are in best agreement with the Langmuir model. It was found that the equilibrium data could best be explained by a pseudo-second-order model. Studies have shown that, in comparison with the original products, the adsorption capacities of which were 408 and 513 mg/g, the modified adsorbents have a higher adsorption capacity for Pd (II) ions and amount to 690 and 579 mg/g, respectively.

The synthesized adsorbents were characterized by scanning electron microscopy (SEM) with energy-dispersive X-ray spectroscopy (EDS) and ultraviolet-visible spectroscopy (UV/Vis). The temperature stability of the adsorbent was studied by thermal analysis methods (TG, DTA, DDTA).

Table 1.

Main indicators of static sorption experiments (d=14 mm)

Element	Sorbent	SE, mq/q	$pH_{opt.}$	μ*, mol/l	Time, min.
Pd(II)	M_1	690	4	0,8	90
	M_2	579	3	0,8	60

**-value of ionic strength, which contributes to a strong decrease in the degree of sorption*

Resulting products were applied for determination of Pd(II) ions in fruits (Table 1).

THERMOELECTRIC CONVERTERS OF IR RADIATION BASED ON $Ag_3In_5Te_9$

*Rahimov R.Sh., Sarmasov S.N.
Baku State University, Azerbaijan
rehim@rehimli.info

Thermomagnetic and thermoelectric phenomena are one of the main sections of semiconductor physics. They are interrelated, their study allows a deeper understanding of electronic processes occurring in semiconductors. In recent years, interest in the development of thermomagnetic and thermoelectric IR converters based on new semiconductors with small lattice thermal conductivity has increased significantly.

To create a thermomagnetic IR converter with significant specific sensitivity, it is necessary to choose a material with low thermal conductivity, but a large value of the H-E coefficient. Dimensionless H-E field coefficient is of great importance in materials, in which at not very high concentrations of carriers have a large mobility, and in the region of mixed conductivity under the condition $U_n/U_p \gg 1$ (U_n and U_p – are mobilities of electrons and holes, respectively).

It follows from the formula ($Z = \frac{(\frac{k_0}{e}\varepsilon_y)}{\chi}\sigma$), that to create converters with a high quality factor, a material with low thermal conductivity and a high value of ε_y is required. To do this, it is necessary that the material has high electrical conductivity, i.e. high mobility of carriers. If you increase ε_y due to the participation of minority charge carriers in the conductivity, then the electrical resistance also increases greatly, which can lead to a worsening in the quality factor.

To develop low-inertia receivers, it is necessary that the sensitive element have a minimum thickness and have high thermal conductivity. The detection ability of receivers mainly depends on specific sensitivity and electrical conductivity.

For modern thermoelectric materials ΔT =1K and $f(z)$ =0.2, ε=60. At ΔT<1 K, ε increases even more and the energy consumption for controlling the temperature of the amplifier decreases accordingly. The thermal generator battery is assembled from series-connected elements with dimensions of 0.8x0.8x1mm^3. It is attached to a Peltier thermoelement, p -

branch of which is made of Bi-Te-S and, n - branch of Bi-Te-Se,

The paper presents the main characteristics of IR radiation converters based on $Ag_3In_5Te_9$ and identifies these as the most promising materials for an IR radiation receiver. It has been shown that in a narrow temperature range the thermal emf increases sharply. This also allows it to be used as a thermoelectric transducer used in measurement technology to amplify weak electrical signals.

INFLUENCE OF ZINC-CONTAINING NANOPARTICLES ON THE PROPERTIES OF COMPOSITIONS BASED ON ISOTACTIC POLYPROPYLENE CONTAINING A MIXTURE OF $C_{60/70}$ FULLERENES

[1*]Dunyamalieva A.I., [1]Kurbanova N.I., [2]Zeynalov E.B.

[1]Institute Polymer Materials, Ministry of Science and Education, Azerbaijan
[2]Institute Catalysis of Inorganic Chemistry, Ministry of Science and Education, Azerbaijan
dunyamaliyeva89@list.ru; ipoma@science.az

Materials with nanoscale structures often have excellent optical, thermal conductivity, mechanical, chemical or electronic properties compared to their bulk counterparts. The development of nanotechnology and related research and production methods have led to an increase in interest in nanomaterials. The molecular composition, size, structure and surface chemistry of nanomaterials can be precisely controlled to tailor their properties for specific devices or applications in various fields; based on this controlled functionality, nanomaterials have many potential commercial applications.

Functionalized carbon nanomaterials exhibit various physical and chemical properties, including chemical stability, good thermal conductivity, unique mechanical properties, high electrical conductivity, and improved optical properties, and hence have attracted much attention since they were first reported.

The presented work is devoted to the preparation and study of the properties of composites based on isotactic polypropylene (PP): 1 - PP, zinc oxide nanoparticles (ZnO NPs); 2-PP, mixture of fullerenes $C_{60/70}$; 3 - PP, a mixture of $C_{60/70}$ fullerenes and zinc oxide nanoparticles (ZnO NPs);

Nanocomposite polymer materials were obtained by mixing PP in the presence of nanofillers: a mixture of $C_{60/70}$ fullerenes and ZnO NPs on laboratory rollers at a temperature of 160-165 °C for 15 minutes. To carry

out mechanical tests, the resulting mixtures were pressed into plates 1 mm thick at 190 °C and a pressure of 10 MPa for 10 minutes.

It has been shown that the introduction of zinc oxide nanoparticles into a composition based on isotactic polypropylene containing a mixture of fullerenes at a ratio of PP/$C_{60/70}$/ZnONPs=100/0.02/0.5. helps to increase tensile strength from 31.44 to 33.28 MPa, Vicat heat resistance from 165 to 180°C, while maintaining elongation at break.

INFLUENCE OF EXCHANGE INTERACTION AND BAND GAP ON THE THERMODYNAMIC PROPERTIES OF DILUTED MAGNETIC SEMICONDUCTOR FILMS

Figarova S.R., *Mahmudov M.M., Damirov R.Y.
Baku State University, Azerbaijan
ragibdamirov@bsu.edu.az

Size effects and exchange interaction between band electrons (s, p) and d electrons localized on magnetic ions in diluted magnetic semiconductor (DMS) films lead to a band parameters changing, as a result of which the energy spectrum becomes very sensitive to the magnetic field and other external parameters, in particular of the sample size.

As a result, their physical characteristics: thermodynamic, kinetic and optical have a number of features. In this work the influence of energy spectrum parameters, magnetic impurities concentration, temperature and film thickness on the thermodynamic properties of diluted magnetic semiconductor films are studied.

It has been shown that the specific heat capacity of degenerate electron gas in diluted semi-magnetic semiconductor films at low temperatures is greater than the heat capacity of non-magnetic structures. Excess heat capacity is due to an increase in the density of states and the magnetic properties of impurities. With increasing of the impurities concentration, the dependence of the heat capacity on temperature is non-monotonic. At very high concentrations $x = 0.8$ this dependence has a maximum at $T = 20K$.

The appearance of the maximum is associated with the phase transition of the paramagnetic state to the antiferromagnetic state. It was found that for ultrathin diluted semi-magnetic semiconductor films the heat capacity is directly proportional to the band gap square, which increases with the concentration of the magnetic impurity. For example, when the

concentration increases threefold, the band gap increases from 1.4 to 2.9 eV (for $Cd_{1-x}Mn_xTe$).

It was found that the heat capacity of a non-degenerate electron gas depends significantly on the exchange interaction energy. The entropy and heat capacity of diluted semi-magnetic semiconductor films are determined by the density of states, which depends on the impurities concentration, exchange interaction and film thickness. It is also noted that entropy and heat capacity oscillate with film thickness and when the Fermi energy coincides to the size-quantized level they experience a jump.

THERMOPOWER IN A SEMICONDUCTOR QUANTUM WELL WITH MODIFIED PÖSCHL-TELLER CONFINING POTENTIAL

*Babayev M.M., Sultanova Kh.B.
Institute of Physics, Ministry of Science and Education, Azerbaijan
mirbababababayev@yahoo.com

The study of electron transport phenomena in low-dimensional systems, including thin films (quantum wells), is one of the most important issues related to the problem of reducing the size of electronic devices. At low crystal temperatures, the drag of electrons by phonons plays a significant role in thermoelectric phenomena. In this work, the thermopower in a semiconductor quantum well was studied taking into account the drag of electrons by phonons.

Actual shape of the confinement potential is unknown, and so different models are used. The most-used models are the square well potential and the parabolic well potential. In the present work, the modified Pöschl-Teller potential is used as a potential that confines the motion of electrons in a quantum well. The shape of this potential is intermediate between that of square and parabolic wells.

We consider the case when the temperature gradient is created parallel to the plane of quantum film. In this plane, the motion of electrons is not confined, so Boltzmann's kinetic equation can be used to determine the electron distribution function and the thermopower. The scattering of electrons by ions, acoustic and piezoacoustic phonons, as well as the screening of scattering potentials by charge carriers are taken into account. The scattering times due to these scattering mechanisms, the chemical potential of electrons and the electron mobility have been calculated.

Within the above conditions, a general expression of thermopower in a quantum well has been found. On the basis of the obtained theoretical results, the temperature dependence of thermopower in a $GaAs/Al_xGa_{1-x}As$ quantum well at low temperatures has been studied. Numerical calculations show that our theoretical results are in good agreement with experimental ones. This indicates that the modified Pöschl-Teller potential describes well the confinement potential in semiconductor quantum wells.

INTERBAND LIGHT ABSORPTION IN QUANTUM FILM OF $Hg_{1-x}Cd_xTe$

*Ismayilov T.H., Aslanli A.F.
Baku State University, Azerbaijan
tariyel.i@gmail.com aslanliaysel90@gmail.com

Spectra of optical parameters contain unique information about electronic phenomena in semiconductors. In recent years, structures based on narrow-gap $Hg_{1-x}Cd_xTe$ solid solutions have attracted increased interest.

Thanks to significant progress in growth technology (molecular beam epitaxy) achieved in the last decade, it has become possible to obtain high-quality HgCdTe-based epitaxial structures, both bulk layers of the $Hg_{1-x}Cd_xTe$ solid solution and heterostructures with HgTe/CdHgTe quantum wells (QWs). HgTe/CdHgTe QWs have many different interesting properties, such as a topological insulator state, a gapless band structure with a linear (graphene-like) dispersion law, giant Rashba splitting. Structures based on Hg_{1-x}CdxTe compounds are also of interest from the point of view of a material for mid- and far-IR detectors. Since HgTe has a so-called inverted band structure with a “negative” band gap, and CdTe has a normal band structure, in Hg_{1-x}CdxTe solid solutions it is possible to obtain an arbitrary band gap from 0 to 1.6 eV. As a result, such structures are the main material for interband detectors in the mid-IR range in atmospheric transparency windows of 3 – 5 μm and 8 – 14 μm and may have prospects for use in the far IR range. On the other hand, such structures with HgTe/CdHgTe QWs, due to the high mobility of charge carriers in QWs with a thickness close to critical and topological protection of edge states, can be used as a material for field-effect transistors (FETs) with high mobility that detect THz radiation.

In this article the interband light absorption in quantum films of $Hg_{1-x}Cd_xTe$ is studied theoretically. Previously from the Schrödinger equation

the wave functions for arbitrary wave vector k and energy spectrum of electrons and holes are found. Then, based on them, the optical absorption coefficient was calculated. The analytical expression depending on the frequency of incident light, band-gap of Hg_{1-x} Cd_xTe and width of quantum well is obtained. The various cases of incident light polarizations are considered. The selection rules have been established.

DETERMINATION OF BAND GAP OF $(AgSbTe_2)_{0.8}(PbTe)_{0.2}$ FROM ELECTROPHYSICAL AND OPTICAL PROPERTIES

[1,2*]Ragımov S.S., [3]Hashımova N.N.
[1]Baku State University, Azerbaijan
[2]Institute of Physics, Ministry of Science and Education, Azerbaijan
[3]Azerbaijan State Oil and Industry University, Azerbaijan
sadiyar.raqimov@bsu.edu.az; sadiyar@mail.ru

$AgSbTe_2$ is a promising p-type thermoelectric material and has been studied by many authors. Based on this thermoelectric material, various thermoelectric compositions have been created. Based on the compounds $AgSbTe_2$ and PbTe the system is called LAST and can be represented as $(AgSbTe_2)_X(PbTe)_{1-X}$. Note that both $AgSbTe_2$ and PbTe crystallize in a cubic lattice structure. At different values of the components, it is possible to obtain a series of solid solutions.

Manipulation of the band structures is a key strategy for improving the thermoelectric properties of materials. By this way can achieve to obtain a high value of thermal power and electrical conductivity coefficients.

Electrical conductivity and Seebeck coefficient are determined only by the electronic properties of the material. By changing the composition, it is possible to vary the parameters of band structure of materials. This is very important for optimizing their thermoelectric properties.

In this work are presented the results of the temperature dependencies of electrical conductivity and Seebeck coefficient of $(AgSbTe_2)_{0.8}(PbTe)_{0.2}$. The experiments were provided in the 80-550K temperature range.

According to experimental results of electrical conductivity and Seebeck coefficient was estimated the band gap width of $(AgSbTe_2)_{0.8}(PbTe)_{0.2}$ (E_g=0.23 эВ).

The band gap width was also estimated using the formula of Goldsmith-Sharpe and the Vegard rule.

It was carried out the spectroscopic ellipsometric optical measurements of $(AgSbTe_2)_{0.8}(PbTe)_{0.2}$. According to experimental results of optical measurements it was estimated the value of band gap width also.

STUDY OF PARTICLE ACCELERATION MECHANISMS IN THE ANISOTROPIC SOLAR WIND

Bashirov M.M.
Baku State University, Azerbaijan
mbashirov@bsu.edu.az

The work examines Compton and inverse Compton effects in solar wind plasma, equations obtained on the basis of magnetohydrodynamic (MHD) theory for single-particle plasma. The radial dependences of the solar wind speed were obtained and analyzed. A MHD approximation in collisionless plasma was carried out, and the problems and many of their special solutions were considered, taking into account thermal effects. Radial and stationary flow from the Sun is considered with isotropic MHD equations, taking into account the heat fluxes.

$$3r^3\frac{dX(x)}{dx}+\frac{f_1(x)}{f(x)}=0,\ \ 6r^3\frac{dY(x)}{dx}+\frac{f_2(x)}{f(x)}=0,\ \ 6x^3X(x)\frac{dZ(x)}{dx}+\frac{f_3(x)}{f(x)A(x)}=0.$$

Where

$$x=\frac{r}{R},X=X(x)=\frac{V^2}{v_0^2},Y=Y(x)=\frac{u_{\parallel}^2}{v_0^2},\ Z=Z(x)=x^2\frac{u_{\perp}^2}{v_0^2},\ A(x)=\frac{Y(x)}{X(x)}-1,$$

$f(x)$; $f_1(x)$; $f_2(x)$ and $f_3(x)$ are a function of x.

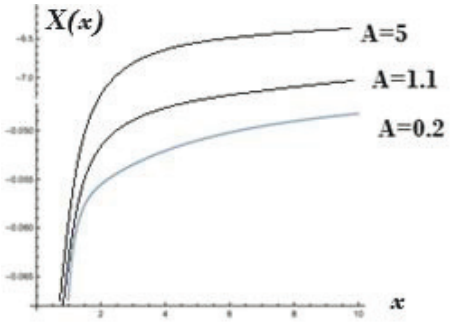

Figures of the X(x) parameter, which characterizes the speed of the solar wind, as A function of the x distance for different values were determined. it can be seen from the graphs that the value of the quantity X(*x*) characterizing the solar wind starts from the point *x*=1. It was bought as such for all special occasions. From here, it is possible to give the physical meaning of the quantity R (characteristic distance): since the solar wind originates from the surface of the

Sun, it is created due to coronal mass ejections, so the distance R can be taken as the radius of the sun or the distance from the center of the sun to a middle point where coronal mass ejections occur. Thus, the quantity R carries the essence of the distance from which the solar wind starts. This distance can be taken as the radius of the Sun at first approximation. As it moves away from the Sun, the speed of the solar wind plasma first increases and then remains constant starting from a certain distance, and decreases near the heliosphere. It can be seen from the graphs that the speed of the solar wind increases sharply at first, and then this rate of increase weakens. Since the equations written for the solar wind do not show the heliospheric boundaries and do not take into account the effects of extrastellar winds, this speed will simply increase in the graphs.

The results are important in explaining the acceleration mechanism of cosmic plasma particles, in studying the evolution process of the Sun and stars, as well as in the study of the factors affecting the operation of radio electronic control devices.

SPATIAL STRUCTURE OF HEPTAPEPTIDE MOLECULE

*Ismailova L., Akhmedov N.A.
Baku State University, Azerbaijan
lara.ismailova.52@mail.ru

Nociceptins are a new type of regulatory peptides of medical interest. Their mechanisms of action are considered anti-opioid. Natural nociceptin reduces motor activity, causes a stress response and modulates spatial attention. For medicine and pharmacology, knowledge of the structural and functional properties of peptide molecules is of great practical importance. This scientific work is devoted to study the spatial structure and conformational possibilities of the heptapeptide Phe1-Gly2-Gly3-Phe4-Pro5-Gly6-Pro7. This neuropeptide molecule is stable analogue of the nociceptin. It was found that the N-terminal tripeptide and tetrapeptide of this molecule are active.

It is known that short linear peptides in solutions do not have a fixed spatial structure. The amino acid sequence and physicochemical properties of the solvent determine the set of low-energy conformations of the peptide molecule. The biologically active conformation of the peptide molecule, which is realized upon interaction with the receptor, is included in the set of low-energy structures that exist in an aqueous solution. Therefore, the study of the spatial structure of peptide molecules is of great interest.

The conformational possibilities of the heptapeptide Phe1-Gly2-Gly3-Phe4-Pro5-Gly6-Pro7 were studied in fragments. First, the conformational properties of the tripeptides Phe1-Gly2-Gly3 and Pro5-Gly6-Pro7, tetrapeptide Phe1-Gly2-Gly3-Phe4 were determined based on the stable conformations of the monopeptides. And finally, the addition of the tetrapeptide Phe1-Gly2-Gly3-Phe4 and tripeptide Pro5-Gly6-Pro6 allowed us to calculate the spatial structure of the heptapeptide molecule. It is known that the active site of the molecule that activates the receptor is the N-terminal tetrapeptide Phe1-Gly2-Gly3-Phe4.

The calculations were carried out by the method of theoretical conformational analysis with regard to nonvalent, electrostatic and torsional interactions, energy of the hydrogen bonds and a special computer program. The low-energy conformations of this molecule and the values of the dihedral angles of the main chain and side chains are found and the energy of the intra- and inter-residue interactions was estimated. The conformational mobility of the Phe1 and Phe4 amino acid side chains is investigated and the amino acids with specific interplays with different receptors are founded. The relative energy of the conformations of this molecule varied within the range 0–8 kcal/mol. Study of the spatial structure of heptapeptide have almost 11 low-energy conformations. The global conformation (U_{rel}=0 kcal/mol) is $B_{11}LPB_{11}RBR$ (fffefe). This shape includes 4 more main chain forms: $B_{11}PRB_{11}RBR$, $B_{11}LPB_{21}RBR$, $B_{11}LPB_{21}BLR$ and $B_{21}PRB_{11}BLR$. It is revealed that low energy conformations of these molecule have the folded and half folded types of backbone.

The results can be used to study the spatial structure of heptapeptide molecule as well as to study the conformational possibilities of side chains when interacting with receptor molecules.

CONFORMATIONAL PARTICULARITIES OF ANTIBACTERIAL, ANTICANCER AND ANTIOXIDANT CYCLIC DIPEPTIDE CYCLO(D-TYR-D-PHE)

***Agaeva G.A., Agaeva U.T., Godjaev N.M.**
Baku State University, Azerbaijan
gulshen@mail.ru

The roles of many proteins and peptides have been identified as novel targets in cancer therapy, allowing for the design of more selective agents. The cyclic dipeptide (diketopiperazine) cyclo(D-Tyr-D-Phe) is a new biologically active natural product, isolated from the culture filtrate of *Bacillus*

sp. N strain. Diketopiperazines are not only a class of naturally occurring privileged structures that have the ability to bind to a wide range of receptors, but they also have several characteristics that make them attractive scaffolds for drug discovery. They are small, conformationally constrained heterocyclic scaffolds in which diversity can be introduced at up to six positions and stereochemistry controlled at up to four positions, and they are stable to proteolysis. Cyclo(D-Tyr-D-Phe) had greater antibacterial, anticancer and antioxidant activities than cyclo(L-Tyr-L-Phe). showed that cyclo It is showed that (D-Tyr-D-Phe) significantly inhibits the growth of cancer cell A549. Furthermore cyclo(D-Tyr-D-Phe) induced apoptotic cell death in A549 cells, suggesting the potential to inhibit the growth of tumors in vivo. It is known that chemical and physical properties of L-amino acid-containing peptides and D-amino acid-containing peptides are structural nearly identical, but they have different bioactivities.

In this investigation our purpose is to search for an energetically probable conformations of the two cyclic dipeptides cyclo(D-Tyr-D-Phe) and cyclo(L-Tyr-L-Phe). The major aim of the present work is the investigation of the three-dimensional structure and conformational dynamics of its side chains relatively of their peptide ring, called diketopiperazine ring. The spatial structure of cyclic dipeptides have been investigated by molecular mechanics method. This approach involves quantitative estimation of all nonbonded interactions. The nonbonded and electrostatic interactions, intramolecular hydrogen bonds, and restricted rotation about all single bonds of side chains are taken into account. The atomic partial charges for two cyclic dipeptides are computed by AM1 calculation method. For investigation of the behavior of the side chains within the energy preferred conformations were obtained the conformational maps around dihedral angles χ_1,χ_2,χ_3 for Tyr and χ_1, χ_2 for Phe residues. The comparison of results of theoretical conformational analysis of both cyclic dipeptides enable us to support the proposal that both peptides are free of any intramolecular hydrogen bond in order to be available for the formation of the complex with the receptor. Our calculations bring out for both cyclic dipeptides the different conformations as the most favorable. One of them cyclo(D-Tyr-D-Phe) formed asymmetric arrangement of side chains concerning peptide ring, but second dipeptide cyclo(L-Tyr-L-Phe) formed conformation with symmetric arrangement of side chains.

KINETIC AND THERMODYNAMIC PARAMETERS OF Cl^- TRANSPORT IN PLANT ROOTS DUE TO CHANGES IN TEMPERATURES

*Abdiyev V., Aliyeva N.
Baku State University, Azerbaijan
vilayet.abdiyev@mail.ru

Using the chemokinetic method, it was established that the penetration of chlorine ions into the root system of barley is fast at first and then slows down, i.e. curves consist of at least two exponential components. Temperature changes affect the value of the first and second kinetic components in the temperature range of 1°C -50°C. It was found that at low temperatures (1°C-10°C) the absorption of Cl^- ions by plant roots from a NaCl solution at a concentration of 100-50 mM is reduced to 70%-80% compared to the control. Kinetic curves of Cl^- intake in the range of 1°C-50°C showed that at low (1°C) and high (40°C-50°C) temperatures the second kinetic component is completely absent when the seedlings are exposed (for 160 min) to 50 mM NaCl.

Calculated apparent activation energy (E_{act}) for the transport of Cl^- into barley roots turned out to be equal to 3.10 kcal/mol in the range of 10°C-30°C. To obtain information about the mechanism of reactions responsible for the transport of ions into the plant cell, we determined the temperature coefficients (Q_{10}) of the transfer of Cl^- ions in the temperature range of 1°C-50°C.

The data obtained showed that the temperature coefficient Q_{10} of the transfer of Cl^- ions from a solution of 50-100 mM NaCl during 160 minutes is slightly different. Thus, for 50 mM NaCl, this coefficient has values of ∼3.53, ∼1.66, ∼1.2, ∼0.19, and ∼0 respectively, in the temperature ranges of 1°C-10°C, 10°C-20°C, 20°C-30°C, 30°C-40°C, and 40°C-50°C, while for 100 mM NaCl, it amounted to ∼2.0, ∼1.28, ∼1.5, ∼0.37, and ∼0 respectively. However, the pattern of change in Q_{10} at both NaCl concentrations is almost adequate.

In our experiments, the temperature maximum for Cl^- transport into the cell was at 30°C. Along with this, the value of free energy /ΔG/ of Cl^- entry into the roots was also determined depending on temperature (1°C-40°C) in different time intervals, as one of the thermodynamic indicators of the transport process. The temperature maximum of the free energy value was also found at 30°C. It has also been established that an increase in exposure contributes to an increase in the value of free energy; this may be one of the arguments in favor of the metabolic nature of the transport of Cl^- into the roots.

The study of kinetic, temperature characteristics, as well as the dependence of the entry of Cl^- into the root system of plants on the concentration of NaCl in the medium, showed that the first component is due to passive diffusion, while the second component is metabolic in nature.

MOLECULAR MODELING OF ILE-TRP DIPEPTIDE

*Rahimzade S.G., Akverdieva G.A.
Baku State University, Azerbaijan
sara.rehimzade@gmail.com

At work, computer modeling techniques have been used to study the Ile-Trp (isoleucyl-tryptophan) dipeptide. Peptides are involved in a wide range of biological processes, so understanding their structure is essential for developing new drugs and therapies. The medicines based on the Ile-Trp dipeptide are used as an immunomodulators for conditions and diseases accompanied by immunosuppression. It is known the dipeptides containing tryptophan can serve as bioactive food additives that have beneficial effects on the cardiovascular system. So, Ile-Trp dipeptide may be used as an antihypertensive drug because it inhibits ACE, an enzyme involved in blood pressure regulation. Ile-Trp dipeptide has been proven to have antioxidant properties, i.e. it can scavenge free radicals and protect cells from damage. This makes it a potential candidate for treating diseases related to oxidative stress, such as cancer and Alzheimer's disease.

The molecular mechanics method was applied to analyze the molecule's conformations. The HyperChem 8.03 software package with the PM3 semi-empirical quantum chemical method, which is suitable for computing biomolecule structures, was used to explore the electronic structure of the preferred conformations of this dipeptide. The study found the most stable conformations of the peptide backbone, both folded and extended. The noncovalent interactions within the molecule that stabilize these structures were analyzed, and it was observed how the hydrogen bonding influences the molecule's shape. In the extended structure of the dipeptide, one hydrogen bond is formed between the α-amino group hydrogen atom of the molecule and the oxygen atom of the carbonyl group of the isoleucine backbone. In the folded structure, two hydrogen bonds are formed between the hydrogen atom of the amide group of the tryptophan backbone and the oxygen atoms of the C-terminal carboxyl group of the molecule. The electronic parameters of the optimized folded and

extended conformations of Ile-Trp dipeptide have been computed (Table 1).

Table 1. The electronic parameters of the optimized folded and extended conformations of Ile-Trp dipeptide

Electronic parameters of the molecule	Folded structure	Extended structure
Total energy, kcal/mol	-86050.99	86089.30
Binding energy, kcal/mol	-4588.90	-4627.31
Isolated atomic energy, kcal/mol	-81461.99	-81461.99
Electronic energy, kcal/mol	-714467.96	707289.87
Core-Core interaction energy, kcal/mol	628416.97	621200.57
Heat of formation, kcal/mol	32.16	-6.16
Dipole moment, debyes (D)	22.48	24.14
E_{HOMO} (eV)	-7.34	-7.28
E_{LUMO} (eV)	-1.98	-1.68
Energy gap, ΔE (eV)	5.36	5.60
Polarizability (Å)	34.70	3.18

THE BINDING OF IRON IONS WITH MELANINS OF PLANT ORIGIN

Bagirov R.M.
Baku State University, Azerbaijan
rafiqbagirov@list.ru

In this study, melanins were isolated from the rind of elderberry black and ivy ordinary fruits. The isolated pigments were subjected to a comprehensive analysis, which included Electron Paramagnetic Resonance (EPR) and Infrared (IR) spectroscopy.

Furthermore, our investigation delved into the intriguing binding interactions between these plant-derived melanins and iron ions. We utilized the advanced technique of Gamma Resonance Spectroscopy (GRS) to explore this binding phenomenon. Our findings reveal that melanins of plant origin exhibit remarkable proficiency in chelating iron ions, regardless of their oxidation state, whether divalent or trivalent.

It is noteworthy that when interacting with Fe^{2+} ions, these plant melanins exhibit an intriguing behavior. They not only efficiently bind Fe^{2+} ions but also catalyze their partial oxidation to Fe^{3+}. This transition is significant as Fe^{3+} ions are known to be less prooxidant and more stable. The melanins demonstrate their ability to bind both Fe^{2+} and Fe^{3+} ions effectively, showcasing their potential in mitigating prooxidant activity.

The characteristics of the GR spectra acquired from the analyzed samples point to the formation of high-spin (HS) complexes involving Fe^{2+} and Fe^{3+} ions within an octahedral ligand environment. This insight into the structural aspect of iron-ion binding is a key contribution to our understanding of melanin-metal interactions.

Moreover, our study postulates that the capacity of melanins of plant origin to efficiently bind prooxidant Fe^{2+} ions may serve as a significant mechanism underlying their antioxidant and radioprotective properties. This research opens new avenues for exploring the potential applications of these natural pigments in various fields, including medicine and materials science.

All of the aforementioned mechanisms for binding iron ions should result in an inhomogeneous distribution of iron ions within the melanin polymer's volume, as evidenced by the results of the GR study. This is apparent in their oxidizing ability from Fe^{2+} to Fe^{3+}, as well as in their capacity to bind iron ions to plant melanins. Based on the data obtained, it can be reasonably assumed that these melanins all contain similar functional groups involved in the binding of iron ions.

Consequently, the results suggest that plant melanins can form complexes with iron ions in both their divalent and trivalent states. Notably, plant melanins can directly bind to Fe^{2+} ions and subsequently oxidize them to their trivalent state, rendering them inactive as prooxidants. The efficiency of both of these processes increases with the rising pH of the reaction medium.

MODIFICATION OF ZINC-ALUMINIUM LAYERED DOUBLE HYDROXIDES WITH FULLERENE AND INVESTIGATION OF PHOTOCATALYTIC ACTIVITY OF OBTAINED NANOCOMPOSITES

***Israfilli T., Balayeva O.**
Baku State University, Azerbaijan
turkan.israfill@gmail.com

Because of the possibilities for their applications, carbon-based nanomaterials include graphene, fullerene, and carbon nanotubes (CNTs) have attracted a lot of interest. Furthermore, fullerene has encouraging photocatalytic capabilities similar to those of graphene and carbon nanotubes. Fullerenes have potential for photocatalytic applications because of their substantial absorption of UV light and moderate just broad absorption of

visible light. Moreover, fullerenes have been found to be effective photosensitizers, possessing a high quantum efficiency of nearly 1.0.

A category of ionic lamellar compounds referred to as layered double hydroxides (LDHs) is made up of positively charged layered hydroxides with charge-compensating anions contained in the interlayer region. These substances, when combined with a polymer matrix, contribute as precursors for LDH/polymer nanocomposites.

Using polyvinyl alcohol (PVA) as a stabilizer, 1% fullerene (C_{60}) was introduced to the ZnAl LDH synthesis to generate a novel nanocomposite. Using methylene blue (MB) and congo red (CR) as model pollutants, the photocatalytic activity of this nanocomposite was examined and the active species in charge of the degradation process were identified. To be more precise, 5 ppm, 10 ppm, 15 ppm, and 20 ppm methylene blue solutions were incorporated with 0.005 g of ZnAl LDH@C_{60}/PVA. After a day, the sorption reached equilibrium, and the mixtures were exposed to 150 W of visible light. The samples were subjected to UV spectrophotometer analysis at multiple intervals. The photodegradation of MB was determined after 8 hours to have removal degrees of 78.62%, 81.61%, 88.62%, and 93.27% at 20 ppm, 15 ppm, 10 ppm and 5 ppm concentrations of MB, respectively.

In a 10 ppm CR solution, we added 0.01 g of ZnAl LDH@C60/PVA and the identical quantity of ZnAl LDH (without C60). Sorption equilibrium was achieved after a day, and then 150 W of visible light was exposed to the sample. UV spectrophotometer analysis was subsequently carried out at different intervals. In the absence of C60 and with C60 present, the photodegradation percentages for CR were determined to be 91.43% and 99.6%, respectively.

A potential photocatalytic process in MB was examined using •OH and •O_2^- radicals onto ZnAl LDH@C60/PVA nanocomposite, based on the active species trapping tests. With trilon B, IPA, ascorbic acid, and without reagent, the removal degree for the photodegradation of MB was 64.80%, 54.93%, 52.71%, and 56.54%, respectively. •OH and h^+ radicals were employed in CR to perform the same process. The percentages of CR that were removed by photodegradation with IPA, trilon B, ascorbic acid, and without reagent were 96.98%, 98.79%, 100%, and 99.8%, respectively. The degradation of MB and CR undergoes with presence of •O_2^- anionic radicals and •OH radicals, respectively. Although all the active species formed in process, the nature of dye molecules influence the process.

INCORPORATED TiO_2 NANOPARTICLES INTO PVC POLYMER FOR ENHANCING THE DIELECTRIC PROPERTIES

Rahimli A.M.
Baku State University, Azerbaijan
rahimli.almara@gmail.com

It was discovered that by including fillers having luminescent, magnetic, photovoltaic, photoresistor, and other active qualities into the polymer matrix, the active properties of the nanocomposite may be altered. Therefore, by adding metal oxides to the polymer matrix, nanocomposites' dielectric, photoluminescence, electret, photovoltaic, photoconductivity, magnetic, and other properties can be altered. Rutile and anatase, the two most frequent phases of TiO_2 nanoparticles, are luminous compounds having a broad luminescence peak in the visible range due to oxygen vacancies.

In this work, a comparative study of the temperature-frequency dependence of the dielectric properties of the composites obtained by modifying the PVC polymer with TiO_2 nanoparticles at different concentrations is presented. A comparative analysis of the dielectric parameters (ε, tgδ and ρ) of the composites obtained by incorporating nanoparticles in different concentrations into the polymer matrix was performed, the relaxation processes in the system were studied, and the interaction in the polymer matrix and at the polymer-filler interphase boundary was described. All nanocomposites exhibit the same pattern of variation as a function of frequency. As a result, it first goes down in the low frequency zone and sharply increases in the relatively high frequency range. This is explained by the fact that introducing nanoparticles into the polymer modifies the internal field in the polymer; as a result, when the value of the external field changes at higher frequencies, the polymer's resonance maximum is lost in response to these changes, and the amount of scattering increases. If the polarization of a material under an electric field happens weakly due to a change in the electric field, then dielectric relaxation loss occurs. The frequency dependence of the dielectric loss tangent graph revealed that the dielectric loss angle increases slowly at low frequencies and fast at high frequencies. At low frequencies of the field, the amount of energy scattered in the dielectric is relatively small, so the dielectric loss is small, but as the frequency of the field increases, the energy scattering also increases, which is reflected in the increase in the value of the dielectric loss.

Thus, it was determined that the inclusion of TiO_2 nanoparticles into

the PVC matrix leads to an increase in the value of dielectric constant of nanocomposites at all concentrations compared to the dielectric constant of pure PVC. This indicates the increase in the polarizability of polymer nanocomposites, and it can be assumed that such materials can be widely used as electret polymer nanocomposite materials in the future.

MWCNT/CuS NWS BASED MATERIALS FOR PHOTOVOLTAICS

[1]Nuriyeva S.G., [1*]Jafarova S.R., [2]Aguas H.
[1]Baku State University, Azerbaijan
[2]Nova University Lisbon, Portugal
snuriyeva@bsu.edu.az

A combination of two 1D materials (NWs and MWCNT) can improve physical properties, indicating possible applications in the PV electrode of solar cells. They can also be easily manufactured into thin films with interconnected networks that have tunable optical transparency and electrical conductivity, as well as superior mechanical flexibility. The MWCNT/CuS NWs-nanocomposites were synthesized using a simple approach based on the bulk heterojunction (BHJ) principle. Various analysis methods were used to investigate the morphology and structure of the generated one-dimensional structures- Cu and CuS nanowires, as well as CNT/CuS nanocomposites. SEM analysis reveals that the Cu NWs have a high aspect ratio, with lengths ranging from 10 to 20 μm and an average diameter of 100 to 300 nm. After sulphidation of CuNWs, the surface of the Cu nanowire is coated by nanoflakes of copper sulfide. The shape of CuS NWs is typical of 1D nanowires with diameters ranging from 200 to 600 nm. The TEM image reveals that the nanowires form a core-shell structure with a wire length of 5 μm and a width of 250 nm.The XRD investigations demonstrate that all of the diffraction peaks in Cu NWs are present and can be easily indexed for face-centered cubic (fcc) crystalline Cu. CuS nanowire XRD patterns can be related to hexagonal CuS structures. The peak at 26.53 in the MWCNT/CuS composite is attributed to MWNT (002) diffraction. These structural characterizations confirm the presence of CuS nanowires in the nanocomposite material. The intimate association of two components-CuS nanowires and MWCNT-suggests that some wires could be linked with multiple MWNTs. Such direct attachments will enable charge transfer networks between nanowires and MWNTs.

SCHOTTKY DIODES BASED ON CdS SINGLE NANOBELTS

*Mamedov R.K., Aslanova A.R.
Baku State University, Azerbaijan
rasimaz50@yahoo.com

In connection with the development of microelectronics and nanotechnology, interest in the development of discrete semiconductor devices and integrated circuit components based on Schottky diodes (SD) with nanostructure has increased significantly. In this case, nanocomposite materials are often used as a metal or semiconductor electrode with a nanostructure. The rectifying properties of such nanostructured SDs are often characterized by a low rectification coefficient and the complexity of the mechanisms for the formation of a potential barrier and the current flow in opposite directions. One of the possible reasons for this behavior of the SD is the appearance of an additional electric field (AEF) due to the limited contact surface in randomly distributed low-dimensional regions of the barrier contact interface. The noticeable effect of AEF on the properties of a SD with a nanostructure can be clearly observed when studying the current-voltage characteristics of a SD with a nanobelts or nanowire.

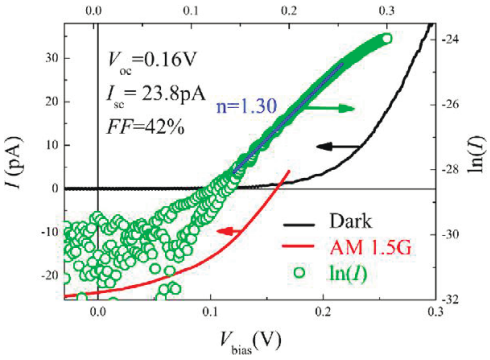

Fig. 1. The *I–V* curves of a typical Au-nCdS NB Schottky diode in the dark, and under AM 1.5G illumination.

Figure 1 shows the current-voltage characteristic of a SD made on the basis of an Au contact with a CdS single semiconductor nanobelts (NBs). The n-type CdS NBs had smooth surfaces and uniform width (1–2 μm) along the growth direction. The thicknesses of the CdS NBs as measured by an atomic force microscope were about 80–200 nm. It is clear from the figure that the forward branch of the current-voltage characteristic of CdS NBs SD is well described by a straight line on a semi-logarithmic scale and is shifted from the origin by a AEF voltage value of about 100 mV. The initial part of the current-voltage characteristic in the voltage range 0-100 mV consists of a reverse

current and in the absence of external voltage in the closed circuit of the CdS NBs DC under the influence of the AEP currents flow with a value of about 10-20 pA. This CdS NBs SD has normal photovoltaic effect and its characteristic parameters under white light are written in the figure.

OPTICAL ABSORPTION AND PHOTOCONDUCTIVITY IN $Cu_3In_5S_9$ SINGLE CRYSTAL

*Jahangirova S. A., Hasanova L.H., Mahammadov A.Z.
Baku State University, Azerbaijan
sona_aliqizi@mail.ru

In recent years $A^I\ B^{III}C_2^{VI} - B_2^{III}C_3^{VI}$ has shown that complex semiconductor compounds with interesting physical properties are obtained in the system. One of them $Cu_3In_5S_9$ is the combination. Its melting temperature is 1083 ^{0}C, it has a layered structure, it is easily separated into layers with a mirror surface. $D_{6h}^1 - (P6/mmm)$ the width of the forbidden band of the compound included in the spatial structure is 1.52 eV. The optical absorption and photoconductivity of the single crystal $Cu_3In_5S_9$ at different temperatures were measured in the considered work. α it was shown that the absorption coefficient can be calculated by measuring the photoconductivity. Since the $Cu_3In_5S_9$ compound has a layered structure, samples of different thicknesses are easily cut from the monolithic compound, and after measuring their thickness, α is calculated based on the Buger formula. Its values calculated from photoconductivity and calculated for transparency differ very little. $Cu_3In_5S_9$ in the single crystal, the absorption coefficient is linearly dependens on the energy in the temperature range of 77-300 K ($\alpha \sim 30\text{–}6 \cdot 10^2\ sm^{-1}$).

For the first time, Urbach showed that the long-wavelength limit of absorption in alkaline hybrid crystals is an exponential function of the photon frequency, i.e.

$$\alpha(v) = \alpha_0\, exp\left[\frac{\gamma(hv_0 - hv)}{kT}\right]$$

Here α_0, v_0 and γ the energetic parameters characterizing the crystal γ/kT show a linear trend corresponding to their dependence on a semi-logarithmic scale at a given temperature.

α_0 and hv_0 for $Cu_3In_5S_9$ crystals are 10 ^{3} and 1.54 eV respectively. It should be noted that γ depends on the temperature.

$Cu_3In_5S_9$ single crystal has an absorption coefficient at small values of energy ≤100 cm^{-1}. This indicates that the incident light is absorbed uniformly throughout the entire volume of the sample and surface recombination is neglected. Then it can be naturally assumed that the dependence of the photocurrent on the energy of the quantum obeys the law of the energy dependence of the absorption coefficient.

ACOUSTIC CHARACTERIZATION OF PHONEMES WITH COMPACT/ DIFFUSE FORMANT STRUCTURE AS A MEANS OF IDENTIFICATION IN PHONOSCOPIC RESEARCH

[1*]Aliyev L.P., [2]Gaziyeva N.G.
[1]Baku State University, Azerbaijan
[2]Institute of Linguistics of ANAS, Azerbaijan
n.gazi@inbox.ru

In phonoscopic research, the speech signal, which acts as a means of identification, plays the role of a "key" thanks to special biometric indicators. Different acoustic qualities determined by the geometrical configuration of the speech tract are reflected in the spectrogram. The acoustic characteristics of vowels are determined by the characteristics of the supralaryngeal cavity, which acts as a resonator. Resonance frequencies depend on the volume and shape of the cavity, i.e. the tongue, lips, etc. depends on the situation. When describing the acoustic properties of vowels, the properties of the first two formants are usually taken into account: FI (the more open the vowel, the higher the FI frequency) and FII - (the more front the vowel, the higher the FII frequency). It should be noted that the sign of labialization reduces the frequency of both formants, nasalization leads to a weakening of the intensity of FI and FII and the creation of an additional "nasalization formant".

In the acoustic classification of vowels, in addition to the actual frequency characteristics of formants, the location characteristics of formants in the vowel spectrum act as an important identification indicator. Depending on which part of the spectrum the energy is concentrated, sounds are divided into two groups: compact and diffuse. If the formants are located in the central part of the spectrum, the sound is called compact, if the formants are located on the edges of the spectrum, it is called diffuse. In compact sounds, the main energy, that is, the dominant formant region, is concentrated in a relatively narrow part of the spectrum,

the formants F1-F3 are close to each other. For diffuse sounds, the energy is distributed throughout the spectrum or along its edges, the distance between F1-F3 is large.

Vowel characteristics are important in the perception of vowel sounds, but experiments show that the change of formant frequencies is considered by people as an important criterion for determining not only the vowel itself, but also the consonant adjacent to it (in most cases, the previous one). An interesting marker is the compact/diffuse feature of formant indicators in the field of consonant-vowel coarticulation: F1 (440 Hz); F2 (2533 Hz); F3 (2544 Hz); F4 (3386 Hz) /ge/ ; F1 (393 Hz); F2 (2084 Hz); F3 (2469 Hz); F4 (3534Hz) /chi/ ; F1 (385 Hz); F2 (983 Hz); F3 (2762 Hz); F4 (3461Hz) /lu/.

STRUCTURE AND PROPERTIES OF PVDF/ZnO-BASED NANOCOMPOSITES

Hacıyeva F.V., *Mehdiyeva S.Z., Eyvazova G.M.
Baku State University, Azerbaijan
simaremehdiyeva@gmail.com

A recent research has indicated that zinc oxide (ZnO) – based polymer nanocomposite materials possess a range of unusual electrical, optical, thermal, mechanical, and biomedical properties, making them suitable for use in gas sensors, catalytic applications, and optoelectronic devices such as piezoelectric converters, optical wave transmitters, UV-laser converters, and solar elements. The present work focuses on the synthesis and study of PVDF/ZnO hybrid nanocomposite materials based on the thermoplastic polymer polyvinylidenefluoride (PVDF) and ZnO nanoparticles. The structure and optical properties of these nanocomposites were examined, and the width of the forbidden zone was calculated via extrapolation method based on UV-transmission spectra. The results showed that the width of the forbidden zone varied with the concentration of ZnO: for the PVDF+1% ZnO nanocomposite – 3,2 eV; – for the PVDF+1% ZnO nanocomposite – 3,0 eV; for the PVDF+3%ZnO nanocomposite – 2,8 eV; for the PVDF+5%ZnO nanocomposite – 2,65 eV; for the PVDF+7%ZnO and PVDF+10% ZnO nanocomposites – 2,3 eV. The crystalline and phase structure of PVDF, ZnO nanoparticles and PVDF/ZnO based nanocomposites were analyzed using Rigaku Mini Flex diffractometer between 20°-80°θ at room temperature. The indexed diffraction pattern for pure ZnO nanoparticles shows that peaks at 2θ=31.8° (100), 34.5° (002), 36.3° (101), 47.6°

(102), 56.6° (002), 62.9° (112) and 66.46° (103) corresponds to hexagonal wurtzite phase structure of ZnO nanoparticles. Have been established that with the introduction of ZnO nanoparticles into PVDF matrix the content of α-phase is decreased and β-phase is increased. It is known that the polarity of the PVDF molecule is related to the content of the β phase and the inclusion of ZnO nanoparticles in the PVDF polymer leads to an increase in the content of the β phase in the polymer nanocomposites.

STABILIZATION OF ZnS NANOPARTICLES BASED ON MODIFIED BUTADIENE RUBBER/EXPANDED PERLITE AND CARBON BLACK COMPOSITES: STRUCTURE, OPTICAL AND CONDUCTIVITY PROPERTIES

[1,2*]Edres N., [2]Buniyatzadeh I., [2]Alosmanov R., [2]Eyvazova G., [2]Mammadayarova S.
[1]Khartoum University, Sudan
[2]Baku State University, Azerbaijan
nadaedres2010@gmail.com

ZnS nanoparticles is one of much interest semiconductors materials it is characterized with wide range of bandgap, nontoxic and chemically stable, mainly exists in two crystalline forms cubic (sphalerite) and hexagonal (wurtzite), with bandgaps of 3.6 eV and 3.9 eV respectively, for cubic and hexagonal forms. due to these properties ZnS exploited in many optoelectronic applications such as sensors, solar cells and magnetic devices. The bulk production of ZnS nanoparticles in liquid phase obtain aggregates due to the high surface energy of the particles which trap the bandgap and shift the light adsorption to a higher energy range resulting in poor properties. Among various methods used to maintaining the nanoparticles chemically stable stabilizing agents of different polymers structures observed remarkable adjust to stabilize the morphology, size, shape and disperse of the nanoparticles. In this project we suggest two different pores/ion exchanger polymer matrixes based on modified butadiene rubber composites one reinforced with expanded perlite and the other with carbon black P234 fillers as stabilizer agents of ZnS nanoparticles, the composites prepared through cholorophosphorylation reaction. ZnS nanoparticles obtained on the base of polymer matrixes in three cycles using SILAR method. For this purpose, 0.1 M aqueous solutions of zinc chloride and sodium hydrosulfide were prepared. The process started by impregnate 0.1 g of polymer matrix in 10 ml of zinc chloride solution for 24 h then sample washed up to neutralization and dried in r.t once more the sample

impregnate in 10 ml of sodium hydrosulfide for 24 h then washed and dried at r.t, in the same manner the three cycles held.

The polymer matrixes allow in-situ stabilizing of cubic ZnS nanoparticles with averages particles sizes of 8 nm and 5 nm respectively for expanded perlite and carbon black modified butadiene rubber composites.

InN NANORIBBON MAGNETIC PROPERTIES

*Ismayilova N.A., Jahangirli Z.A.
Institute of Physics, Ministry of Science and Education, Azerbaijan
ismayilova_narmin_84@mail.ru

In the present work, we investigate the electronic structure and magnetism of InN nanoribbon doped with 3d Mn atoms in different positions by first-principle density functional calculations. To construct InN-NR structure that contains 52 atoms where 24 atoms from 52 are In, 24 is N, and 4 are H atoms that were chosen. In this structure, z-axis was aligned with the chiral vector (n, m) = (3, 3). H atoms were used to passivate the dangling bonds in the edge of NR. Replacing the In atoms by transition has a drastic effect on the electronic and magnetic properties. The calculated spin-polarized band structures of pure and InN NR1, InN NR2, and InN NR3 structures along with the total and partial DOS are displayed in Figs.

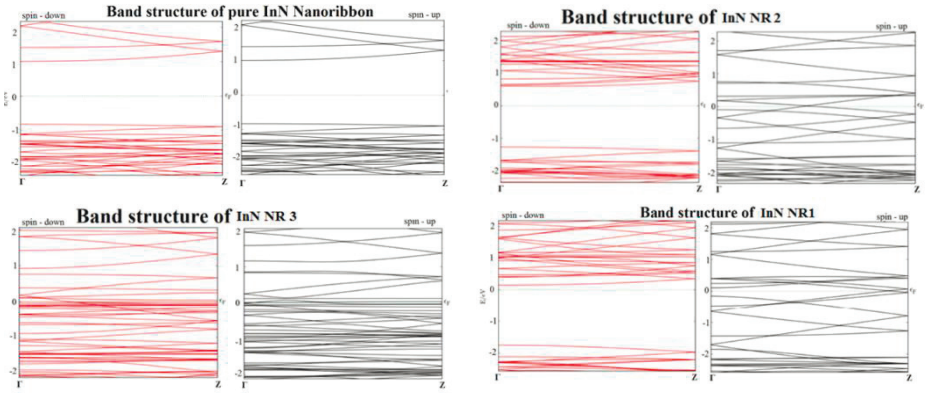

Fig. Electronic structure of InN nanoribbon pure and doped with Mn atoms

Calculation results reveal that pure InN-NR nonmagnetic and spin-dependent variation in the electronic structure is not observed. Mn dopant can result in a remarkable spin polarization and semiconductor ribbon

becomes halfmetallic by doping of InN NR1 and InN NR2 structure with Mn. It shows that the p-d hybridization between the Mn-N atoms is essential for the formation of the spin-dependent energy gap. Due to negligible induced magnetic moments of In and N atoms, total magnetic moments are approximately 16 mB for all InN NR1, InN NR2, and InN NR3 structures, where the most contribution comes from Mn local magnetic moment. These structures are suitable for spintronic and nanomagnetism applications.If you want to receive a formal acceptance of your abstract is funded to come to the conference, please write this in your e-mail when you submit your abstract, and you will receive a prompt reply.

STUDY OF THE SPECTRUM OF NOVA SCO 2023 DURING THE OUTBURST PERIOD

[1]Alisheva K.I., [1]Mikailov Kh. M., [1,2]Rustamov B.N., [1*]Alili A.H.

[1]Baku State University, Azerbaijan

[2]Shamakhy Astrophysical Observatory named after N. Tusi, Azerbaijan

kamalaalisheva@bsu.edu.az

This paper examines the evolution of the spectrum of Nova Sco 2023 during the outburst with a comparison of the light curve constructed according to AAVSO data (https://www.aavso.org/LCGv2/), and also determines the absolute magnitude at maximum ($M_V = -9^m$) and distance to the star (d=4.5±0.2 kpc). The light curve showed that the star belongs to the O-class (oscillation) of light curves.

Moderate resolution spectra (R=11000) of the object were taken from the ARAS astronomical observation database (https://aras-database.github.io/database/novasco2023.html). Further processing of the spectrum was developed using the Dech 30 software package (http://www.gazinur.com/DECH-software.html).

Two high-speed absorptions are observed in the star's spectra. At the moment of maximum brightness (22-04-2023), the Hα and Hβ lines of hydrogen show a P Cyg profile with two absorption components: the radial velocities of these components of each line are, on average, -1770 km/s and -2950 km/s, respectively. Subsequently, for the Hα and Hβ lines of hydrogen, the radial velocity of the second absorption component reached a value of -3350 km/s, and the first component disappeared. The helium line HeI (5876) also shows a P Cyg profile with broad emission and broad absorption components. The radial velocity of the absorption

component is equal to -2921 km/s. For 5 days, the radial speed of the HeI line (5876) increased to -3750 km/s. However, in the following days, the absorption component disappears and a very strong emission component remains. Lines of ionized metals, such as FeII, exhibit a P Cyg profile with a single-component absorption whose radial velocity is -1670 km/s.

The sodium NaI D1 and D2 lines in the spectrum of Nova Sco 2023 consist of two components belonging to both the star itself and the interstellar medium (ISM). The NaI lines associated with the interstellar medium show a radial velocity of -6 km/s, and the stellar lines show a radial velocity of -1670 km/s and after 5 days reach -1930 km/s.

As can be seen, the radial velocities of the hydrogen, helium, ionized iron lines and NaI stellar lines are very close in value. Among the classical nova stars we have studied so far, only Nova Sco 2023 exhibits such high radial velocities of individual absorption components of lines of some elements. This once again indicates a very strong explosion, accompanied by two (1700 km/s and 3000 km/s) powerful emissions of matter.

JOINT SURFACE IONIZATION OF CsCl MOLECULES AND Ba ATOMS ON THE SURFACE OF RHENEIUM COVERED WITH A GRAPHITE MONOLAYER

Orujov A.K.
Baku State University, Azerbaijan
orar@mail.ru

It is known that the monolayer of graphite reduces the dissociation and corresponding surface ionization of many alkali metal halides, the ionization coefficient being practically 10^{-5}-10^{-6}. CsCl molecules practically do not dissociate on the surface of metals with a graphite coating. We obtained the dependence of the coefficient of utilization of Ba atoms in splitting reactions on the temperature of the sample during the joint adsorption of Ba atoms and CsCl molecules on the Re-C surface in various flows (Fig. 1).

These dependences differ significantly from the above works, since it is noted there that the utilization increases with decreasing temperature, and then the dissociation coefficient remains constant, it is also shown that this stability is the result of a chemical reaction between CsCl molecules and Ba atoms, in our opinion, this is impossible from the point of view of the degree of activity of chemical elements. In our case, with decreasing temperature, the dissociation coefficient and the coefficient of

utilization of atoms monotonically increases, passes through a maximum, and with a subsequent decrease in temperature monotonically decreases to zero.

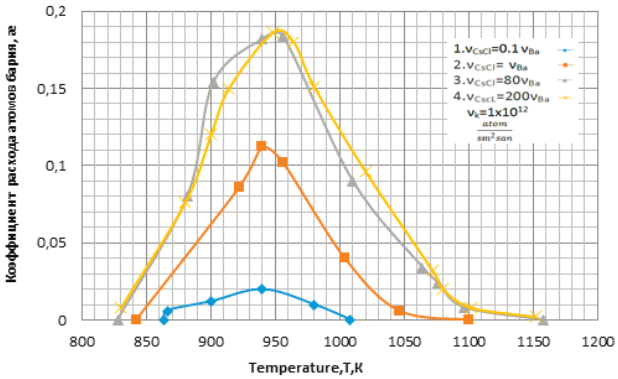

Fig. 1. Temperature dependence of the co-adsorption rate coefficient of CsCl molecules and Ba atoms

This process can be explained as follows: the meeting of CsCl molecules and Ba atoms on the surface during their stay on the surface depends on their migration along the surface.

ELECTRICAL PROPERTIES OF POROUS-Si/NANO-Cd0.4Zn0.6S HETEROJUNCTIONS

1*Mamedov H.M., 2Shah S.I., 1Mansimova F.B.

[1]Baku State University, Azerbaijan
[2]University of Delaware, USA
mhhuseyng@bsu.edu.az

Solar cells based on c-Si/porous-Si/Cd0.4Zn0.6S heterojunctions were synthesized by depositing Cd0.4Zn0.6S films on c-Si/porous-Si substrates by electrochemical deposition. Porous silicon layers with a systematically varied pore diameter (8÷45nm) and were fabricated on p-type c-Si wafers using **electrochemical etching**. Depending on the sizes of the $Cd_{0.4}Zn_{0.6}S$ crystallites and silicon pores, electrical characteristics of porous–Si/$Cd_{0.4}Zn_{0.6}S$ heterojunctions are studied. The optimal pore size (10–16 nm) is determined, which provides the maximum photoelectric conversion efficiency (9.1%) of heterojunctions.

RAMAN STUDIES ON SI/PS NANOCOMPOSITE

Pashayev B.G., *Surxayli.A.E., Shirinova.H.A

Baku State University, Azerbaijan
hshirinova@bsu.edu.az

Nano-sized particles spread in a polymer matrix improve a set of properties of polymers by influencing their structural characteristics. Besides the small size of the nanoparticles and narrow size distribution, the interfacial interaction also plays a vital role in the formation of the unique properties of the nanocomposite. The final features of the nanocomposite depend on the active properties of the dispersed phase. It is known that Si is one of the most common semiconductive materials which is widely used in different areas of electronics. However, the properties of nano silicon differ from bulk Si. From this perspective, investigation of the Si nanoparticle-based polymer nanocomposites is an actual issue for material science and all branches of technology where semiconductive materials are actively used.

Polystyrene and silicon-based nanocomposites were prepared by ex-situ method. The structure of the prepared samples was analyzed by scanning electron microscope and x-ray diffraction technique. Raman spectroscopy is used as one of the fast and nondestructive methods for Raman scattering study. In this study, Raman measurements were carried out at room temperature. It was shown that the peak wavelength of silicon shifts with the increase of the silicon concentration in the polymer matrix. This can be explained by the phonon confinement effect.

DESIGN AND DEVELOPMENT OF ADVANCED MULTICOMPONENT BULK METALLIC GLASSY ALLOYS FOR TECHNOLOGICAL APPLICATIONS

[1]* Mekhrabov A.O., [2]Akdeniz M.V.

[1]Azerbaijan Technical University, Azerbaijan
[2]Middle East Technical University, Türkiye
emdulla.mehrabov@aztu.edu.az

The presentation will be an overview of the main research thrusts at the “Novel Alloys Design and Development Lab” (NOVALAB) of MetE-METU, and at "Novel Materials and Nanotechnology" Research Center of

Azerbaijan Technical University (AzTU) in the designing and development of advanced multicomponent bulk metallic glassy alloys for technological applications. Fundamental principles and main aspects of Computational Materials Science (CMS) for modeling and simulation based "alloy design" which has been developed over 30 years at our Labs, will be presented.

Bulk metallic glasses (BMG) show a unique combination of specific metallic and glassy properties and since most of these properties cannot be found in crystalline materials, the BMG are attractive for practical utilization as a new class of structural as well as functional materials. Bulk glass-forming ability (BGFA) of a melt is frequently evaluated in terms of the critical cooling rate for easy glass formation, which is the minimum possible cooling rate necessary to preserve amorphous structure of melt during solidification preventing nucleation and growth of any crystalline structure in the alloy systems. In spite of great efforts that have been concentrated on the analysis of bulk glass forming ability (BGFA) of various multicomponent alloy systems, the exact nature of the mechanism of BGFA has not been revealed and is largely empirical. Unlike previous approaches, this lecture will address the problem of integrating modeling, computer simulation and atomic level theory into a new coherent methodology of widespread applicability aimed at designing the content and structure of multicomponent alloy systems having high BGFA leading to easy glassy phase formation under conventional solidification conditions. Application of this new approach for the designing and utilization of advanced Fe-based multicomponent BMG with enhanced physico-chemical properties will be discussed.

8th INTERNATIONAL CONFERENCE MTP-2023: MODERN TRENDS IN PHYSICS

DEDICATED TO THE 100th ANNIVERSARY
OF NATIONAL LEADER HEYDAR ALIYEV

NOVEMBER 30 – DECEMBER 01, 2023
BAKU STATE UNIVERSITY BAKU, AZERBAIJAN

BOOK OF ABSTRACTS

Printed: 29.11.2023
Volume 11,5 p.s.. Amount 150

Baku State University Publising House.
33, Acdemician Z. Khalilov street, Baku, Azerbaijan
Tel: (+99412) 538 87 39 / 538 50 16
e-mail: bdumetbee@gmail.com www.bsu.edu.az